University of Salamanca

Institute of Neuroscience of Castilla y León

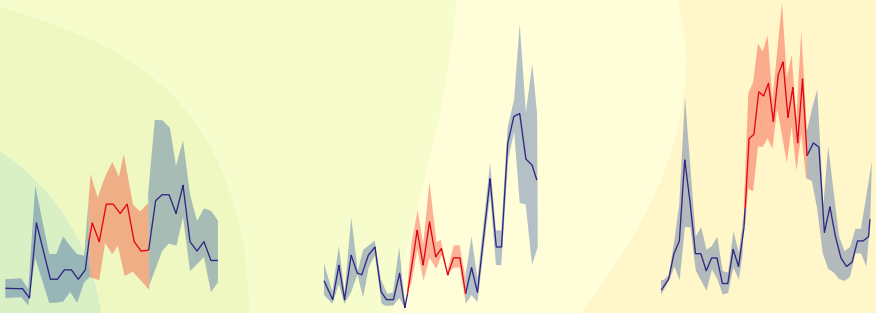

FUNTIONAL MECHANISMS THAT MEDIATE NEURAL ADAPTATION IN THE AUDITORY BRAIN: THE CHOLINERGIC MODULATION AND OMISSION RESPONSES

Ana Belén Lao Rodríguez

Doctoral Thesis
June 2023

VNiVERSiDAD D SALAMANCA

INSTITUTO DE NEUROCIENCIAS CASTILLA Y LEÓN

UNIVERSITY OF SALAMANCA

Institute of Neuroscience of Castilla y León

Cognitive and Auditory Neuroscience Laboratory

FUNCTIONAL MECHANISMS THAT MEDIATE NEURAL ADAPTATION IN THE AUDITORY BRAIN:

THE CHOLINERGIC MODULATION AND OMISSION RESPONSES

Thesis submitted by

Ana Belén Lao Rodríguez

to obtain the degree of

Doctor in Neuroscience

and the

International Doctor Mention

Supervised by

Prof. Manuel S. Malmierca, M.D., Ph. D.

Prof. David Pérez González, Ph. D.

Salamanca, Jun 2023

This work was supported by project PID2019-104570RB-I00 funded by MCIN/AEI/10.13039/501100011033 (to M.S.M.) and Foundation Ramón Areces grant CIVP20A6616 (to M.S.M. and D.P.-G.), European Union's Horizon 2020 grant agreement no. 952378—BrainTwin (to M.S.M., D.P.-G., and A.B.L.-R.).

AKNOWLEDGMENTS

I am deeply grateful to my thesis supervisor, Manuel S. Malmierca, for letting me be part of his group and for his patience in guiding and encouraging me to get this far. His passion and enthusiasm for neuroscience has been a great inspiration, which has led me to find beauty in what we do. Thank you for being my mentor beyond being 'the boss'.

Special thanks to David Pérez González, who also supervised this thesis. Thanks for your guide and support, especially when forces are weak.

To Prof. Gerard Borst for receiving me in his lab and for trust me with implementing new experiments. Thank you for pushing me to a deeper rationale.

To Prof. Bernhard Englizt for sharing with me his knowledge and his courage to take on challenges.

To Gloria G. Parras for accompanying me during my first surgeries and recordings.

To all my labmates: Blanca, Guillermo, Lorena, Flora, Camilo, Cata, Cristian, Laura, Laurita, Jazmín, Alba, Adam y Warren who have been sharing sadness and happiness.

Thanks to my friends for listen to me.

Thanks to Alejandro for being always there.

Thanks to my parents, my all.

TABLE OF CONTENTS

LIST OF ABBREVIATIONS

A1: primary auditory field

AAF: anterior auditory field

ABR: auditory brainstem response

AC: auditory cortex

ACh: acetylcholine

ANOVA: analysis of variance

Aq: aqueduct

AUC: area under the curve

BF: basal forebrain

CO2: carbon dioxide

CSI: common stimulus-specific adaptation index

EEG: electroencephalography

ERP: event related potentials

FRA: frequency response area

IC: inferior colliculus

iMM: index of neuronal mismatch

iPE: index of prediction error

iPR: index of repetition suppression

LDT: laterodorsal tegmental

M: medial

MI: mutual information

MMN: mismatch negativity

nMM: neuronal mismatch

PAF: posterior auditory field

PAG: periaqueductal

PC: predictive coding

PPT: pedunculopontine

PSTH: peristimulus time histogram

RCIC: rostral cortex of inferior colliculus

SC: superior colliculus

SEM: standard error of the mean

SI: specific index

SOA: stimulus onset asynchrony

SRAF: suprarhinal auditory field

SSA: stimulus-specific adaptation

V: ventral

VAF: ventral auditory field

1. Introduction

Understanding an ever-changing environment is crucial for all living beings. Consider a crowded restaurant. As you sit at your table, your sensory systems are bombarded with multiple sensory stimuli. Conversations overlap and blend together, clattering dishes and cutlery create a symphony of noise, and the aroma of various dishes fills the air. In the middle of this sensory chaos, your brain must navigate and make sense of the scene. Despite the cacophony, you are able to focus on a specific conversation at your table, distinguishing the voices of your friends from the surrounding chatter. You can even pick out the subtle sound of a familiar song playing softly in the background. In this scenario, your brain is tasked with isolating and interpreting individual auditory objects, such as voices and music, within a complex auditory landscape.

A key function of the auditory system is to transform complex auditory scenes into meaningful representations that are biologically relevant. For example, a tray full of crystal glasses falling to the floor and shattering into a thousand pieces warns us of dangerous broken glass. Due to the limited mechanical capabilities of our sensory systems, our brain is compelled to generate meaningful interpretations from an excessive amount of fragmented, noisy, and uncertain sensory data. It must filter out irrelevant sounds and extract meaningful information from the sensory overload, allowing you to engage in conversations and enjoy the ambience of the restaurant.

The majority of the sound that reaches our ears is characterized by its repetitive and predictable nature but may have little functional relevance because critical information is usually made of infrequent sounds. The ability of the auditory system to automatically filter out these predictable stimuli and highlight unique, unpredictable sounds is known as *deviance detection* (Grimm and Escera, 2012; Escera and Malmierca, 2014). In other words, deviance detection is a key process that arises from finely tuned internal mechanisms that can discriminate between familiar and novel sounds.

1.1. Mismatch Negativity as the main biomarker of deviance detection

The pioneering work by Prof. Risto Näätänen (1978), who used electroencephalogram techniques (EEG) recorded from the human scalp, described a phenomenon they called *Mismatch Negativity* (MMN) (Näätänen et al., 1978, 2007; Näätänen, 1990, 1992) (Fig. 1). MMN is one component of the auditory *event-related potentials* (ERP) that reflects

the brain's ability to detect changes in the auditory scene, i.e., deviance detection. MMN can be induced by any discriminable alteration in the auditory input using a traditional oddball paradigm, where infrequent auditory inputs (referred to as deviant, unpredictable stimuli, 10% of appearance) are randomly interspersed within a succession of regular inputs (referred to as standard, predictable stimuli, 90% of appearance) (Näätänen, 1992). Furthermore, the amplitude of the MMN reflects the magnitude of the difference between the responses to standard and deviant tones, reaching its maximum amplitude between 100 up to 220 ms after the deviant onset (Näätänen et al., 1978).

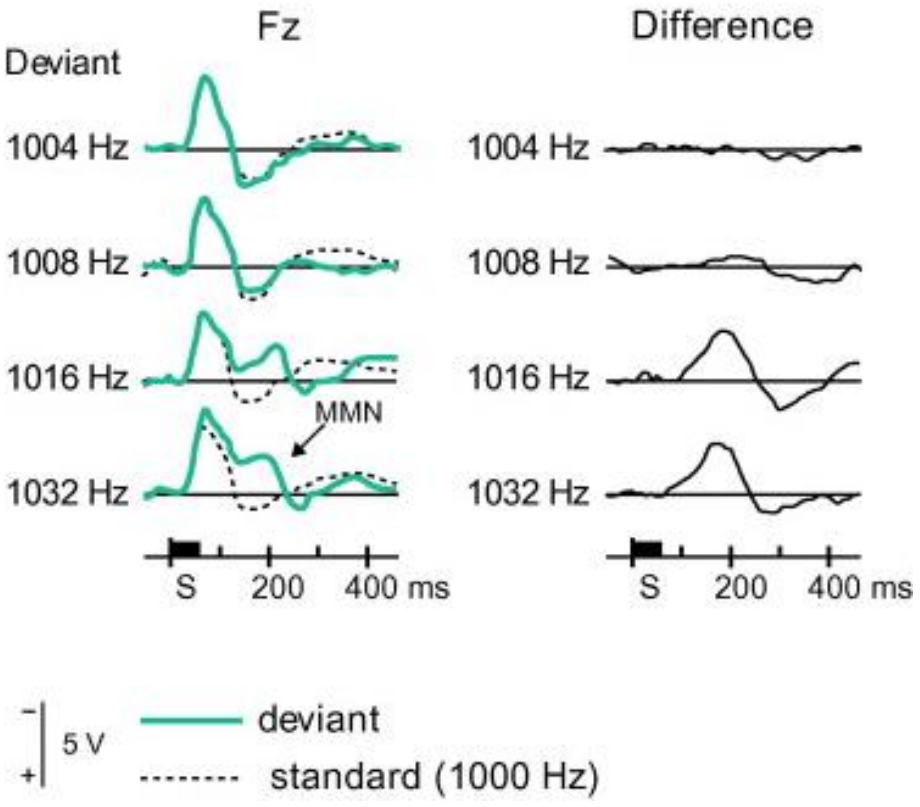

Figure 1. Frontal ERPs averaged across subjects in response to the standard tone (black dotted lines, 80% appearance, 1000Hz) and randomized deviant tones (green lines, 20% appearance of difference frequencies). Adapted from Näätänen et al., 2007.

The MMN has been extensively measured in different brain states: during natural sleep (Nashida et al., 2000; Sculthorpe et al., 2009; Strauss et al., 2015), anaesthesia (Koelsch et al., 2006; Quaedflieg et al., 2014), or coma (Morlet and Fischer, 2014; Rodriguez et

al., 2014). It is currently believed that the computational mechanism underlying deviance detection forms the basis and triggers higher-order cognitive processes (Näätänen et al., 2010), such as attention (Sussman et al., 2003; Fritz et al., 2007) and memory (Ranganath and Rainer, 2003; Bartha-Doering et al., 2015). Therefore, MMN has been extensively used as a biomarker for patients with neurodevelopmental and psychiatric disorders, who typically exhibit a significant MMN decrease such as in schizophrenia (Garrido et al., 2009; Todd et al., 2013; Fisher et al., 2018), Parkinson's disease (Minks et al., 2014; Heldmann et al., 2017), autism spectrum disorders (Goris et al., 2018; Hudac et al., 2018; Schwartz et al., 2018) or Alzheimer's disease (Tsolaki et al., 2017; Jiang et al., 2022) among others.

1.2. From human scalp to single neurons in animals

Due to the extended use and relevance of MMN, many studies have tried to explore this phenomenon at the neuronal level using the same oddball paradigms that are used in human electrophysiology (Ulanovsky et al., 2003; Malmierca et al., 2009; Antunes et al., 2010; Ayala and Malmierca Dr., 2013; Escera and Malmierca, 2014; Duque and Malmierca, 2015; Nieto-Diego and Malmierca, 2016; Carbajal and Malmierca, 2018). These studies described a mechanism shown by many auditory neurons, namely, they exhibited a gradually diminished response to the standard stimulus, which could be re-established by an unexpected deviant sound (Fig. 2). This mechanism is referred to as *stimulus-specific adaptation* (SSA). Due to their common properties, SSA was proposed to be the neuronal correlate of MMN (Ulanovsky et al., 2003).

Theories such as *the adaptation hypothesis* (May and Tiitinen, 2010) and *the model-adjustment or memory trace hypothesis* (Winkler, 2007) have tried to explain deviance detection under different perspectives.

The adaptation hypothesis attempts to explain deviance detection, in particular MMN, based on a physiological mechanism of synaptic adaptation. This theory argues against the existence of a genuine deviance detection process, arguing that the standard stimulus induces SSA due to passive mechanisms such as synaptic depression in auditory cortex (AC) neurons (May et al., 1999; Ulanovsky et al., 2003; Jääskeläinen et al., 2004). Meanwhile, the frequency channels of the AC neurons that are tuned to deviant tones maintain their responsiveness (May and Tiitinen, 2010; Fishman, 2014).

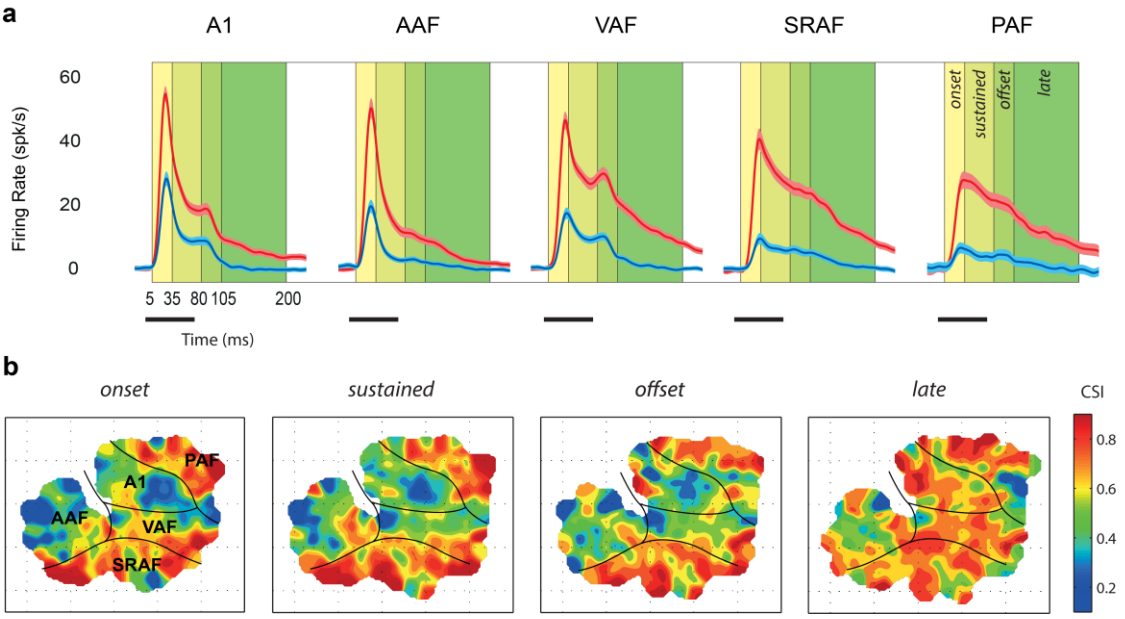

Figure 2. a. Grand-average of responses to standard (blue line) and deviant tones (red line) within auditory cortex (AC) fields (A1, anterior auditory field (AAF), ventral auditory field (VAF), suprarhinal auditory field (SRAF) and posterior auditory field (PAF)). **b.** Topographic distribution of stimulus-specific adaptation index (CSI) showing higher and lower SSA and response time-related behaviour. Adapted from Nieto-Diego and Malmierca 2016.

The classic cognitive interpretation of the MMN, the model-adjustment or memory trace hypothesis, proposes that repeated presentations of a standard stimulus create a sensory-memory trace of acoustic stimuli. This memory trace is mainly encoded in temporary AC sources (Näätänen and Michie, 1979; Näätänen, 1990), allowing the detection of sensory differences between the memory trace and the actual input (Näätänen and Alho, 1995). The memory trace hypothesis interprets the MMN as the result of all the neural activity that meets the cognitive resources to process deviant events (Winkler et al., 1996; Näätänen and Winkler, 1999).

Both theories fail to fully explain deviance detection. The MMN appears without attention or conscious perception of the deviant stimulus. This suggests that the MMN is an automatic process that is not solely dependent on the adjustment of internal models based on attention or conscious awareness. Secondly, the SSA has been observed not only for simple, but also for complex stimuli, such as speech sounds and music (Koelsch et al., 2019; Malmierca et al., 2019). The adaptation hypothesis struggles to account for the

specificity and selectivity of SSA across different sensory domains and stimulus complexities.

Moreover, both the MMN and SSA have been observed at multiple levels of the auditory pathway, including subcortical areas. This indicates that multiple neural processes contribute to these phenomena beyond simple adaptation or model adjustment mechanisms. Consequently, a different approach is needed to understand how MMN is generated, leading to more appealing theories, which I describe presently.

1.3. Predictive coding: The Solomonic solution as a unifying theory

Predictive coding is an all-encompassing theory of neural function that explains how the brain comprehends and interprets the world around us (Friston, 2002, 2012). According to this theory, the brain continuously extracts regularities from the environment to generate predictions or expectations based on prior knowledge, building then an internal model.

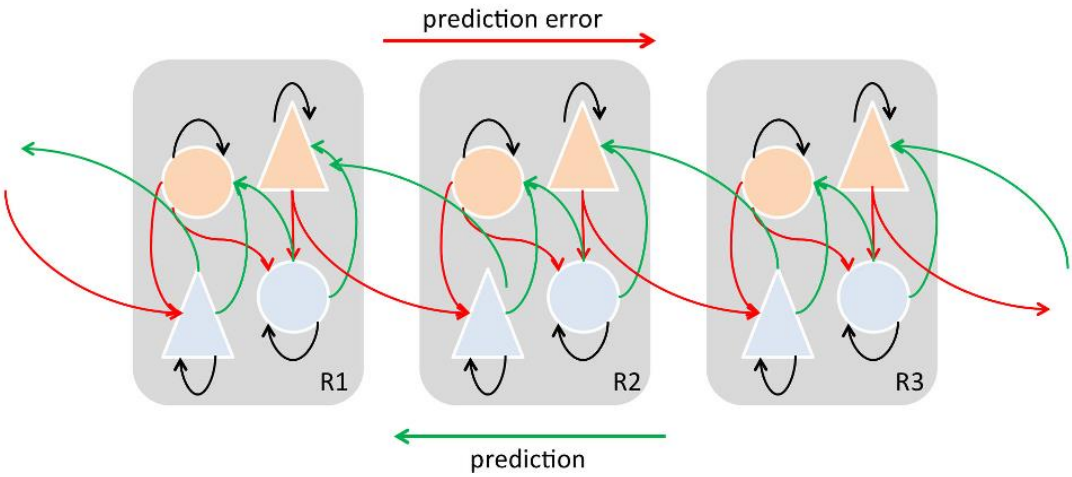

Figure 3. A schematic of hierarchical predictive coding across three cortical regions; the "lowest" (R1) on the left and the "highest" (R3) on the right. Light blue cells represent state units, orange cells represent error units. Note that predictions and prediction errors are sent and received from each level in the hierarchy. Feed-forward signals conveying prediction errors originate in superficial layers and terminate in deep (infragranular) layers. Conversely, feedback signals conveying predictions originate in deep layers and project to superficial layers and are associated with beta-band oscillations. Adapted from Seth et al., 2012.

Then, these predictions are compared to the incoming sensory input and any discrepancies, or *prediction errors*, are used to update and refine the existing model (Fig. 3). The MMN response is widely considered as a neurophysiological prediction error signal (Friston, 2005; Winkler, 2007; Garrido et al., 2008, 2009; Den Ouden et al., 2012; Stefanics et al., 2015; Parras et al., 2017; Casado-Román et al., 2020). It is the result from comparisons between sensory (bottom-up) input and a memory trace, or the prediction, encoded in top-down activity (Yuille and Kersten, 2006; Antunes and Malmierca, 2011; Carbajal and Malmierca, 2018, 2020). A prediction error occurs when the sensory input does not match the internal predictions.

This is one of the most controversial, but also influential theories of neural function. This is because it challenges traditional views of perception and cognition (Heilbron and Chait, 2018). Predictive coding enjoys empirical support, especially from studies on SSA that has been described along the different auditory stations of the auditory pathway (Parras et al., 2017; Casado-Román et al., 2020) (Fig. 4). These studies proposed a new approach to studying neuronal deviance detection. Here neuronal responses have been decomposed into repetition suppression and prediction error components using the no-repetition controls previously introduced in the MMN literature (Schröger and Wolff, 1996; Jacobsen and Schröger, 2001; Jacobsen et al., 2003b, 2003a). The difference between deviant and standard is now referred to as *neuronal mismatch* (nMM).

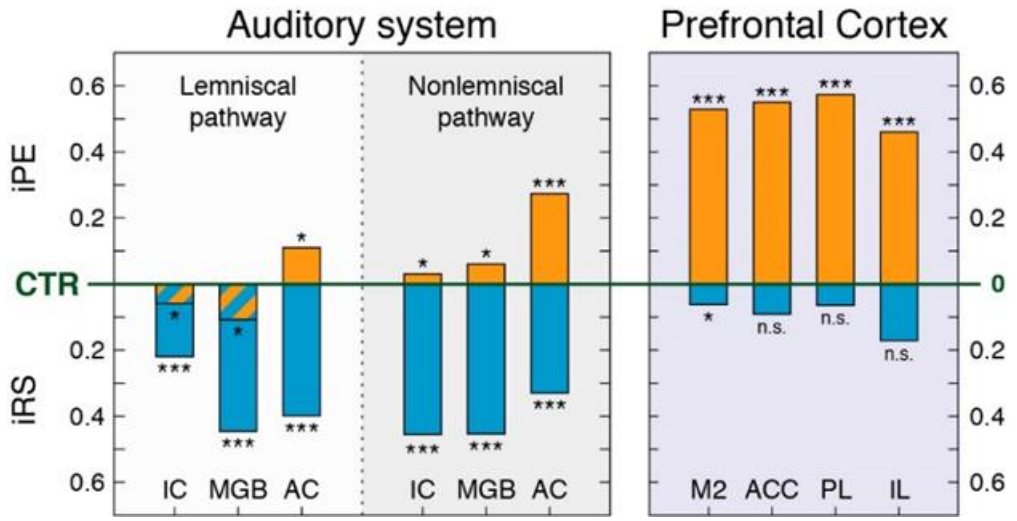

Figure 4. Description of repetition suppression index (iRS, blue vertical bars) and prediction error index (iPE, yellow vertical bars) along the auditory

system (IC (IC), medial geniculate body (MGB) and auditory cortex (AC) and the prefrontal cortex (secondary motor cortex (M2), anterior cingulate cortex (ACC), prelimbic cortex (PC) and infralimbic cortex (IC)). Adapted from Casado-Román et al., 2020.

1.4. Searching for fidelity: the precision of prediction errors

As mentioned before, predictive coding theory posits that there is active hierarchical processing which compares top-down predictions and bottom-up prediction errors (Rao and Ballard, 1999). Rather than processing the entirety of information available, a predictive process would just integrate the prediction error signal (Clark, 2013). Then, as expectations are updated, the number of prediction errors being encoded is progressively diminished. Therefore, reduced prediction error values indicate optimized processing of the information. This is the guiding principle of the predictive coding framework: prediction error minimization (Friston et al., 2006; Friston, 2010; Fields et al., 2022).

A perceptual system could minimize prediction errors adopting a hierarchical generative model within its neural network. This model involves comparing the bottom-up sensory inputs to the top-down predictions at multiple levels of processing, which are strongly interconnected. The *prior beliefs* will be updated at each processing station based on the prediction errors that are forwarded up from the level below. The *posterior beliefs* at one level become the expectations at the next lower level. Thus, the prediction error is forwarded to the next higher level as evidence for updating the prior belief (Friston and Stephan, 2007; Hohwy, 2017). This cycle of updating predictions using prediction errors continues until the prediction error is sufficiently reduced by fitting expectations from the lower levels. Hence, perception is a result of a hierarchy of causal inferences, where each level constrains the processing of its nested levels. In other words, a multilevel representation of the sensory information that does not fit the expectations is encoded through hierarchical prediction error minimization, which involves the convergence of expectations and sensory input across nested levels, allowing perception to emerge with minimal use of processing resources (Carbajal and Malmierca, 2020).

This process may appear finite but it is not. The nervous system is always processing prediction errors because the world is constantly fluctuating, but also because our own nervous system functions erratically. Non-ideal listening situations, such as hearing loss

or signal masking due to a noisy environment can lead to misinformative prediction errors. Consequently, not all prediction error signals should be considered equally.

Here is where the concept of *precision* plays a fundamental role in the formation and the revision of predictions (Fig. 5). This precision refers to the level of reliability of a prediction error. Predictions are examined by discriminating the uncertainty from the prediction error. Meanwhile, as synaptic signals move along the processing hierarchy, they are given different weights depending on how precise they are expected to be (Friston, 2008; Parr et al., 2018; Parr and Friston, 2019). If the brain expects a high level of precision, the prediction error signals will be amplified, increasing how influential they are when updating predictions. On the contrary, when low precision is expected, prediction error signals will be attenuated to avoid inaccuracies and then reinforcing prior beliefs.

Thus, the magnitude of a prediction error signal depends not only on the size of the mismatch, but also on the precision of the prediction. In other words, the precision of a prediction reflects the level of confidence or certainty that the brain assigns to it. Therefore, the expected precision refers to the degree of amplification that the postsynaptic gain applies to prediction error, which adjusts its impact on higher levels of processing. This allows more accurate and reliable prediction errors to contribute to learning processes, rather than less precise and less trustworthy ones (Friston and Kiebel, 2009).

In the literature, prediction has been represented as a Gaussian probability distribution relative to a perceptual feature. In that distribution, the mode represents the most probable prediction, while the inverse of the variance defines the confidence in that prediction, known as precision. Therefore, prediction is the expectation itself and the expected reliability of that expectation. From this, perception, therefore, is the result of a weighted average between the sensory input and the prediction, where the weight is determined by the precision (Sedley et al., 2016).

Prediction errors are weighted and amplified through the regulation of postsynaptic gain driven by neuromodulatory systems (Friston, 2008; Feldman and Friston, 2010; Parr et al., 2018; Parr and Friston, 2019). Proper precision adjustment is crucial for the function of the entire perceptual system. Dysfunctional neural receptors could lead to incorrect

weighting of precision, resulting in signs and symptoms of neuropsychiatric disorders and neurogenerative diseases, as auditory hallucinations, schizophrenia and Alzheimer´s disease (Tandon, 1999; Adams et al., 2013; Hullfish et al., 2019; Friston et al., 2021).

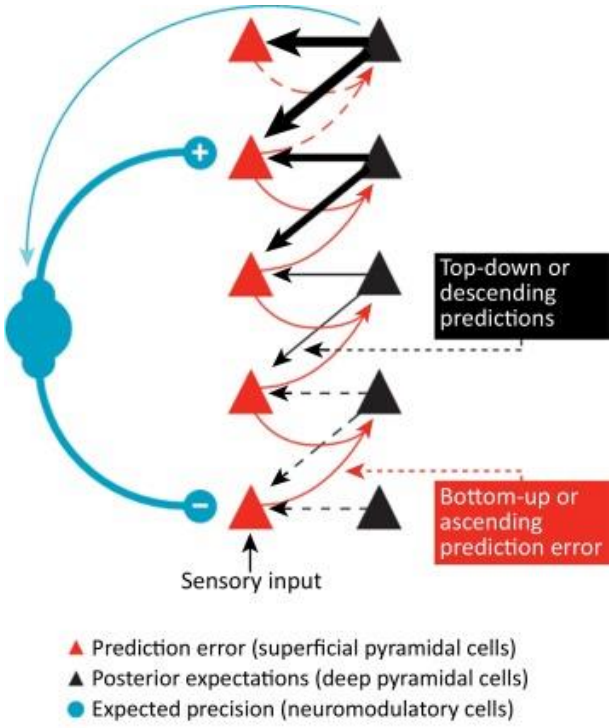

Figure 5. Decreasing influence of top-down predictions on ascending prediction errors. The image illustrates the precision-weighted decrease of top-down (descending) predictions towards lower levels of the processing hierarchy. Adapted from Koelsch et al., 2019.

One candidate for signalling precision is neuromodulation. Originally Yu and Dayan, proposed that the cholinergic and dopaminergic systems implement precision in terms of neuromodulation (Yu and Dayan, 2002, 2003, 2005). Also studies by (Moran et al., 2013) and (Friston et al., 2012, 2014), has tested how the natural release of neurotransmitters such as acetylcholine (ACh) and dopamine could be playing a fundamental role in the balance of the expected precision, respectively. The framework of Yu and Dayan (Yu and Dayan, 2002) proposes that ACh modulates uncertainty associated with top-down signals and modulates the interaction between top-down and bottom-up when processing in determining the appropriate neural representations for

inputs in high-level representations, illustrating how cholinergic modulation leads to appropriate perceptual inference.

Miasnikov and colleagues demonstrated that a sensory "memory" relies on cholinergic modulation in the auditory domain (Miasnikov et al., 2008). Further studies have analysed the simulated and empirical responses about the role of cholinergic signalling in perception and attention (Moran et al., 2013). Their results fit with previous theoretical and empirical accounts, supporting that ACh boosts bottom-up signals in response to uncertainty (Yu and Dayan, 2002, 2003; Bentley et al., 2004).

Summarizing, there is a preponderance of theoretical and empirical evidence for indicating a computational role of ACh in promoting the influence of sensory evidence in perception and attention.

1.5. The sound of silence: omission responses

Although there is a wealth of data in support of predictive processing along the different sensory modalities (for a review see (Bendixen et al., 2012)), it is currently unknown how predictions are generated and what is the neural coding representation once a prediction has been formulated.

It has been argued that the *omission responses* would provide conclusive, empirical evidence of the predictive process, as it occurs in the absence of sensory input (Wacongne et al., 2011, 2012; Heilbron and Chait, 2018; Braga and Schönwiesner, 2022). The absence of a tone in an otherwise regular sequence of stimuli may activate a neuronal response. This activation is not caused by afferent sensory pathway but rather is reflective of an internal efferent expectation, built over the prior pattern of stimulation when a stimulus should occur.

Hence, predictions can be studied by examining the neuronal signature to the omission of an expected sound. This is important because it confirms that MMN is not simply a passive, bottom-up process that leads to synaptic adaptation to repeated stimuli due to a constant stimulation of the same afferent pathways (Parras et al., 2017; Casado-Román et al., 2020). Therefore, omission responses could be a crucial and underestimated tool for disentangling the underlying mechanisms of predictive processing, especially in animal models. Thus, since the neural activity evoked by the deviant stimulus reflects the

difference between a sensory input and the downstream prediction, the omission of an expected stimulus reflects the pure prediction signal (Bendixen et al., 2009; Den Ouden et al., 2009; Todorovic et al., 2011; Wacongne et al., 2011, 2012; Cornella et al., 2015; Schröger et al., 2015).

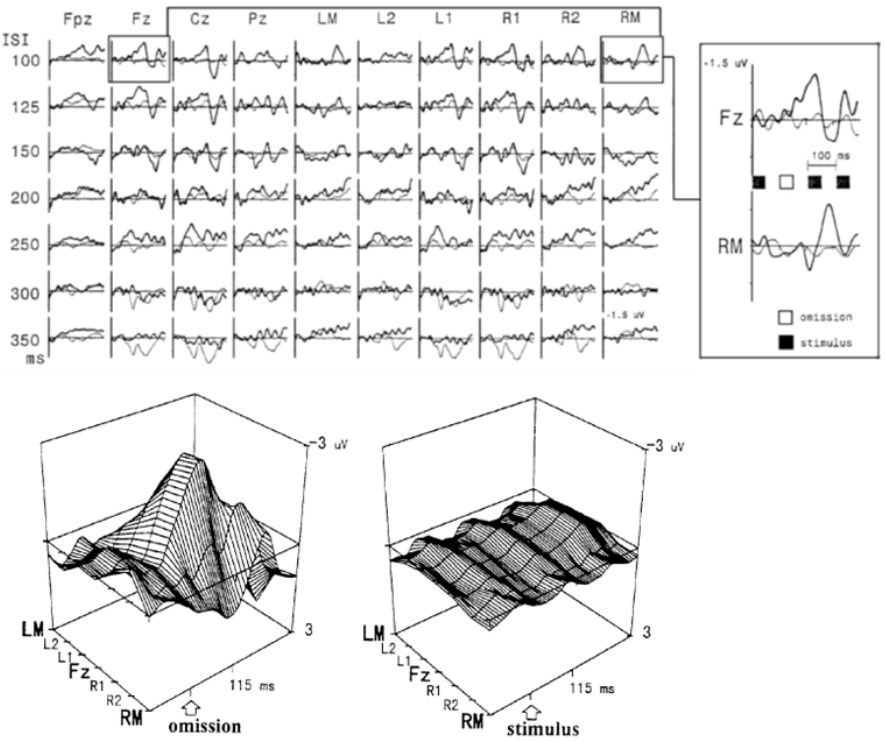

Figure 6. ERPs grand-average for omitted tones (thick line) and standard stimuli (thin line). *Stimulus onset asynchronies* (SOAs) varied from 100 to 350 ms. The response to the omitted tone peaks around 120 ms after the omission onset. Omission responses were found with the two shortest SOAs of 100 and 125 ms. Adapted from Yabe et al., 1997.

Omission responses have been shown in human studies (Fig. 6) where MMN is elicited by the omission of an expected auditory stimulus (Tervaniemi et al., 1994; Raij et al., 1997; Yabe et al., 1997; Horváth et al., 2010; May and Tiitinen, 2010; Wacongne et al., 2011, 2012; Heilbron and Chait, 2018; Fonken et al., 2019). More specifically unexpected omissions of predictable sounds usually evoke an early negative omission response (oN1) that peaks between 45 and 100 ms in the electroencephalography (EEG) which is related to the omission onset where the sound was expected (SanMiguel et al., 2013a, 2013b; Stekelenburg and Vroomen, 2015; van Laarhoven et al., 2020).

Studies investigating omission responses in the MMN have revealed intriguing findings. First, the neural mechanisms underlying omission responses appear to involve similar generatoss as those responsible for conventional MMN responses. These generators include the AC (Raij et al., 1997; Kraemer et al., 2005; Suda et al., 2022) and frontotemporal regions (Yabe et al., 1997; Suda et al., 2022), suggesting a shared neural substrate for the detection of both deviant stimuli and omissions.

Secondly, studies exploring omission responses have the potential to provide insights into disorders characterized by impaired auditory processing, such as schizophrenia (Kreitschmann-Andermahr et al., 1999; Kirino et al., 2019; Mori et al., 2021) and autism spectrum disorders (van Laarhoven et al., 2020) (Fig. 7). Despite its relevance, evidence of auditory omission responses at the neuronal level is still elusive.

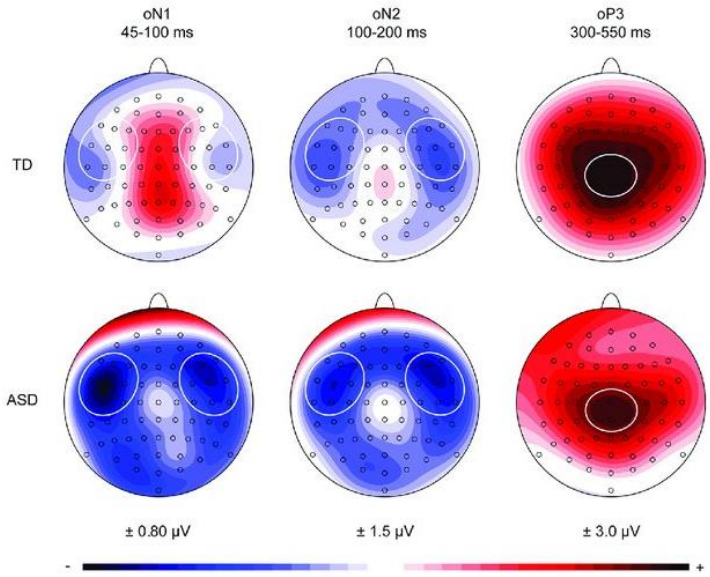

Figure 7. Scalp potential maps for typical development individuals (top row) and individual with autism spectrum disorder (bottom row) related to the omission of an expected stimulus after a visual trigger. Group-averaged and visual-corrected auditory omission responses in the denoted oN1 (45-100 ms), oN2 (100-200 ms), and oP3 (300-550 ms) time windows. Based on these scalp distributions, a left-temporal (F7, F5, F3, FT7, FC5, FC3, T7, C5, C3) and right-temporal (F4, F6, F8, FC4, FC6, FT8, C4, C6, T8) region of interest were selected for the oN1 and oN2 time windows. A central-parietal (C1, Cz, C2, CP1, CPz, CP2) region of interest was selected for the oP3 time window. oN1 for the ASD group was more pronounced compared to the oN1 for the TD group, while the oN2 and oP3 deflections appeared to be similar for both groups. Adapted from Laarhoven et al., 2020.

2. Hypothesis

Prediction has been described throughout the auditory pathway in support of the predictive coding hypothesis (Parras et al., 2017; Casado-Román et al., 2020). These studies recorded single-unit activity from the inferior colliculus (IC), medial geniculate, AC and prefrontal cortex. The oddball paradigm, and the no-repetition controls, were used to discriminate responses related to a prediction error from those due to adaptation effects. They reported not only that prediction errors are already present in subcortical regions, but also that prediction errors are hierarchically organized and increase as they are forwarded to temporal and prefrontal areas (Casado-Román et al., 2020). These studies demonstrate that prediction errors are a fundamental component of deviance detection in auditory single units.

Predictions errors are modulated by precision. One of the candidates for this modulation is ACh (Yu and Dayan, 2003, 2005). In 2015, Ayala and Malmierca reported that the application of this neuromodulator in the IC neurons reduced SSA by increasing the response to the repeated tone (Ayala and Malmierca, 2015a). However, the effect of ACh on nMM responses in AC neurons is still unknown.

Furthermore, previous studies have demonstrated that MMN can be elicited by the omission of deviant tones using the classical oddball paradigm (Rüsseler et al., 2001; Dercksen et al., 2020; Horváth et al., 2010 Bendixen et al., 2009)). In 1997, Yabe and colleagues studied the MMN elicited by the omission of an expected sound with constant stimulus onset asynchronies (SOAs). They showed a clear MMN response driven by the omitted tone only when the SOA was shorter than 150 ms, suggesting an estimation of the duration of the temporal integration window (Yabe et al., 1997).

At the neuronal level, omission responses have been measured in visual cortex (Fiser et al., 2016; Solomon et al., 2021) but currently, empirical data to support the predictive coding theory at the auditory single-neuron level in animal models is limited.

Considering the findings reported above, I propose the following hypothesis:

I. Cholinergic inputs mediate the precision of the prediction error by changing and adjusting precision in AC neurons.

II. A subset of neurons in the auditory pathway may be considered pure prediction error neurons because they are sensitive to the omission of an expected stimulus, i.e., neurons may respond even in the absence of a sensory input.

3. Objectives

Based on my hypothesis, I propose to study the following objectives:

I. Test whether cholinergic inputs affect prediction error signals in AC neurons.

II. Determine whether auditory neurons can signal the omission of an expected stimulus.

To answer the questions that originate from these objectives I have made two sets of complementary experiments:

I. Microiontophoretic injections of ACh in AC while neuronal activity is recorded under the oddball paradigm, and the cascade and the many standard paradigms, which are the non-repetition controls.

II. Recordings of single units in the IC and AC, under the oddball paradigm but with the deviant stimulus being omitted.

4. Summary of materials and methods and main results

4.1. Study I

4.1.1. Materials and methods

The experimental protocols were approved conforming to the University of Salamanca Animal Care Committee standards and the European Union (Directive 2010/63/EU) for the use of animals in neuroscience research. Experiments were performed on 37 adult female Long-Evans rats with body weights within 180-250 g. Surgical anaesthesia was induced and maintained with urethane (1.5 g/kg, intraperitoneal), with supplementary doses (0.5 g/kg, intraperitoneal) given as needed. Dexamethasone (0.25 mg/kg) and atropine sulfate (0.1 mg/kg) were administered at the beginning of the surgery to reduce brain edema and the viscosity of bronchial secretions, respectively. Normal hearing was verified with auditory brainstem responses (ABR) recorded with subcutaneous needle electrodes, using a RZ6 Multi I/O Processor (Tucker-Davis Technologies, TDT) and processed with BioSig software (TDT). ABR stimuli consisted of 100 μs clicks at a 21/s rate, delivered monaurally to the right ear in 10 dB steps, from 10 to 90 decibels of sound pressure level (dB SPL), using a closed-field speaker. After the animal reached a surgical plane of anaesthesia, the trachea was cannulated for artificial ventilation and a cisternal drain was introduced to prevent brain hernia and bran edema. Isotonic glucosaline solution was administered periodically (5–10 ml every 7 h, subcutaneous) throughout the experiment to prevent dehydration. Body temperature was monitored with a rectal probe thermometer and maintained between 37 and 38°C with a homoeothermic blanket system.

The AC surgery was performed as described in previous works carried out in our laboratory (Nieto-Diego and Malmierca, 2016; Parras et al., 2017). The temporal bone was exposed and the AC was located using stereotactic coordinates (Paxinos et al., 1997). A craniotomy was performed over the AC, the dura was removed carefully, and the exposed area was filled with a layer of agar to prevent desiccation and to stabilize the recordings. Before applying the agar, a magnified picture (25×) of the exposed cortex was taken with a digital camera coupled to the surgical microscope (Zeiss) through a lens adapter (TTI Medical). The picture included a pair of reference points previously marked on the dorsal ridge of the temporal bone, indicating the absolute scale and position of the image with respect to bregma (the reference point). This picture was displayed on a

computer screen and was overlapped with a micrometric grid, over which the placement of the multibarrel for every recording was marked. The micrometric grid allowed to generate coordinates in a two-dimensional axis, from the superimposed image of the AC of each animal. Once the coordinates of each of the recorded units of all the animals were obtained, I used the functions 'griddata' and 'contourf' of MATLAB to generate topographic maps (through a graduation of colors) of the characteristic frequency (CF), Common SSA Index (CSI) levels (see index formula in section 5.1.1.2.), and deviant and standard tone responses in all auditory cortical fields.

4.1.1.1. Electrophysiological recording and microiontophoresis injection of Acetylcholine (ACh)

A tungsten electrode (1–3 MΩ) was used to record multiunit neuronal activity. This tungsten was attached to a 5-barrel multibarrel borosilicate glass pipette that carried drug solution to be delivered in the vicinity of the recorded neuron. The multibarrel's tip was cut to a diameter of about 20-30 μm approximately. The center barrel was filled with saline solution for current compensation (165 mM NaCl) whereas the other barrels were filled with 1 M acetylcholine chloride (Sigma, catalog no. A6625). The pH was adjusted between 4.0-4.2 (Ayala and Malmierca, 2015b). The drug was retained by applying a -15 nA current, and were ejected when required, typically using 30–40 nA currents (Neurophore BH-2 System, Harvard Apparatus). The duration of the drug ejection usually lasted 8–10 min and the recording protocols were extended until the effect of the drug had disappeared (60 to 90 minutes approx.). The multibarrel assembly was positioned over the pial surface of the AC, forming a 30° angle with the horizontal plane towards the rostral direction, and advanced using a piezoelectric micromanipulator (Sensapex) until I observed a strong spiking activity synchronized with the train of search stimuli. Analog signals were digitalized with a RZ6 Multi I/O Processor, a RA16PA Medusa Preamplifier and a ZC16 headstage (TDT) at 12 kHz sampling rate and amplified 251x. Neurophysiological signals for multiunit activity were band-pass filtered between 0.5 and 4.5 kHz.

4.1.1.2. Experimental Design and stimulation paradigms

Sound stimuli were generated using the RZ6 Multi I/O Processor (TDT) and custom software programmed with the OpenEx Suite (TDT) and MATLAB. Sounds were

presented monaurally through a speaker, in a close-field condition to the ear contralateral to the left AC. The speaker was calibrateed to ensure a flat spectrum up to ~75 dB SPL between 0.5 and 44 kHz; the second and third harmonics were at least 40 dB lower than the fundamental at the loudest output level for all the frequencies. The experimental stimuli were pure tones in the range 0.5–44 kHz, with a duration of 75 ms, including 5 ms rise/fall ramps presented at a rate of 4 stimuli/s. Once a suitable neuron was found, the frequency response area (FRA) of the cell, i.e. the combination of frequencies and intensities capable of evoking a suprathreshold response, was obtained automatically using a randomized paradigm that presented tones between 0.5-44 kHz in 25 logarithmic steps, with intensities spaced by 10 dB steps, from 0 to 70 dB SPL, at a repetition rate of 4/s. Based on this information, I selected a pair of frequencies evoking similar responses at 10–30 dB above threshold. I used pure tones at these frequencies as the stimuli in the oddball paradigm. Oddball sequences consisted of frequently repeating stimuli (standard tones) which were pseudo-randomly interleaved with rare events (deviant tones). Two oddball sequences with fixed parameters (400 trials each, 75 ms stimulus duration, 0.5 octaves frequency separation, 10% deviant probability, 250 ms onset to onset, and a minimum of three standard tones before a deviant) were presented for every pair of stimuli thus selected. In one of the sequences, the low frequency (*f1*) was the "standard" and the high frequency (*f2*) was the "deviant," and in the other sequence their roles were inverted. The order of presentation of these two sequences was randomized across sites. In some cases, one or more extra pairs of stimuli were selected, and the oddball sequences were repeated with the new stimuli. According to the predictive coding framework, mismatch responses like those obtained during an oddball paradigm can be divided in two components: repetition suppression (RS), a reduction in the response caused by a repeated stimulus, and prediction error (PE), an increased response caused by the violation of a regularity (Parras et al., 2017; Carbajal and Malmierca, 2018).

For this, in a subset of the experiments, I used control sequences to evaluate the separate contribution of RS and PE. Control sequences consisted of 10 tones evenly spaced by 0.5 octaves (same as in the oddball sequences), including the tones used in the oddball paradigm, and all stimuli at the same previously chosen sound level. Each control sequence lasted 400 trials, the duration of all stimuli was 75 ms and the presentation rate 4/s. I used two different control sequences, namely the many-standards and cascade sequences. The many-standards control is the consecutive presentation of blocks of 10

tones randomly ordered within the block, each tone with a 10% probability of occurrence (Schröger and Wolff, 1996). In this sequence the tones are unpredictable, and it is not possible to establish a rule which could be used to predict the following tones. On the other hand, the cascade control consists of the regular presentation of the same 10 tones in ascending or descending frequency succession (Ruhnau et al., 2012). This sequence also avoids the effects of the repetition of a single stimulus, but in this case, it maintains a predictable context. Cascade sequences are considered a more rigorous control than many-standard sequences because like the oddball sequence, a regularity is established (Carbajal and Malmierca, 2018).

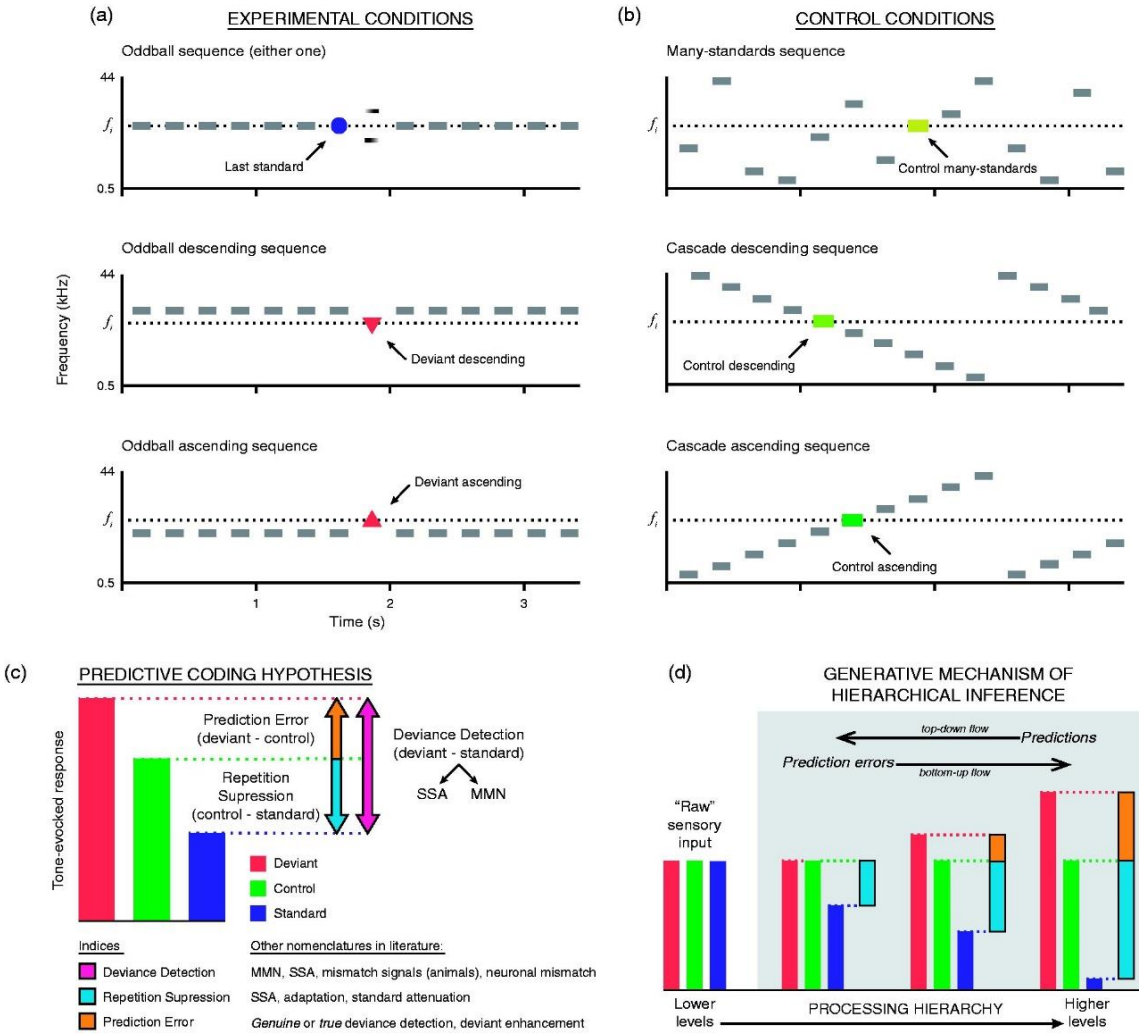

Figure 8. a. Classical oddball paradigm, displaying three possible experimental conditions for a given *f* target tone. **b.** Control sequences highlighting the *f* target tone. In the many-standards sequence, the target tone

is embedded within a random succession of assorted equiprobable tones, making impossible for the system to establish a predictive rule. The two versions of the cascade sequence (descending and ascending) are compared with the corresponding version of the oddball sequence. In both versions, the target tone is embedded in a predictable succession of equiprobable tones, allowing the system to establish a predictive rule that is not broken by the appearance of the target tone, as opposed to what happens in the oddball sequence. **c.** Decomposition of deviance detection signals (deviant–standard) according to the interpretation of the predictive coding hypothesis. The difference between the response to the target tone in the control sequence and its evoked response when presented as a standard in the oddball sequence would constitute the component of repetition suppression. On the other hand, the difference between the deviant-evoked response and the response to that target tone within a control sequence, if positive, would unveil a component of prediction error. **d.** Hierarchical processing scheme. Adapted from Carbajal and Malmierca, 2018.

Here I describe the analysis performed using the cascade condition as control (CTR). Baseline-corrected spike count responses of a neuron to the same tone in the three conditions (DEV, STD, CTR) were normalized using the following formulas:

$$N = (DEV^2 + STD^2 + CTR^2)^{1/2}$$

$$DEV_{Normalized} = DEV/N$$

$$STD_{Normalized} = STD/N$$

$$CTR_{Normalized} = CTR/N$$

These indices, consequently, always range between −1 and 1, and provide the following quantitative decomposition of nMM (Fig. 8) into repetition suppression and prediction error:

$$iMM = DEV_{Normalized} - STD_{Normalized}$$

$$iRS = CTR_{Normalized} - STD_{Normalized}$$

$$iPE = DEV_{Normalized} - CTR_{Normalized}$$

$$iMM = iRS + iPE$$

The iMM index is largely equivalent to the typical SSA index: SI or specificity index, commonly used in most previous studies of SSA in single units (Fishman and Steinschneider, 2012):

$$\mathrm{SI} = \frac{DEV(f1) - STD(f1)}{DEV(f1) + STD(f1)}$$

Another index related to SSA is CSI or Common SSA index, which considers the two frequencies used to perform the oddball paradigm:

$$\mathrm{CSI} = \frac{DEV(f1) + DEV(f2) - STD(f1) - STD(f2)}{DEV(f1) + DEV(f2) + STD(f1) + STD(f2)}$$

4.1.2. Main results

I studied the influence of cholinergic modulation on CSI and prediction error in AC neurons. For this purpose, I recorded a total of 113 neurons before, during and after the microiontophoretic injection of ACh. Recordings were performed in all the subdivisions of the AC: primary auditory field (A1), anterior auditory field (AAF), ventral auditory field (VAF), posterior auditory field (PAF) and suprarhinal auditory field (SRAF), and the recording depths ranged 120–1191 μm including neurons from all layers in urethane-anaesthetized rats.

In order to allocate each recorded neuron to a specific field in the AC, I recorded the frequency-response area (FRA) and analysed the topographical distribution of the characteristic frequency (CF) for each unit. Each recording was assigned to a dorsoventral and rostrocaudal coordinate system relative to bregma following previous studies (Polley et al., 2007; Nieto-Diego and Malmierca, 2016; Parras et al., 2017). This analysis allowed us to pool the data from all animals (Fig. 9a) and construct a synthetic map of the CF across the entire rat AC (Fig. 9). Similar to these previous works, I found a high-frequency reversal zone between VAF (caudally) and AAF (rostrally), a low-frequency reversal zone between A1 and PAF (dorsocaudally), and a high-frequency reversal between VAF and

SRAF (ventrally). Thus, I could reliably define the lemniscal (A1, AAF, and VAF) and non-lemniscal (SRAF, PAF) auditory cortical fields (Fig. 9).

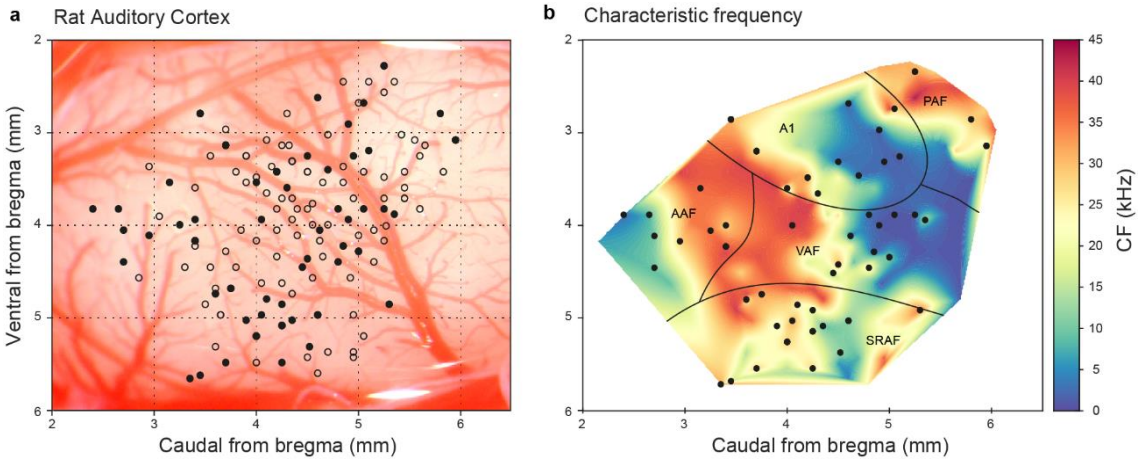

Figure 9. Map of all recording locations. **a.** All recording sites drawn over the cortex of a representative animal. At every site, the CF was determined and then I presented an oddball paradigm and the corresponding control sequences. Empty dots indicate sites used only for CF determination. Filled dots indicate sites where oddball paradigm was recorded. **b.** Distribution of the CFs across the entire rat AC. Note how each field shows a characteristic CF gradient. Filled dots indicate sites where oddball paradigm was recorded.

4.1.2.1. ACh modulates the magnitude of the nMM

Two neurons of the lemniscal subdivision shown in Figure 10 illustrates representative FRAs that reflects the modulation of the CSI during ACh release (Fig. 10a, b; decreased and increased CSI respectively). The neurons of the non-lemniscal subdivision (Fig. 11) also present a decreased or increased CSI during ACh application (Fig. 11a, b; respectively). In both, peri-stimulus time histograms (PSTH) are also depicted for standard and deviant (blue and red lines respectively lines). Most neurons recovered their basal firing rates after 60-90 minutes post ACh injection (recovery mean: 6.5 ± 8.1 spikes/stimulus). After the visualization of the FRA, I selected a pair of pure tones within this area (10–30 dB above minimum threshold) at each recording site to test the adaptation sensitivity of the neuronal response under the oddball paradigm, to study CSI. To analyse the effect of ACh on CSI, I recorded the neuronal responses under an auditory oddball paradigm. With this aim, I previously checked that our sample neurons responded to both selected frequencies in the oddball paradigm.

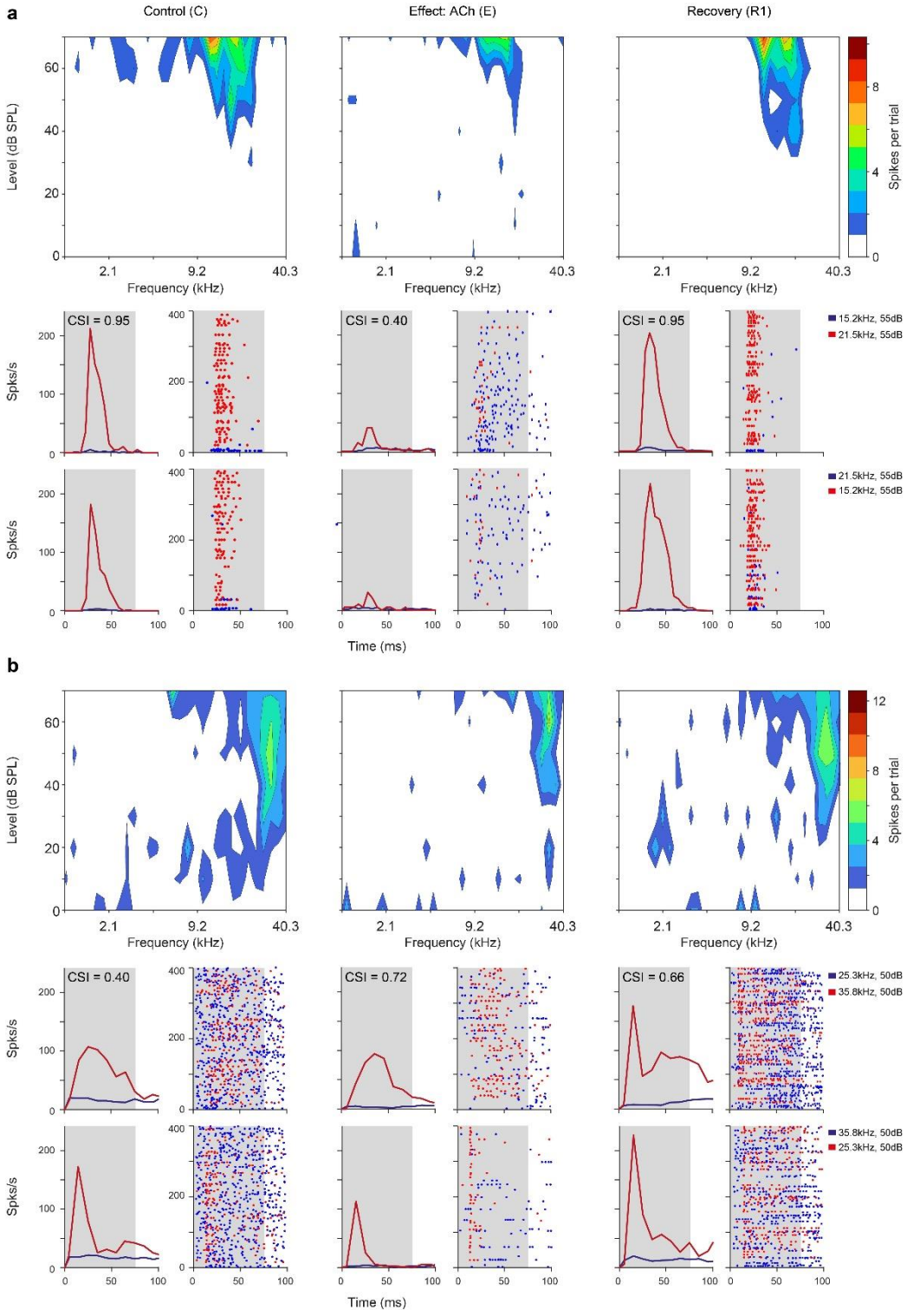

Figure 10. Lemniscal AC units modulated by ACh. Left, middle and right columns show the responses before (control), during (effect) and after (recovery) ACh application, respectively. **a.** FRAs and PSTHs from a unit located in A1. This specific neuron shows a CSI decrease during ACh application and recovery to baseline levels (CSI = 0.95, CSI= 0.4 and CSI = 0.95, respectively) **b**. FRAs and PSTHs from an AAF unit with increased CSI (CSI = 0.4, CSI= 0.72 and CSI = 0.66, respectively) during ACh application.

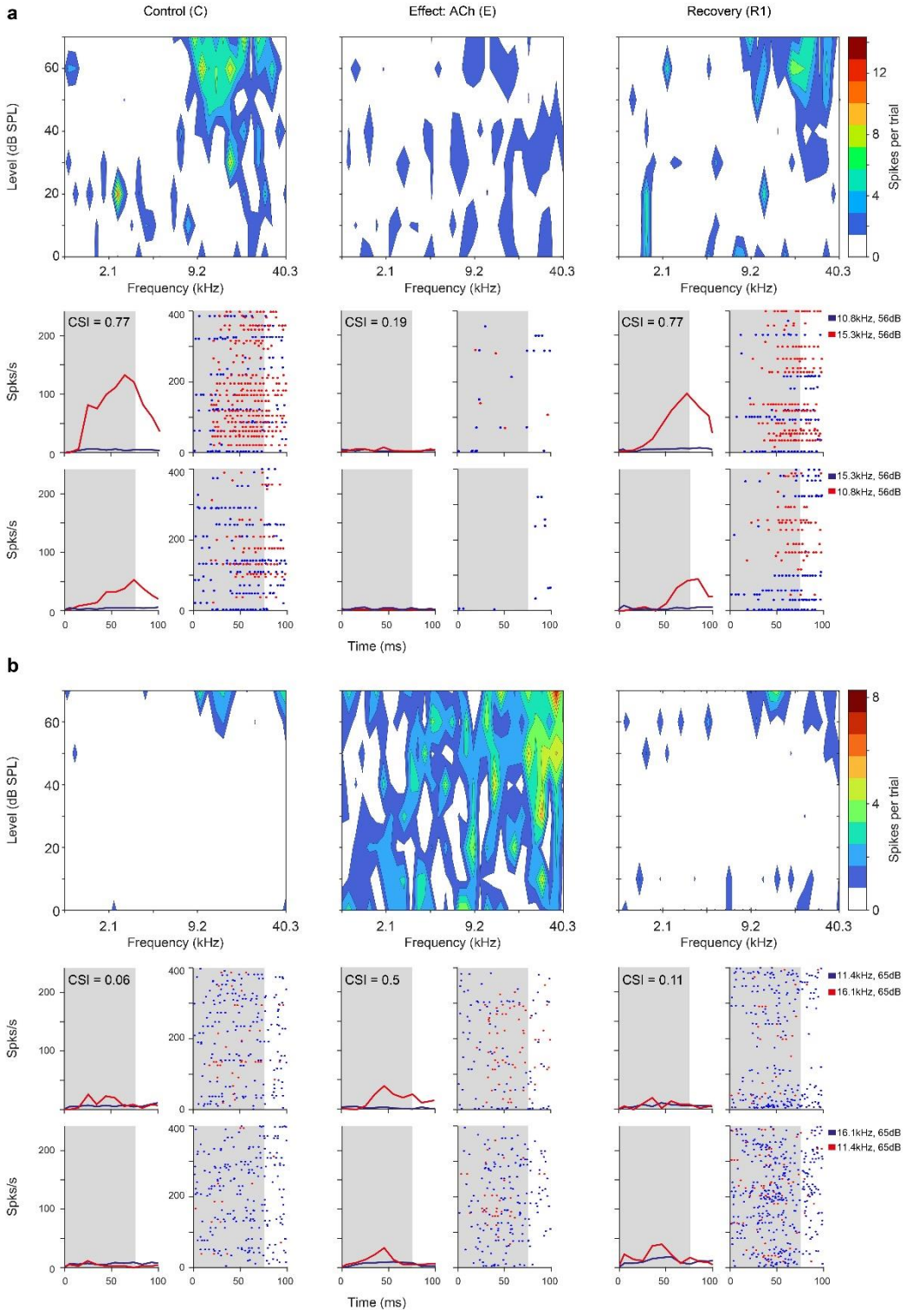

Figure 11. Non-lemniscal AC units modulated by ACh. Left, middle and right columns show the responses before (control), during (effect) and after (recovery) ACh application, respectively. **a.** FRAs and PSTHs from a unit located in SRAF. This specific neuron shows a CSI decrease during ACh application and recovery to baseline levels (CSI = 0.78, CSI= 0.19 and CSI = 0.77, respectively). **b.** FRAs and PSTHs from a PAF unit with increased CSI (CSI = 0.06, CSI= 0.5 and CSI = 0.11, respectively) during ACh application.

Next, I computed the CSI in 85 neurons with significant responses to both *f1* and *f2* auditory stimuli. Modulation of CSI levels is observed in all individual examples. ACh produced a significant increase of the CSI value in 25.9% of the recorded neurons (Fig. 12a, purple dots; 22/85, bootstrapping, 95% c.i.). Thirty-seven units (43.5%) were unaffected by ACh (gray dots) and 26 (30.6%) showed a significant decrease of their CSI (orange dots). The average CSI during ACh injection (CSI = 0.54 ± 0.27) was similar to that of the control condition (CSI = 0.57 ± 0.23; Wilcoxon Signed Rank test, p=0.359; Fig. 12b). After that, I analysed the effect of ACh on the response to the deviant- or standard stimuli separately. Results show that ACh produced a significant decrease in the mean firing rate in response to the deviant tones (11.75 ±17.46 Hz), as compared to the control condition (16.51 ±16.19 Hz; Wilcoxon Signed Rank test, $p < 0.001$). This effect was also observed in the mean firing rate in response to standard tones (4.58 ±6.38 vs 3.97 ±9.90 Hz, control vs ACh; Wilcoxon Signed Rank test, $p = 0.001$) (Fig. 12c).

In order to better understand how ACh affects discriminability of deviant- and standard stimuli, I calculated the area under the curve (AUC) of the receiver operating characteristic (ROC) for each tone (Fig. 12d, left panel). The mean AUC decreased significantly during the application of ACh (0.74 ±0.13 vs 0.67 ±0.15, control vs. effect; Wilcoxon Signed Rank test, $p < 0.001$). The same happened for the mutual information (Fig. 12d, right panel; 0.09 ±0.07 vs 0.07 ±0.08, control vs. effect; Wilcoxon Signed Rank test, $p = 0.003$).

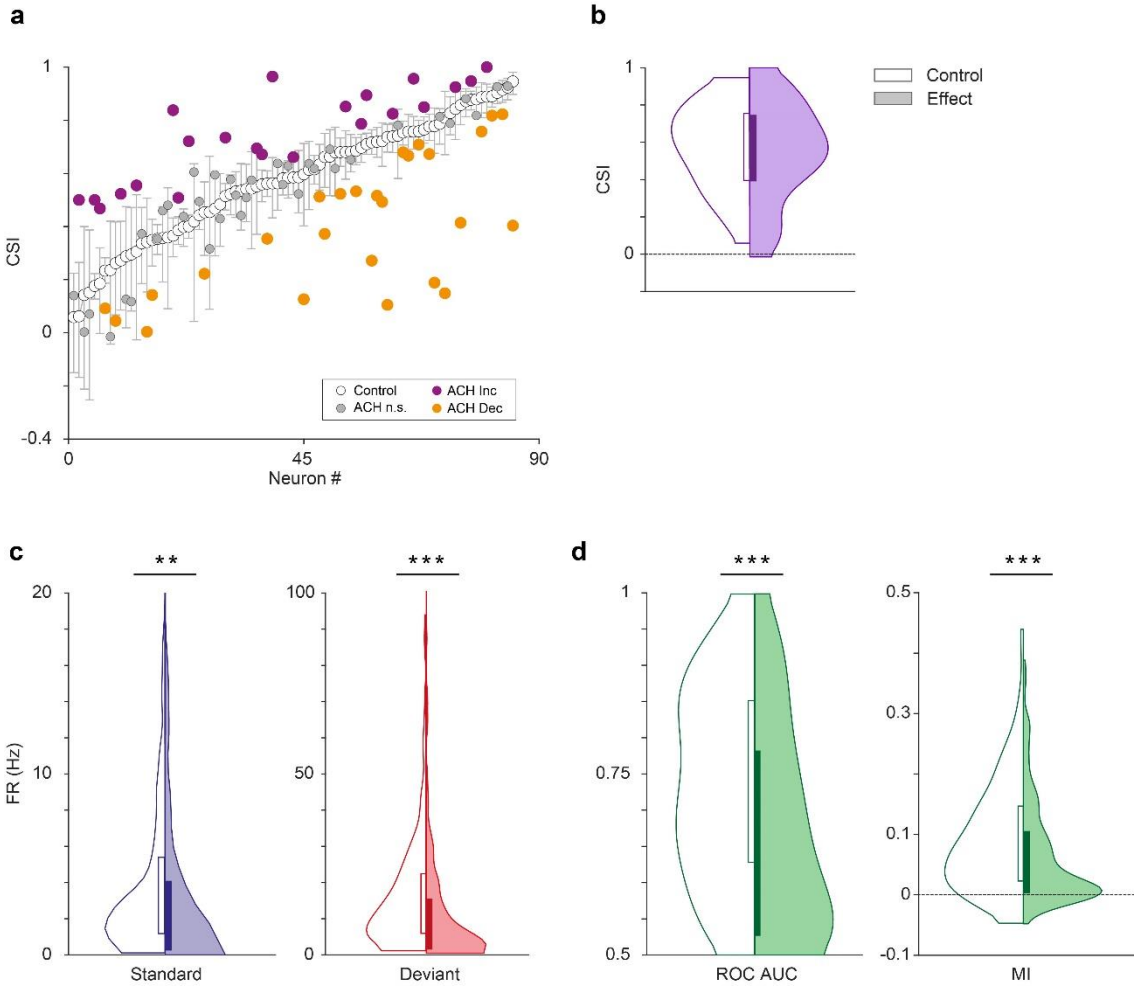

Figure 12. Effect of acetylcholine on CSI. **a.** Changes on the CSI due to the effect of ACh, for each recorded unit. The units are sorted based on their CSI in the control condition (white dots). The vertical bars indicate the 95% confidence interval for the CSI in the control condition. **b.** Violin plots showing the CSI measured in control and effect conditions. The CSI did not change significantly during the application of ACH. In this and similar violin plots, white background indicates the control conditions, while shaded background indicates the effect condition. **c.** Distribution of firing rates in response to the deviant (red) and standard tones (blue), in control and ACh conditions. The application of ACh caused a significant reduction in the response to both deviant and standard tones. **d.** Distribution of AUC and Mutual Information values in control and ACh conditions. The application of ACh caused a significant decrease of both AC and Mutual Information. In this and similar figures: *p<0.05; **p<0.01; ***p<0.001.

4.1.2.2. ACh effect on nMM as a function of topographic distribution.

Another aspect of interest is whether the effect of ACh show a homogeneous distribution across AC neurons in different fields and layers. Figure 13 shows the CSI (first row) and spike count levels for the standard and deviant tones (middle and bottom rows, respectively) before and after ACh application, as well as the difference between the ACh and control conditions. ACh application produced an overall increment of CSI in AAF and a decrement in the rest of the fields. However, these changes were not significant ($p > 0.79$ in all fields, Wilcoxon signed rank test with Holm-Bonferroni correction). Looking at the response to the standard, ACh application caused a firing rate increase in A1 and PAF, and a decrease in AAF, VAF and SRAF, but such changes were only significant in AAF ($p=0.001$, Wilcoxon signed rank test with Holm-Bonferroni correction). By contrast, the firing rates in response to the deviant decreased in all fields during ACh application, with significant changes in AAF, VAF and SRAF ($p=0.011$, $p=0.026$ and $p=0.009$, respectively; Wilcoxon signed rank test with Holm-Bonferroni correction).

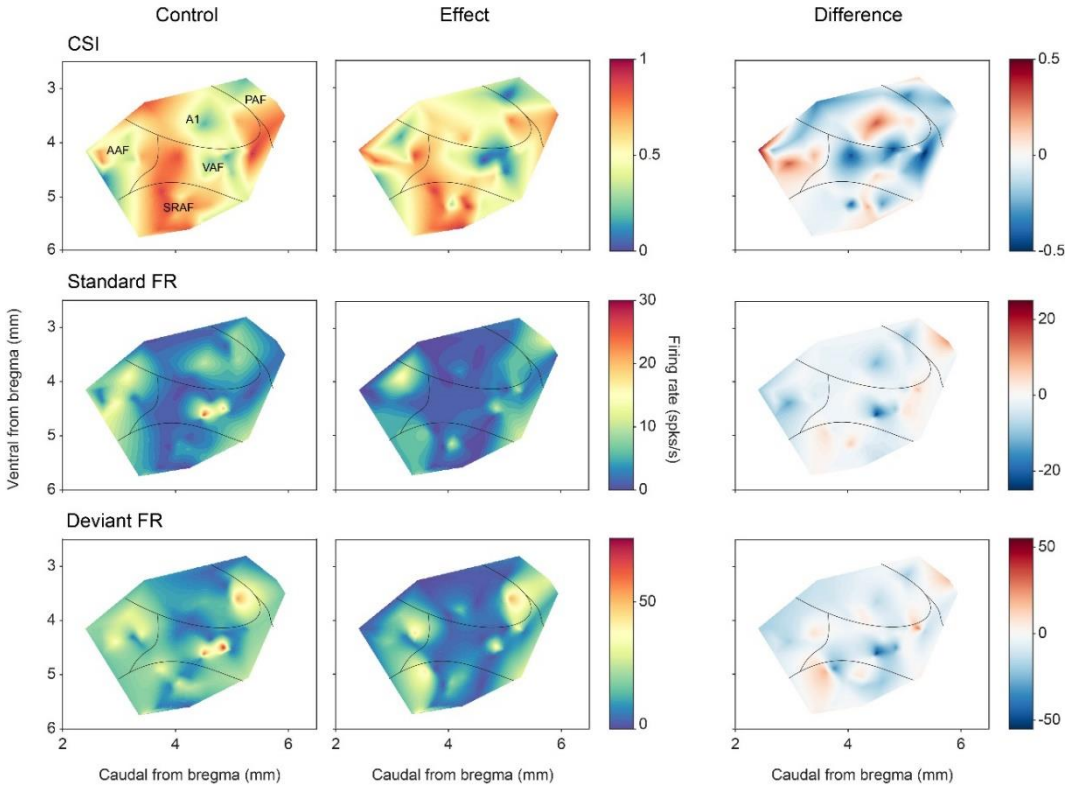

Figure 13. Anatomical localization of CSI and responses to the deviant and standard tones. Distribution of CSI (top row) and responses (spikes per trial) for deviant (bottom row) and standard tones (middle row), before and after ACh application, as well as the difference between both conditions.

With the aim to better understand how ACh affected the responses to the individual frequencies of the oddball paradigm (*f1* and *f2*). I calculated SI index independently for each of these frequencies (Fig. 14). The results showed that ACh was more likely to cause a decrement on SI in all AC fields except in AAF, were SI increased (Fig. 14a). I also looked at the effect of ACh along AC layers. The analysis showed that units experiencing a SI decrease are more prevalent around the granular layer (layer IV), while units experiencing a SI increase, are more commonly found in the infragranular layers (Fig. 14b).

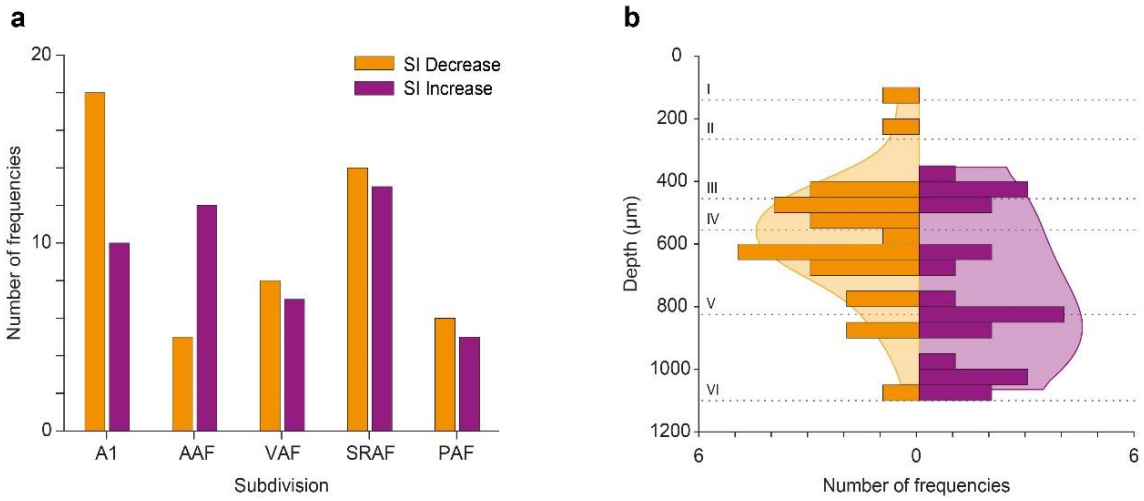

Figure 14. Effect of ACh on SI in AC fields and layers. **a.** Mean CSI (and standard deviation) in the different AC fields, before (white bars) and during the application of ACh (shaded bars). CSI changes are not significant in any of the fields. **b.** Distribution of units in which SI decreased (orange) or increased (purple) significantly due to the effect of ACh, across AC layers. The shaded background depicts the probability density functions. Note that units experiencing SI decrease are more prevalent around the granular layer (layer IV), while units experiencing SI increase, are more commonly found in the infragranular layers.

4.1.2.3. Different mechanisms for SI increase or decrease during ACh application

Next, I calculated the SI for 205 individual frequencies, from 113 units, that elicited a significant response from the whole AC sample. ACh produced a significant increase of

the SI value in 27% of the frequencies recorded (Fig. 15a, purple dots; 55/205, bootstrapping, 95% c.i.), 31% (64/205; Fig. 15a, orange dots) showed a significant decrease of their SI and 42% frequencies (86/205) were unaffected by ACh. The mean SI (SI = 0.55 ± 0.31, control condition) was reduced during ACh injection (SI = 0.40 ± 0.50) although not significantly (Wilcoxon Signed Rank test, p=0.086; Fig. 15b).

Afterwards, I looked at the firing rates in response to deviant- and standard stimuli, separately for those frequencies. In both cases, responses to deviant- and standard sounds were affected differently, when measuring the firing rate change ratio (amount of change caused by ACh, relative to the baseline-firing rate). In frequencies showing a SI decrease, the effect of ACh was significantly different for deviant- and standard stimuli (Fig. 15c, top panel; $p<0.001$, Wilcoxon signed rank test). Furthermore, this ratio was clearly negative for deviant responses ($p<0.001$, Wilcoxon signed rank test) and not significant for standard responses (p=0.256, Wilcoxon signed rank test), indicating that ACh caused a reduction of the firing rate exclusively during deviant stimuli. On the other hand, in frequencies showing an increased SI, the effect of ACh also had a different effect on deviant and standards (Fig. 15d, top panel; $p<0.001$, Wilcoxon signed rank test), but in this case the effects were opposite: the change ratio was clearly negative for standard sounds (p=0.001, Wilcoxon signed rank test) and not significant for deviant ones (p=0.379, Wilcoxon signed rank test), so now ACh caused a reduction of the firing rate solely during standard stimuli. In other words, while the main effect of ACh was a reduction of the firing rates, in some frequencies it only affected responses to the deviant stimuli, thus decreasing SI (Fig 15c, top panel), while in others it only affected responses to the standard stimuli, resulting in an increment of the SI (Fig 15d, top panel).

Interestingly, ACh affected stimuli discriminability differently in both groups. In frequencies showing SI decrease (Fig. 15c, bottom panel) both ROC AUC and mutual information decreased significantly during ACh application ($p<0.001$in both cases, Wilcoxon signed rank test), in line with the results obtained for the whole sample (compare to Fig. 12d). However, in frequencies showing SI increase (Fig. 15d, bottom panel) ROC AUC did not change significantly (p= 0.339), while mutual information increased slightly (p= 0.008). These results suggest that frequencies showing SI decrease are the ones mediating the main effects of ACh in the population.

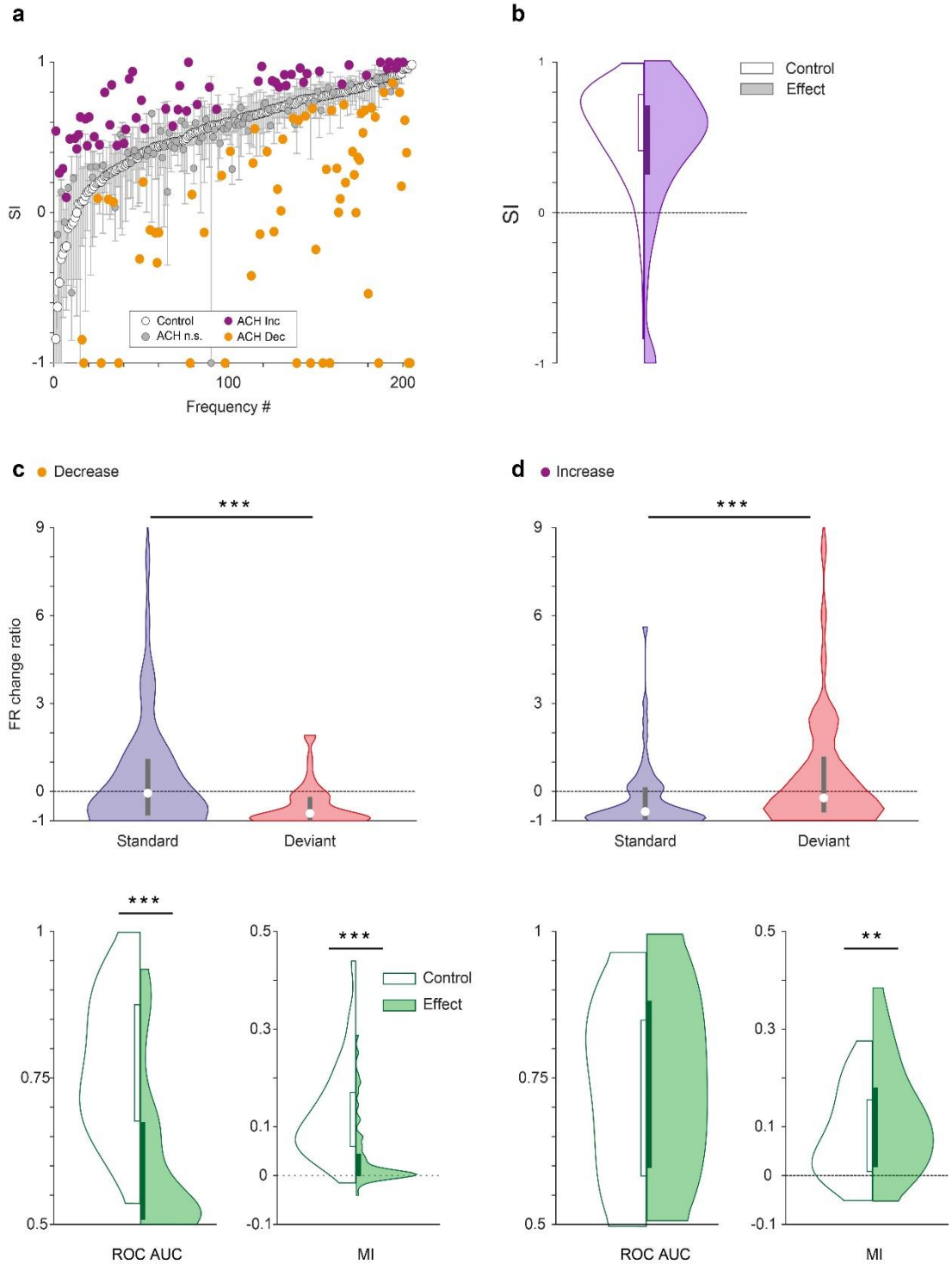

Figure 15. Characteristics of units depending on the effect of ACh on SI. **a.** Changes on the SI due to the effect of ACh for each tested tone. The units are sorted based on their SI in the control condition (white dots). The vertical bars indicate the 95% confidence interval for the SI in the control condition. **b.** Violin plot depicting the overall effect of ACh on the SI, for the complete sample. **c.** Firing rate change ratio due

to ACh application, relative to the control condition. In units showing SI decrease (left column), it was caused by a significant reduction of the firing rate in response to deviant tones. By contrast, in units showing SI increase (right column) it was caused by a significant reduction of the firing rate in response to standard tones. d. In units showing SI decrease (left column) there was a significant reduction of both AUC and Mutual Information.

4.1.2.4. Precision of the prediction error

Under the predictive coding framework, the precision (inverse of variance) of prediction errors would encode the certainty of such errors (Friston, 2008), increasing the weight of highly precise errors. Then, as a deeper analysis, I calculated the inverse of the variance of the iPE distributions as an estimate of precision of the prediction error (Fig. 16e, f). For this, I used a 1000-sample bootstrap strategy in order to obtain distributions of the prediction error precision in each condition, showing that the PE precision decreased during the application of ACh both in units with decreased or increased SI. This analysis revealed that ACh application reduced the prediction error precision for decreased and increased SI neurons (14.29 ±3.18 vs 7.63 ±2.01, control vs. effect; Fig. 16e; and 8.50 ±2.66 vs 5.99 ±1.61; $p<0.001$; Fig. 16f; Wilcoxon Signed Rank test; respectively). Notably, ACh caused a convergence on the precision of both groups, making precision distributions more similar.

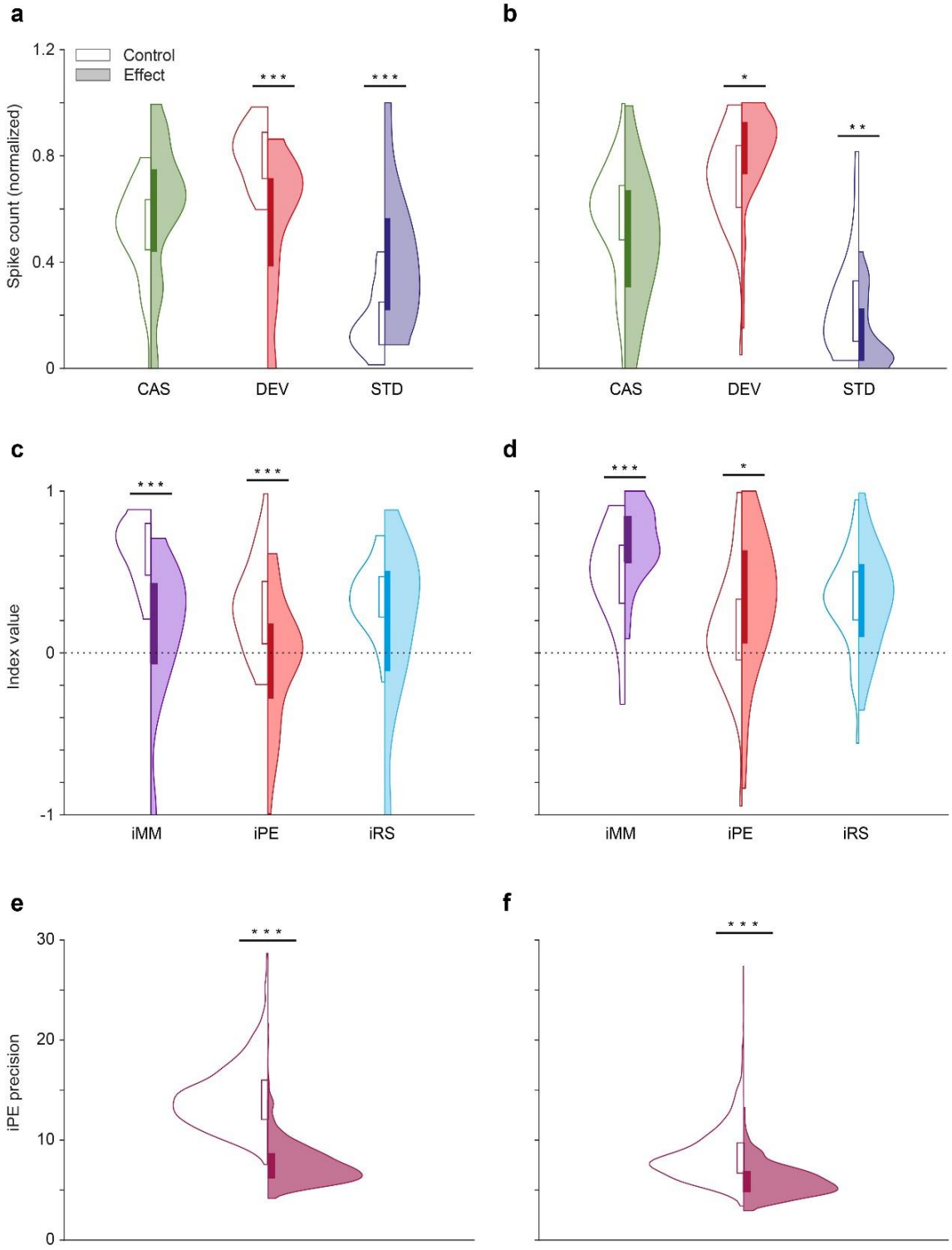

Figure 16. Predictive coding indices depending on the effect of ACh on SI. The application of ACh decreased the normalized spike counts in response to deviant stimuli (red) and increased the normalized spike counts in response to standard stimuli (blue) in those units where SI decreased due to the application of ACh (**a**), while the changes were opposite in those units where SI increased due to the application of ACh (**b**). In neither case, the response to the cascade condition (green) changed significantly, but there was a slight trend in the

same direction as the changes of the standards. In consequence, the neuronal mismatch index (iMM, purple) and prediction error indexes (iPE, light red) decreased significantly in those units where SI decreased due to the application of ACh (**c**) but increased in those units where SI increased due to the application of ACh (**d**). The repetition suppression index (iRS) in light blue, did not change significantly in any case. The PE precision decreased during the application of ACh both in units with SI decrement (**e**) or increment (**f**).

4.2. Study II

4.2.1. Materials and Methods

4.2.1.1. Experimental procedures

Experiments were performed on 22 anaesthetized adult female Long-Evans rats (9 rats were used for IC recordings and 13 rats for AC recordings) and 6 C57/B6 mice (3 awake, 3 under urethane anaesthesia). Awake mice experiments were performed in collaboration with the Computational Neuroscience Laboratory of Bernhard Englizt. The body weight ranged from 200–300 grams in rats (9 to 17 weeks of age) and 25–35 g in mice (14-18 weeks of age). Each individual animal was used to record a single auditory station, either IC or AC. Experimental procedures in anaesthetized rats were carried out at the University of Salamanca and all the experimental procedures and protocols were adjusted to the directives of the Directive of the European Communities (86/609/CEE, 2003/65/CE and 2010/63/UE) and RD53/2013 Spanish Legislation for the use and care of animals. All the details of the study were approved by the Bioethics Committee of the University of Salamanca (USAL-ID-195). Experiments in awake mice were performed at the Central Dierenlaboratorium at the Radboud University Medical Center. The experimental procedures and protocols were approved by the Dutch central commission for animal research (Centrale Commissie Dierproeven) and implemented according to approved work protocols from the local animal welfare body (project number 2017-0041).

4.2.1.1.1. Experimental and surgical procedures in anaesthetized rats (IC and AC)

The experiments were carried out inside a chamber with acoustic insulation and electrical protection. Sound stimuli were generated using the RZ6 Multi I/O processor (Tucker-Davis Technologies, TDT). Sounds were presented monaurally (right ear) through a closed system using a custom-made earphone (1–45 kHz) coupled to a custom-made cone, as a substitute for traditional ear bars. Thus, sounds were presented through the speaker in a closed field condition to the ear contralateral to the left IC or AC. The software was programmed with OpenEx Suite (TDT) and MATLAB. The sound system response was flattened with an on-site calibrated finite impulse response system using a ¼-inch condenser microphone (Model 4136, Brüel & Kjaer), a conditioning amplifier (Nexus, Brüel & Kjaer), and a dynamic signal analyzer (Photon+, Brüel and Kjaer). The

speaker output was adjusted to ensure a flat spectrum (±2 dB) between 0.5 and 44 kHz, and the second and third harmonic components in the signal were >40 dB below the level of the fundamental at the highest output level (~76 dB SPL). A single neuron was recorded at a time, using a self-made glass-coated tungsten electrode whose impedance ranged from 1.5 to 3 MΩ at 1 kHz. Analog signals were digitized with an RZ6 multi-I/O processor, Medusa RA16PA preamp, and ZC16 main stage (TDT) at 25 kHz sample rate and amplified 251x. The neurophysiological signals for multi- or single-unit activity were bandpass filtered between 0.5 and 4.5 kHz.

The initial surgical procedures were the same for the two auditory areas to be recorded (IC and AC). Electrophysiological procedures differed only in craniotomy location and recording electrode placement for each station. Anaesthesia was induced and maintained with urethane (1.9 g/kg, intraperitoneal) with supplementary doses (~0.5 g/ kg, i.p.) administered as necessary. These replenishments were given to ensure a deep and stable anaesthetic level whenever corneal or pedal retraction reflexes appeared. Urethane maintains a balanced neuronal activity better than other anaesthetic agents that have a slight effect on inhibitory and excitatory synapses and that is why it was the selected anaesthesia method (Hara and Harris, 2002).

At the beginning of surgery, both dexamethasone (0.25 mg/kg) and atropine (0.1 mg/kg) were administered to reduce cerebral oedema and bronchial secretions, respectively. Lidocaine was also injected around the pinna tissue to achieve a higher anaesthetic level in these areas. In addition, an isotonic glucosaline solution (5–10 ml every 6–8 h, s.c.) was periodically administered to avoid dehydration. During all the experimental procedures, the animals were artificially ventilated controlling the CO_2 levels and the temperature was monitored with a rectal probe (36–38 °C) and maintained with a heating blanket (Cibertec) placed under the animal.

Once the animal reached a surgical state of anaesthesia, the ears were prepared by removing the cartilage to obtain a greater exposure of the ear canal. The trachea was cannulated to maintain ventilation artificially, and corneal and pedal withdrawal reflexes were constantly monitored to ensure that I maintained a deep anaesthetic level during surgery and as uniform as possible throughout the recording procedure. Once the animal was prepared, it was placed on the stereotactic frame, the upper jaw was attached to a bite

bar and the restraint was carried out using ear bars. At this time, the speaker was also placed on the right ear of the animal, while the left ear canal was covered with plasticine.

For IC recordings, a craniotomy was performed on the left parietal bone to expose the cerebral cortex overlying the left IC. The dura was removed and the surrounding tissue was covered with cotton balls soaked in 0.9 % saline solution to maintain hydration of the area. An electrode was placed orthogonal to the surface of the brain (forming an angle of 20° with the horizontal plane, oriented caudally), and advanced between 7500–10000 μm from lambda to bregma and 500–3000 μm to the left ear. Then, it was lowered into the brain between 4400–5600 μm using a piezoelectric micromanipulator (Sensapex) until I observed strong spike activity synchronized with the search stimulus train.

For AC recordings, the skin and temporal muscles were removed from the left side of the skull and a 6x5 mm craniotomy was performed on the left temporal bone to expose the entire AC. The dura was removed and the cisterna magna was drained to prevent brain herniation. The exposed cortex area and surrounding tissue were covered with a transparent layer of agar to prevent desiccation and thus stabilize the recordings. For AC measurements, I placed the electrode in contact with the AC and as perpendicular as possible to its surface. After this, I advanced it between 0–2000 μm in depth. The recording tracks were spaced 250–500 μm and placed through the cortical regions of interest, while blood vessels were avoided. The vascular pattern was used as a local reference to mark the position on the image where the tract was made, considering that this map varies between animals. At the end of the experiment, the limits and the relative position of the auditory fields were identified according to the pure-tone frequency response topographies in rats (Nieto-Diego and Malmierca, 2016). I estimated the depth of each neuron from the reading of the micromanipulator relative to the brain surface. I used the depths of the layers in the rat AC as stated in Pérez-González et al. (Pérez-González et al., 2021) (i.e., the granular layer would extend between 457–614 μm).

The sounds used to search for neuronal activity were trains of noise or pure tones (1–4 stimuli per second). These stimuli had a short duration (30 ms) in order to avoid a strong adaptation. Sound parameters such as frequency, intensity, presentation rate or type of sound such as white noise, narrow band noise or pure tones, were manually varied as necessary to facilitate mismatch.

For each neuron recorded, the frequency response area was calculated, which is the response magnitude map for each pair of frequency / intensity data. This was calculated in the first place to ensure that the frequencies and intensities used were contained in the response range. To obtain this frequency response area, a sequence of tones was presented at a rate of 4 Hz, randomly varying the frequency and intensity of the tones presented (3–5 repetitions of each tone). The sounds used for stimulation were sinusoidal tones of 75 ms duration, including up and down ramps of 5 ms, at a frequency and intensity within the response area of the neuron. In the single electrode recordings in the rat, the frequency-intensity combination could be chosen specifically for the single neuron recorded at a time. In the many-electrode recordings in the mouse, I chose a set of frequencies that made a good match with the frequency response areas of the currently recorded cells. I used a fixed set of three intensities in the mouse ([50, 60, 70] dB SPL) which were intense enough to activate all recorded neurons. These sounds were presented in an oddball sequence 400 tones long. The oddball sequence consisted of a repeating tone (90% standard probability) that was occasionally omitted (10% deviant probability).

For the AC recordings, the coordinates of the neurons over the AC extension were measured from the micromanipulator as the position of the recording electrode in reference to bregma. For the IC recordings, at the end of the recording session a 5 µA current was driven for 5 seconds through the recording electrode, in order to produce an electrolytic lesion. Animals were euthanized with a lethal dose of pentobarbital, and the head was removed and immersed in a mixture of 1% paraformaldehyde and 1% glutaraldehyde in 1M PBS. After fixation, tissue was cryoprotected in 30% sucrose and sectioned in a freezing microtome to obtain 40-µm thick coronal sections. The sections were stained using 0.1% cresyl violet to facilitate identification of cytoarchitectural boundaries.

I visualized the electrophysiological recordings online using custom-written software with MATLAB (Mathworks) and OpenEx Suite (TDT). Multiple unit activity was automatically extracted by manually setting a unilateral action potential threshold above the background noise as an accurate estimate of neuronal population dynamics (Trautmann et al., 2019). Once a neuron was isolated and confirmed to be stable, the stimulation protocol described in the next section was applied. For the awake experiments, the activity was monitored online using the OpenEPhys GUI, and stimuli were presented if single unit neural activity could be visually detected.

The omission of the tone was presented in two different ways within the oddball sequence: periodically or randomly, always with the same probability of appearance. A minimum of 3 standard tones were presented before each deviant. These sequences were presented with different SOAs (125 ms, 250 ms, and 500 ms) to control for confusion between actual responses to omissions and responses to previous standard stimuli.

In the single electrode recordings in the rat the standard and deviant frequencies were chosen to lie symmetrically around the characteristic frequency at the same intensity in order to elicit similar response rates. The paradigm was run with either of the two stimuli as standard and deviant. The output of the system was also recorded using a ¼-inch condenser microphone (Model 4136, Brüel & Kjaer) to ensure the absence of any sound or noise during omissions (Fig. 17). The spectrogram in Fig. 17a shows a portion of the presented periodic omission sequence reflecting the intensity of the sounds that the system reproduces. The power spectrum shown in Fig. 17b allows comparison between the signal produced during a real stimulus (blue) with the omitted signal (red) and confirms that no sound was reproduced during the omission.

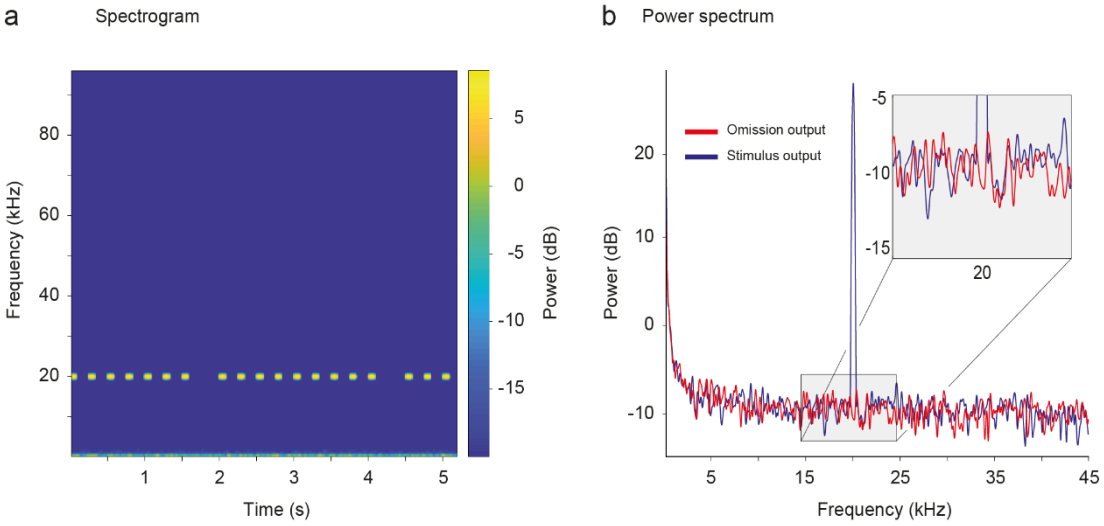

Figure 17. Sound/omission stimulation controls. **a.** Spectrogram of the output of the speaker recorded with a microphone, during the presentation of the omission stimulation paradigm. Note the gaps between the 20 kHz tones (yellow), showing the lack of stimulus during the omission periods. **b.** Power spectrum showing a direct comparison of stimuli periods (blue) and omissions periods (red), demonstrating the absence of acoustic stimulation beyond system noise.

4.2.1.1.2. Experimental and surgical procedures in anesthetized- and awake mice

The experiments were carried out inside an acoustically insulated and electromagnetically shielded and grounded booth. Sound stimuli were generated and recorded using a multichannel data-acquisition device (USB-6351, National Instruments) through a custom-written MATLAB GUI (Controller). Sounds were presented to both ears by a speaker (T250D, Fostex) placed in front and above the animal. The output of the speaker was calibrated to have a flat spectral profile over the range 2–80 kHz within 5 dB using an inverse linear filter, estimated before the experiment using an ultrasonic microphone (CM16/CMPA, Avisoft Bioacoustics) corrected for its own frequency-dependent sensitivity curve.

Mice were implanted with a headpost for head fixation at the age of 8-12 weeks. In the second surgery, performed when animals were 12–16 weeks old, mice were implanted with a silicon NeuroNexus neural probe aiming at the left primary AC, field A1, based on stereotaxic coordinates (3.2 mm post-bregma, 5.9 mm lateral from the midline, measured on the skull, estimated from (Tsukano et al., 2016) and confirmed pre-implantation via intrinsic optical imaging of noise burst sequences (0.2 s long, 0.1s interstimulus interval, 70 dB SPL, 10 sounds per trial, 30 trials). A craniotomy (~1x2mm) was opened using a microdrill centred on the part of AC that showed the strongest response in the intrinsic imaging. In the awake mice, the implant was chronic, mounted in a custom designed drive (variant of the EDDS drive, Microprobes for Life Science) allowing the electrode array to be repositioned. The surgery was performed under general isoflurane anaesthesia (1.5–2% dosage, E-Z Anaesthesia, E-Z Systems Corporation). From 24h before to 48h after the surgery the animal received an analgesic dissolved in water (1 ml/L water, Carprofen (Rimadyl cattle), Zoetis), supplemented by another dose of Carprofen at the start of the surgery (5 mg/kg, s.c.). In the anaesthetized mice, the electrode array was inserted acutely for the period of the recordings under urethane anaesthesia using one initial dose (1.7 g/kg i.p.) and 1-2 supplementary doses (0.2 g/kg i.p.). Additionally, Dexamethasone (0.2 mg/kg, s.c.) was given in both conditions after induction of anaesthesia to reduce local bulging of the brain and a ground screw was implanted over the right frontal cortex.

In awake mice, for the time of recording the animal was placed on a platform located in the middle of a booth and head-fixated using an implanted headpost. All recordings were performed using NeuroNexus silicon probes with 64 channels. The recording sites were

distributed differently per probe, in particular I used two 4x16 (A4x16-Poly2-5mm-23s-200-177, A4x16-2.5mm-tet/lin-300/125-333-121/177-PC) configurations. Data was digitized using a combination of a 64 channel (Intan Technologies) headstage connected to an OpenEphys recording system (Open Ephys, Cambridge USA). Data was collected at a sampling rate of 30 kS/s, bandpass filtered between 0.3–6 kHz and spikesorted to get multi- and single unit responses using the openly available function autoSortC from the Controller package. The sorting used automatic criteria for cluster-cutting rather than human decisions, which are prone to be variable from day to day. Sorting was performed separately for each prong. The average number of cells/electrode in a single session was 0.71 after spike-sorting, which is a typical yield, e.g. in comparison to other recording techniques (0.625 cells/electrode, (Voigts et al., 2013)). I estimated the depth of each cell from the depth of the array relative to the brain surface and the position of the recording sites in each array configuration. The depths of the layers were estimated from a coronal section of the mouse AC in the Allen Brain Atlas (Allen Institute for Brain Science, 2011) (i.e., the granular layer would extend between 355–477 μm).

In the multielectrode recordings in the mouse the pair of frequencies were chosen to provide the best match with the currently recorded cells, and also ran the paradigm with both frequencies for standard and deviant. All subsequent analysis for omissions and deviants was identical.

4.2.2. Main results

We tested whether neurons of the auditory pathway exhibit elevated responses to the omission of sounds within a fixed-rate, repetitive sequence, i.e., whether their response signifies a violated expectation of a regularly repeating sequence. For this purpose, I recorded neuronal activity in the IC (IC, n=48) and AC of urethane-anaesthetized rats (AC, n=77) and the AC of awake mice (AC, n=635) in response to a set of pure-tone sequences.

The sequences corresponded to an oddball paradigm where the deviant was an omitted stimulus (Fig. 18). I tested each neuron with a set of six sequences, with fixed frequencies and intensities chosen to fall within the frequency response area. Sequences differed in their SOA (125, 250 or 500 ms) and precise sequencing, either with a random number of tones before an omission or a fixed number (periodic). The spontaneous activity of each

neuron was recorded for 2.5–10.0 s (equivalent to ≥ 20 stimuli for each respective SOA) before each sequence as a control to compare with the evoked activity (Fig. 18).

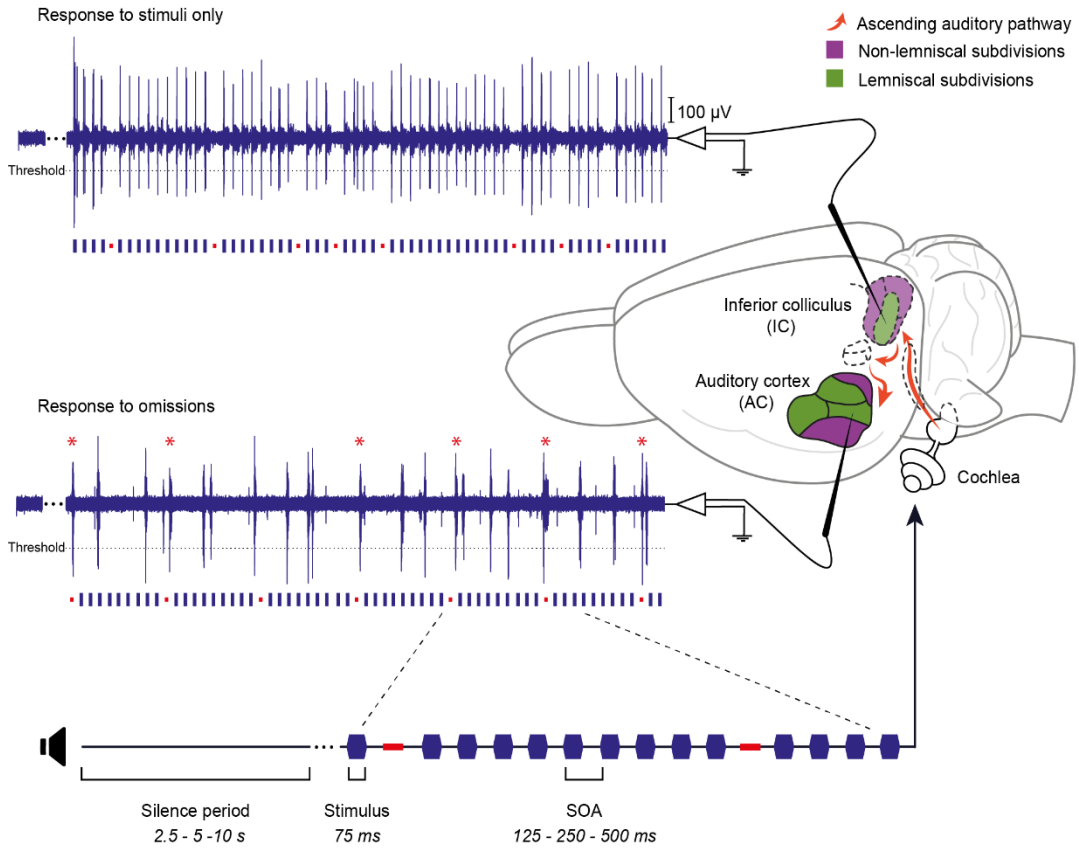

Figure 18. Experimental setup and design for recording from the IC and AC. While stimulating with sequences of pure tones, neuronal activity was recorded using microelectrodes in the urethane-anaesthetized rats (AC and IC) as well as urethane-anaesthetized and awake mice (AC). The long tone sequence consisted of a repeating tone (stimulus probability: 90%) that was occasionally replaced by an omitted tone (average deviant probability: 10%). Traces correspond to actual recordings (from the IC and AC of urethane-anaesthetized rats, respectively). Red stars indicate neuronal responses during an omitted tone. SOA denotes the amount of time between the start of one stimulus and the start of the following stimulus.

Omission responses were defined as a temporally localized elevation of spiking activity occurring during the periods of silence when a stimulus was periodically or randomly omitted (10% probability in both cases) in a long sequence of tones. This elevated

neuronal activity should be significantly different from (i) the spontaneous activity of the cell, prior to the entire stimulation sequence and (ii) the neuronal activity recorded just before each omission trial (-25 to 5, -75 to 5 and -195 to 5 ms time-windows, while the considered response windows were 5 to 120, 5 to 150 and 5 to 225 ms, respectively; two-sided Montecarlo test with Benjamini-Hochberg correction for multiple comparisons, $p<0.05$, see Methods for details). From the cases that were significant for both tests, I only used those where the omission-evoked firing rate was larger than both (i) and (ii). This separates systemic from spurious increases in firing rate, which may occur by chance in some trials. Due to the low spontaneous activity of IC neurons, a minimum firing rate of 1 spks/s during omitted tones was also required for IC neurons. I recorded the output of the speaker while playing the stimulation sequence to check that there was no acoustic signal during the omissions (Fig.17).

Importantly, I performed much of the significance assessment on the level of the presented stimulus sequences, as the omission response could depend on the parameters governing the sequence, i.e., rate (SOA: 125, 250 and 500 ms), sequencing (random vs. periodic), area/state and lastly neuron. The latter is particularly important, as the classical theory of predictive coding predicts only a subset of neurons to elevate their rate for certain conditions, in particular inhibitory neurons. Hence, not all neurons are expected to enhance, or more generally change their firing rate during omissions.

4.2.2.1. Evidence of omission responses in auditory neurons

Following the previous criteria, 2.2 % (16/713 sequences), 10.9 % (119/1092 sequences) and 15.1 % (1373/9075 sequences) from IC, and AC from anaesthetized rats and awake mouse responses to omitted tones immersed into different stimulation sequences were classified as significant omission responses.

The omission responses were induced at different SOAs suggesting that omission neurons represent a heterogeneous neuronal population. I found that the omission response is already apparent in a subset of IC neurons recorded at 125 ms SOA under anaesthesia and it is also present in AC neurons being robust and more frequent in awake animals (Fig. 19c).

Previous studies have questioned the existence of genuine omission responses, considering that these responses may represent rebound effects. Rebound and entrainment

effects should occur within a short period after the preceding stimulus, and their latency is expected to be constant regardless of SOA. To check for these effects, I analysed how the SOA affects the omission responses (Fig. 19). If a rebound would occur, an obvious and clear neuronal activity should appear in a time range that coincides with this specific time window after the previous tone. Detailed inspection of these time windows demonstrated that this was not the case for any of the recordings. Thus, the analysis of longer SOAs provides a robust control that these responses are, indeed, genuine omission responses.

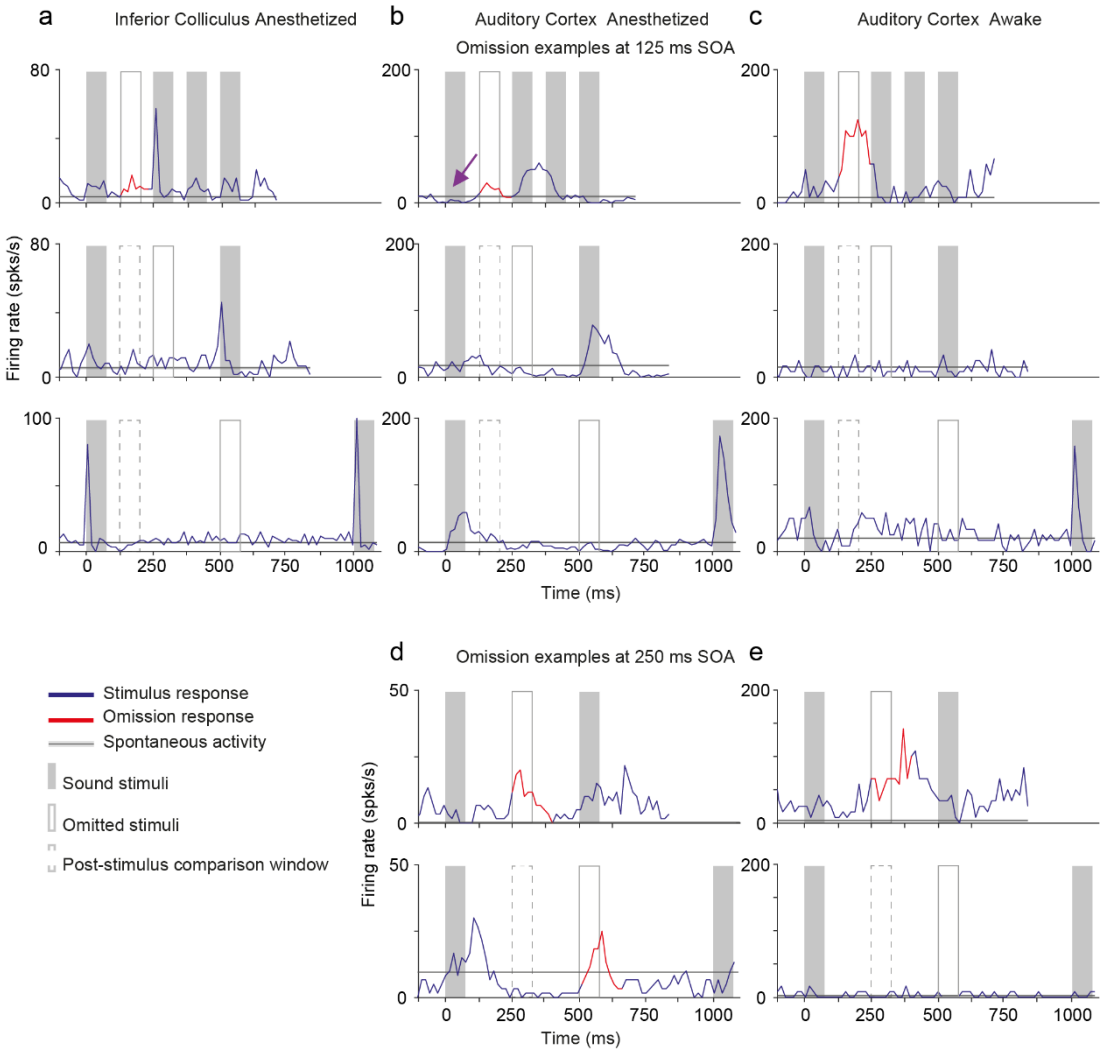

Figure 19. Representative examples of PSTHs. PSTHs for significant omission responses (red traces) and that of the stimulus response (blue traces). The three recorded areas are shown in the different columns (IC anaesthetized rat, AC anaesthetized rat and awake mice; from left to right respectively). Firing rates (spks/s) and time (ms) are represented in vertical and horizontal axes. The duration of the stimuli and omitted tones (75 ms) is represented by

vertical grey-shaded and white continue-lines boxes respectively. Each plot is aligned to the last stimulus prior to the omission (see columns). The omission signal (red line) has been computed as centred on the omitted tone whose response is occurring during the white vertical reference box. Grey-shaded vertical boxes indicate the location of the stimuli previous and following the omission. The spontaneous activity recorded before the stimulation sequence is also depicted as reference (grey horizontal line). **a-c** show examples of neurons with significant omission responses occurring at 125 ms SOA (upper panels) and their corresponding sequences at SOAs of 250 and 500 ms (middle and bottom panels, respectively). **d, e** show examples of neurons with significant omission responses occurring at 250 ms (upper panels) and their corresponding 500 ms sequences (bottom panel). Grey dotted lines show comparison windows for post-stimulus activity control.

In summary, omission-evoked responses occurred more frequently for the 125 ms SOA (16.82%, 1245/7401 sequences) particularly in the awake condition, but they may also occur at 250 ms SOA (10.98%, 200/1822 sequences) and 500 ms SOA (3.8%, 63/1657 sequences).

4.2.2.2. Comparison between sound- and omission responses

In order to obtain a more general picture of omission responses in the auditory brain, I compared the firing rate during the silent periods (omission deviants) and the sound stimuli, both referenced to spontaneous activity (paired t-test with Bonferroni correction, $p<0.05$; Fig. 20), for all conditions. In IC and AC neurons (Fig. 20a, b) from urethane-anaesthetized rats, omission responses were very similar to the sound evoked activity, showing a relatively minor enhancement of the omission response for 125 ms in AC. However, when looking at the awake mice AC (Fig. 20c), there is a robust and highly significant enhancement of the omission response as compared to the sound response at all random presentations and also periodic/125 ms SOA presentation.

This effect was observed as a main effect when pooling over SOAs and was specifically pronounced in the awake mice AC responses for SOA 125 (14.93 vs. 18.06 spks/s for periodic and random presentations respectively; $p<0.0001$, type II ANOVA with Bonferroni correction; $p<0.05$; Fig. 20c). In the present 3-way ANOVA 105 post-hoc tests were conducted systematically, which places rather strict requirements for significance on individual condition comparisons after Bonferroni correction.

In summary, there are two important features regarding the omission firing rates. First, the firing rate for the omission is larger than the one for sound stimuli in awake mice AC, but not in the IC and AC of anaesthetized rats, which show similar magnitudes. Second, the periodic and randomly occurring omissions lead to significant differences in the omission related neural response. Thus, showing that the omission response is highly dependent on the auditory processing hierarchy, pattern of stimulation, and the individual neuron.

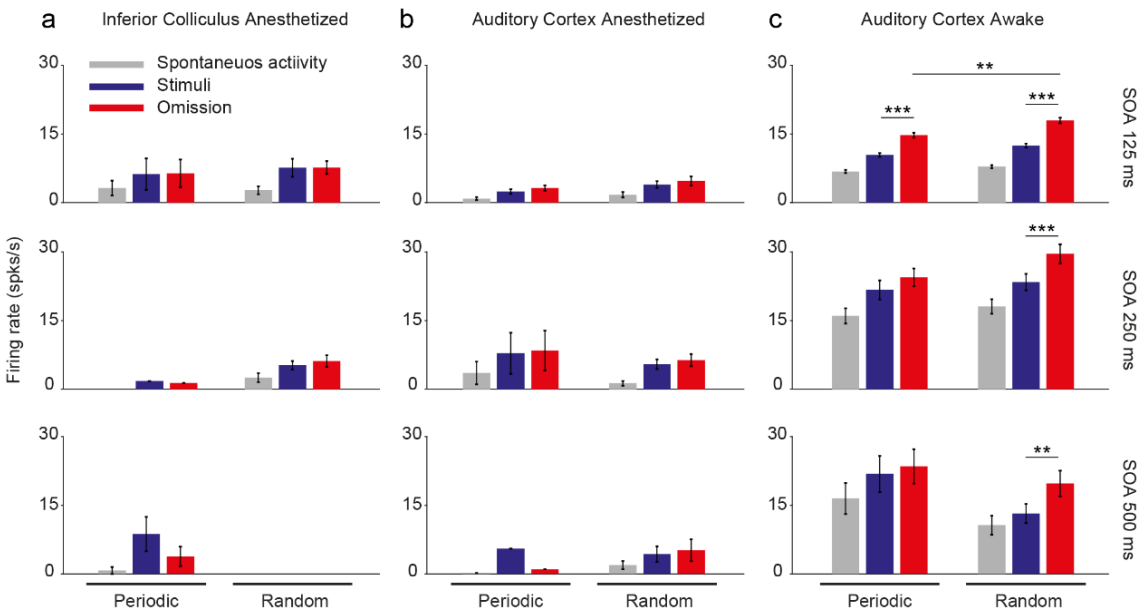

Figure 20. Firing rates average of neural responses. **a-c** Spontaneous, sound- and omission-evoked activity are represented by gray, blue and red boxes respectively. Columns and rows represent the recorded areas and SOA conditions respectively. Within each column, periodic and random conditions are sorted. Error bars denote mean stimulus deviation. Asterisks indicate statistical significance of omission responses against basal and pre-omission activity and also statistical significance between periodic/random omission deviants (*$p < 0.05$, **$p < 0.01$, ***$p < 0.001$; paired t-test with Bonferroni correction). Note that a significant difference between periodic/random omission deviants has been found for 125ms SOA in awake mice.

In order to quantify the comparison between sound- and omission-evoked activity, I computed an *omission index* [iOmi = (Omi FR – Stim FR)/(Omi FR + Stim FR)] for the

three recorded areas (Fig. 21a-c). The iOmi ranges from -0.9 to 0.6 in IC, -1 to 1 and -0.7 to 1 in in AC from anaesthetized and awake animals. Some stimulation sequences show negative or positive iOmi values that exhibit a larger response to the sound or to the omission, respectively (Fig. 21a-c). The average of iOmi gives an idea of the omission detection power of the neurons in each auditory area. In anaesthetized rats, iOmi values are negative for IC neurons, becoming positive for AC neurons (Fig. 21a, b). When moving from anaesthetized to awake animals, iOmi values increases for AC neurons (iOmi = -0.0084, 0.0771 and 0.1594, respectively). Interestingly, AC neurons show normal distributions, and those omission responses whose iOmi > 0.33 will be referred to as *omission selective responses*, as this value corresponds to a factor 2 difference (Fiser et al., 2016). Thus, a total of 30/119 (25.21% sequences) and 311/1373 (22.65% sequences) in AC of anaesthetized and awake animals are omission selective responses. All IC responses show an iOmi < 0.20, except for one single response that shows an iOmi of 0.54.

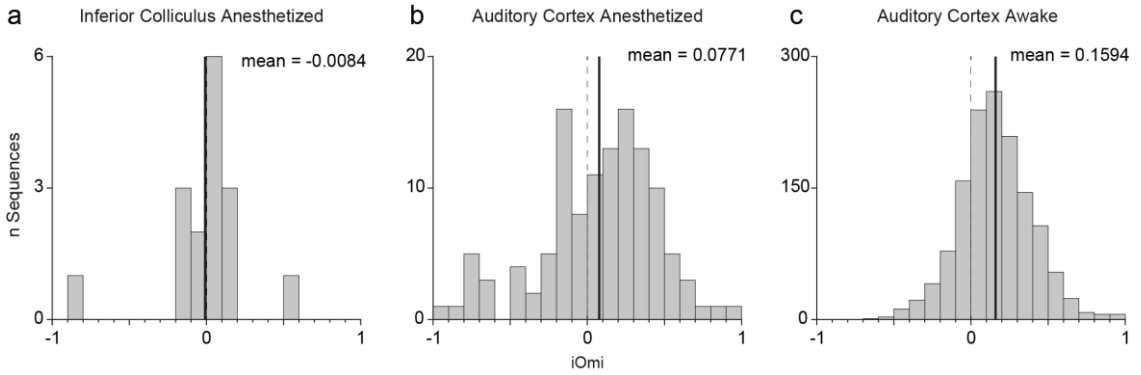

Figure 21. Omission index of significant omission responses. The three-recorded areas show different omission index (iOmi) from negative to positive values (-0.0084, 0.0771 and 0.1594 for IC and AC in anaesthetized rats and awake mice AC neurons respectively; see columns). The iOmi was computed for significant omission responses as iOmi = (Omi FR – Stim FR)/(Omi FR + Stim FR].

In order to explore the omission responses further, I measured and compared the peak latency for the omission and sound evoked activity (paired t-test with Bonferroni correction, $p<0.05$). In all SOAs and conditions, stimulus- and omission latencies were

not significantly different except for 125ms SOA in awake animals. A real and genuine omission response should be time-locked to the period when the stimulus is expected to happen (but it is omitted). Hence, these latency data strongly support the notion that there is a population of auditory neurons that unambiguously respond to the omission of a stimulus.

4.2.2.3. Histological distribution of omission responses across AC fields and layers

In order to test if omission responses show any specific distribution across AC fields and/or layers, I analysed where neurons with omission responses were located in the different AC regions (Fig. 22a, b). In order to allocate each recorded neuron to a specific field in the rat AC, I recorded the frequency response areas and analysed the topographical distribution of CFs for all units. Each recording was assigned to a dorsoventral and rostrocaudal coordinate system relative to bregma as in previous studies (Polley et al., 2007; Nieto-Diego and Malmierca, 2016; Parras et al., 2017). Omission responses are distributed in all fields, the highest levels of iOmi were found in SRAF and PAF. As the recordings in the mouse were targeted towards A1 only, no data is presented from these recordings.

Next, I analysed the iOmi across layers in this case for both, anaesthetized and awake animals (Fig. 22c-d). For anaesthetized rats, the proportion of omission responses over the total recordings were 10.73% (44/410 sequences), 10.04% (23/229 sequences) and 10.36% (40/386 sequences) for supragranular, granular and infragranular layers, respectively. For awake mice, these proportions are slightly larger; thus, 14.97% (417/2786 sequences) of the sequences in our AC sample were located in the supragranular layers, 16.45% (272/1653 sequences) in the granular and 14.75% (684/4636 sequences) in the infragranular.

When looking at the distribution of the omission selective responses for the anaesthetized rats (Fig. 22c), AC neurons show that 3.90% (16/410 sequences) of the responses were located in the supragranular layers, 2.18% (5/229 sequences) in granular layer, and 1.55% (6/386 sequences) in the infragranular layers. Meanwhile, for the awake mice AC neurons, the proportions were 2.80% (78/2786 sequences), 4.36% (72/1653 sequences) and 3.47% (161/4636 sequences), respectively (Fig. 22d). Therefore, while the

distribution of omission significant neurons is similar across layers, both in the anaesthetized and the awake preparations, omission selective neurons (i.e., those that respond much more to the omission than to the stimulus) are more frequent in the supragranular layer of the anaesthetized rat, and in the granular and infragranular layers of the awake mouse.

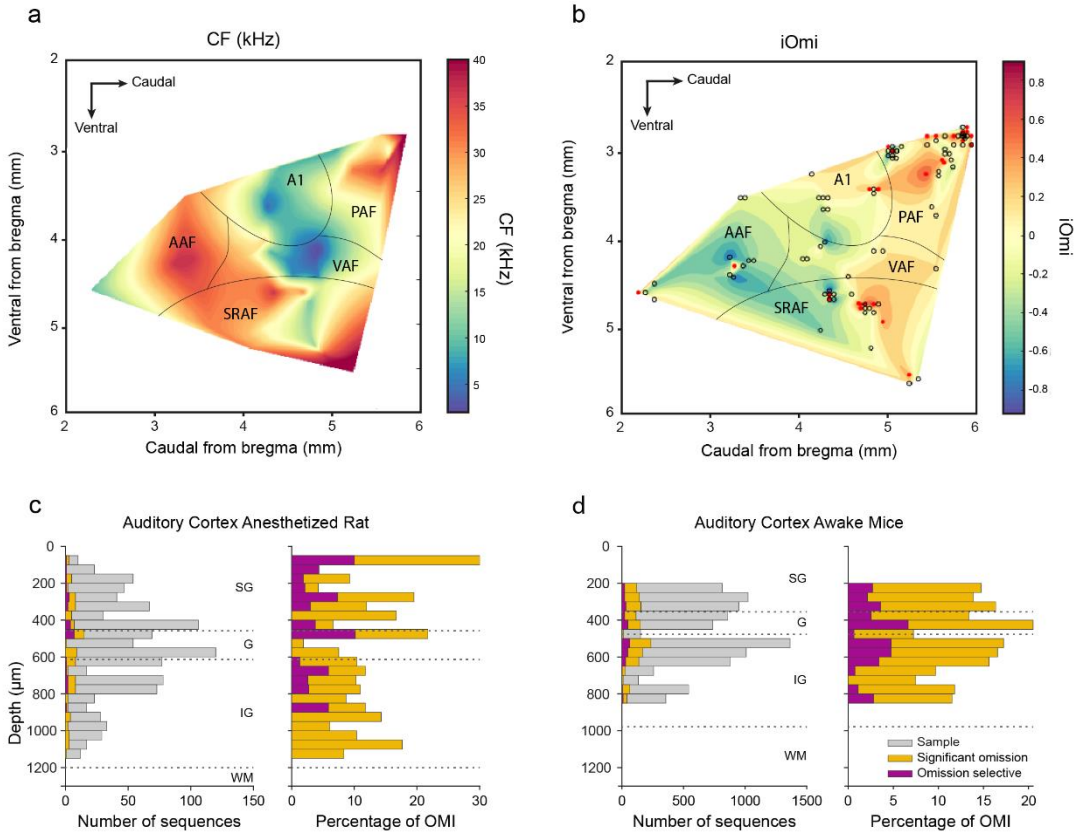

Figure 22. Omission responses in AC fields and layers. **a.** Distribution of characteristic frequencies across the rat AC. The frequency gradients were used to estimate the limits of the different fields. b Distribution of iOmi across the rat AC. Each circle indicates the location of a neuron with omission responses. Red-filled circles indicate neurons with omission-selective responses (iOmi > 0.33). Note how high iOmi neurons tend to be found in PAF and the caudal areas of VAF and SRAF. **c, d**. Distribution of omission sequences in the rat (**c**) and mouse (**d**) AC layers. Horizontal lines indicate the boundaries between supragranular (SG), granular (G) and infragranular (IG) layers. While the percentage of omission sequences (orange bars) over the total sample (grey bars) is similar in all layers in both preparations, omission-selective sequences (purple bars) are more frequent in the supragranular layers of the anaesthetized rat and in the granular-infragranular layers of the awake mice.

These results allowed me to identify the omission responses and some of the details that govern their responses. At the same time, this analysis could be suffering from double-dipping (Kriegeskorte et al., 2009), so I further analysed the data at the neuronal level by performing the statistics on half of the data, and used the other half for plotting. I also performed AC neurons recordings in urethane-anaesthetized mice in order to link the two rodent species.

4.2.2.4. Omission-sensitive neurons

In order to confirm that the omission responses are also genuine responses at the neuronal level, and not simply random variability that could result in false or fictitious significant responses, I averaged all the conditions (sequences) recorded for each neuron. This average was performed regardless of omission responses significance to obtain a single omission significant value per neuron. Thus, when I grouped all values by neuron, I consistently found omission responses (Fig. 23a, red traces) for 125 ms SOA at the neuronal level in all three recording conditions. I referred to these neurons as *omission-sensitive* neurons. Omission responses in the AC of anaesthetized rodents (Fig. 23a, left and middle) are clearly noticeable in comparison to the preceding stimulus response, which is the last stimulus in the stimulation sequence prior to the omission. The omission response for the awake mouse AC neuron is very distinct, in both size and timing (Fig. 23a, right).

Next, in order to analyse omission responses at the population level, I computed grand-average PSTHs including all neurons showing significant omission responses (Fig. 23b). The whole population also reflected the trend shown in the individual cells. The omission responses are more robust when comparing results from anaesthetized to awake animals. Significantly, while positive omission responses are present in anaesthetized rodents AC populations (Fig. 23b, left and middle) they are even more pronounced in awake mice (Fig. 23b, right). The stimulus-evoked response (blue) shows less adaptation in awake mice (Fig. 23b, right) as opposed to cortical neurons in anaesthetized rats and mice (Fig. 23b, left and middle). In awake mice, the onset responses to each stimulus are clearly visible and the omission-evoked activity (red) is readily recognisable (Fig. 23b, right). The firing rate in response to sound stimulation is low in anaesthetized rodents, except for the first stimulus after the omission, and it tends to increase during omitted tones (Fig. 23b, left and middle).

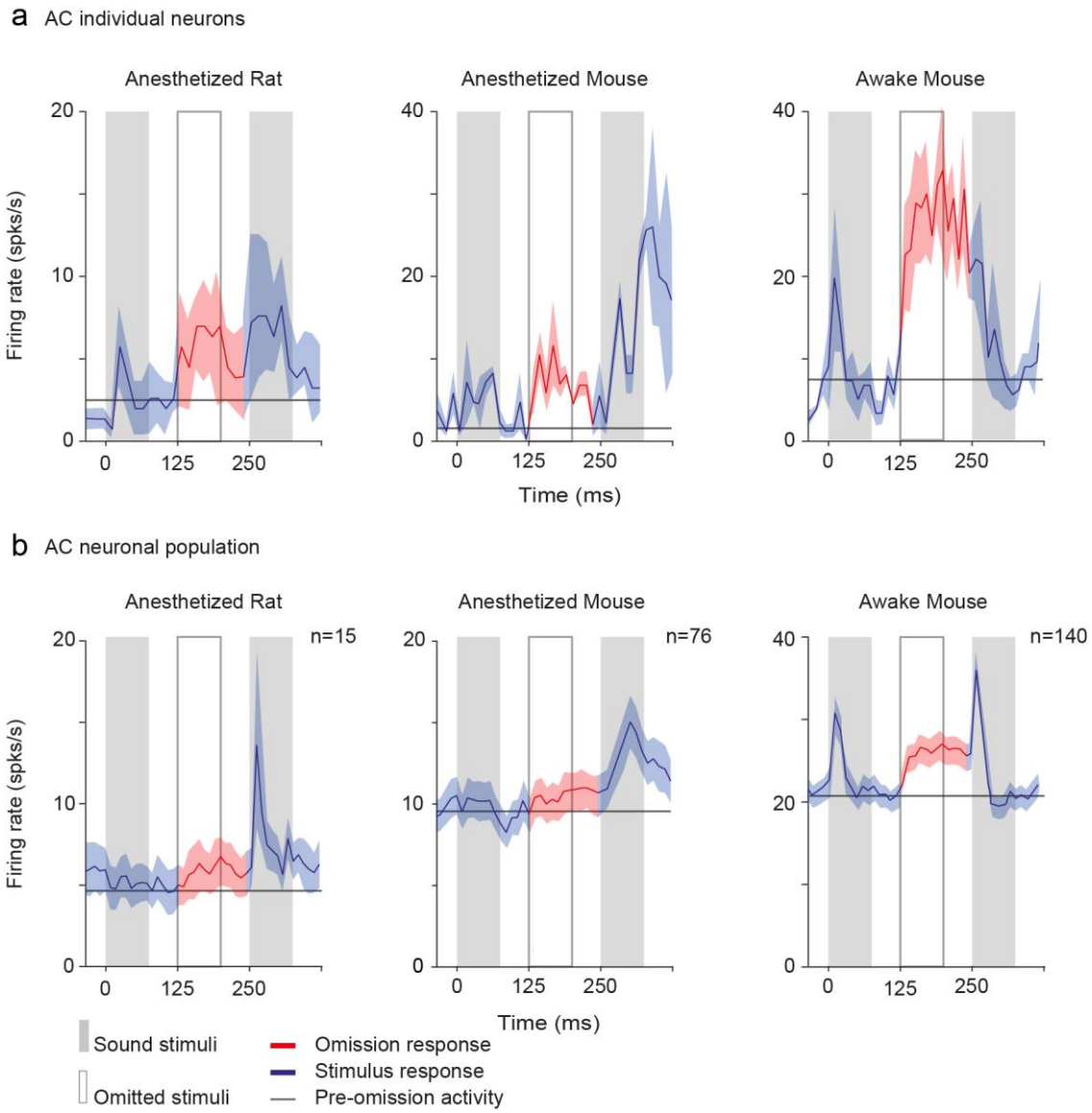

Figure 23. PSTHs of omission-sensitive neurons. **a.** Representative examples of omission responses in individual AC neurons. Neurons from the three recorded conditions are shown in the different columns (anaesthetized rat, anaesthetized mouse and awake mouse; from left to right respectively). Firing rates (spks/s) and time (ms) are represented in vertical and horizontal axes. The duration of the stimuli and omitted tones (75 ms) is represented by vertical gray-shaded and white continue-lines boxes, respectively. The responses have been computed as centred on the omitted tone whose response is occurring during the white vertical reference box. The red traces indicate responses during the omission analysis window. The pre-omission activity is also depicted as reference (gray horizontal line). Shaded areas indicate SEM. **b.** Grand average of the responses of all the omission-sensitive neurons, per recorded condition, indicating the number of neurons included.

When looking at the shape of the stimulus responses, omission responses typically had an onset component, both in individual examples as well as at the population level. Using the 115 ms analysis window that includes most of the evoked response, only in the case of the anaesthetized animals I found larger responses to the stimulus after the omission compared to the response to the stimulus before the omission ($p=0.0125$ and $p<0.0001$ for rats and mice respectively; Wilcoxon test). However, when using a 30 ms analysis window encompassing only the onset component, the response to the stimulus after the omission was larger than the response to the stimulus previous to the omission in all conditions (anaesthetized rat: $p=0.0496$, anaesthetized mouse: $p=0.0402$, awake mouse: $p<0.001$; Wilcoxon test). In the awake condition, as opposed to the responses to the stimuli, the omission responses tended to be more sustained, and started from the expected time of occurrence of the omitted stimulus, often continuing to the subsequent stimulus presentation.

In summary, omission-evoked responses are strongly represented at 125 ms SOA occurring both under anaesthetized and awake states in the AC, with a substantial increase in magnitude in the awake state (compared to our smaller dataset from the IC). At longer SOA (250 and 500 ms), I still detected a small subset of omission-sensitive neurons but their average responses (based on the second half of the split-data analysis) did not provide substantial evidence for reliable omission responses at these SOAs.

4.2.2.5. Omission-sensitive neurons sound- and omission responses

Next, I evaluate omission response at the population level and compare it to stimulus responses (not just the preceding one) and responses to the after-omission stimuli. Each of these responses was referenced to the omission preceding activity in order to have a common local baseline. As expected, the spontaneous rate before the stimulation sequence to overestimate the within-sequence spontaneous rate (Wilcoxon test with Holm-Bonferroni correction, $p<0.05$, Fig. 24). AC neurons from anaesthetized rats and mice responded with similar firing rates to stimuli and omissions (Fig. 24a, b; $p = 0.577$ and $p = 0.067$, respectively). On the other hand, awake mice AC neurons showed a significant enhancement of omission responses relative to stimulus responses (Fig. 24c; $p<0.001$).

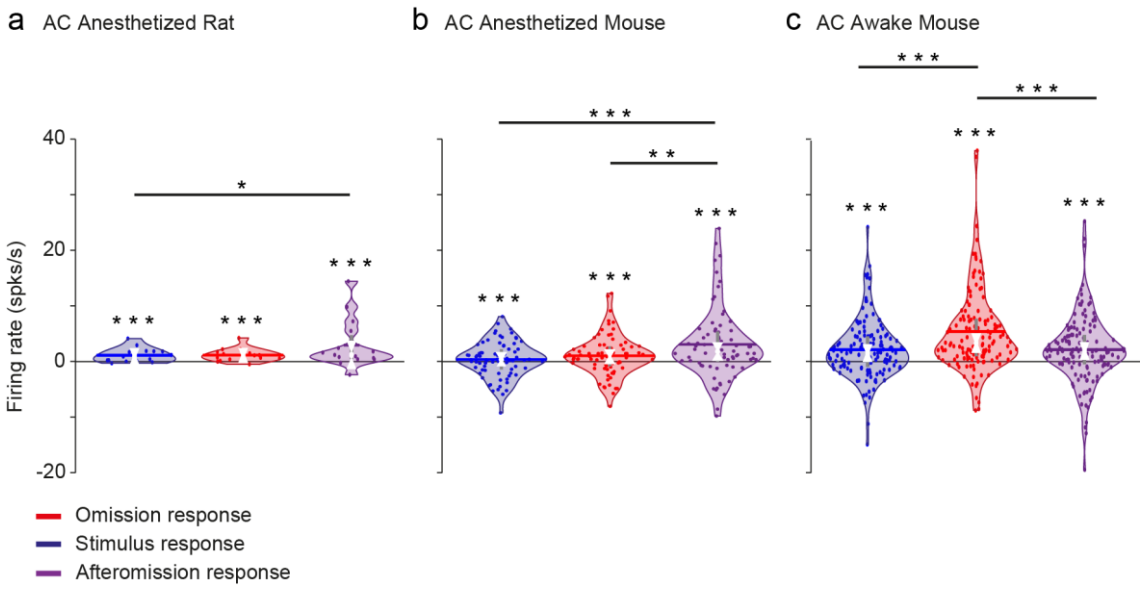

Figure 24. Firing rates of omission-sensitive neurons in the AC of the anaesthetized rat (**a**), anaesthetized mouse (**b**) and awake mouse (**c**). Sound-, omission- and after-omission evoked activity are represented by blue, red and purple violin plots, respectively. In this and similar violin plots, the horizontal solid lines indicate the mean of the distribution, while the inner gray box indicates the interquartile range. Similarly, the white circles indicate the median and the white triangles show the 95% confidence interval for the median. Evoked firing rates have been baseline-corrected, relative to pre-omission activity. Asterisks directly over the violin plots indicate that the distribution is statistically different from 0 (Wilcoxon test with Holm-Bonferroni correction). Asterisks over horizontal lines indicate significantly different distributions (Wilcoxon test with Holm-Bonferroni correction, $*p < 0.05$, $**p < 0.01$, $***p < 0.001$).

The omission response was significantly stronger to the first stimulus after an omission in the awake condition, highlighting the omission response in the sequence ($p<0.001$, Fig. 24c). The average firing rate in response to after-omission stimuli was significantly larger than the average response to the rest of stimuli in anaesthetized rat and mouse neurons ($p=0.038$ and $p<0.001$), but not in awake mice AC neurons ($p=0.276$), although it is also significant when using a 30 ms window, adapted to the brevity of the response. The reduced average response to all stimuli (excluding after-omissions) is probably due to an adaptation effect to the repeated stimuli, which is later released by the occurrence of the omission and subsequent after-omission.

Further, I tested whether there were differences in the response to the omission among the periodic and random conditions (with a common, average probability for omissions of 10%), but there were no significant differences at the population level (p=0.93, Wilcoxon test). As an occurrence of the omission in the periodic sequence is more predictable, I originally hypothesised a greater response in the random condition. The lack of a difference could be explained by the length of our shortest sequence in the random condition in relation to the dynamics of response adaptation.

In summary, I found two important features regarding the omission firing rates: First, for omission-sensitive neurons, the firing rate during the omission is similar to the sound-evoked firing rate in the anaesthetized condition (in both rat and mouse), but in the awake condition the omission response is even larger than the sound evoked activity over the analysis window. Second, the neural response of omission-sensitive neurons exhibits a timed rise at the start of the expected tone following an omission.

In order to quantify the comparison between sound- and omission-evoked activity I computed the omission index at the cellular level [iOmi = (Omi FR – Stim FR)/(Omi FR + Stim FR)], for the omission-sensitive neurons, for the three recorded conditions, where the firing rate for stimuli was averaged from all stimulus presentations (Fig .25a). Negative and positive iOmi values show neurons that exhibit a larger response to the sound or to the omission, respectively.

The average iOmi (Fig. 25a, vertical red-dotted lines) quantifies the response selectivity to omissions for a group of neurons, here applied to the omission-sensitive neurons. Anaesthetized rat AC neurons respond similarly on average to the stimulus and to the omission (iOmi = -0.089, p = 0.661, Wilcoxon test with Holm-Bonferroni correction, Fig. 25a, left), as well as anaesthetized mouse AC neurons (iOmi = -0.006, p = 0.836, Fig. 25a, middle), while in awake mouse AC neurons the average response to the omission is larger than to the stimulus (iOmi = 0.055, p < 0.001, Fig. 25a, right). Notably, the average iOmi is significantly larger in the awake mouse AC than in the anaesthetized mouse AC (p = 0.0013, Wilcoxon sum of ranks).

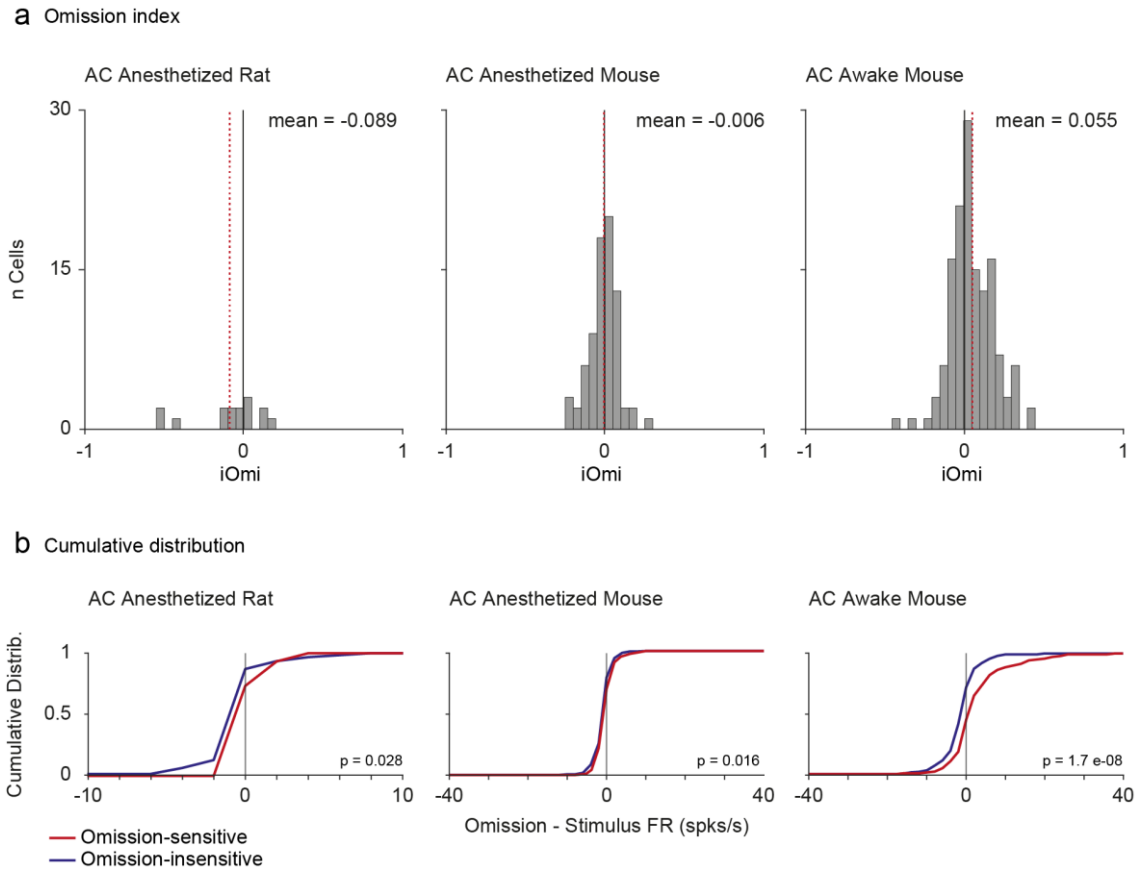

Figure 25. Responses to omission become larger than stimulus responses in the awake condition. Distribution of omission index (iOmi) between the recorded conditions. **a.** iOmi for omission-sensitive neurons show progressively increasing values, from negative in the rat anaesthetized condition, to positive values in the mouse preparations, being highest in the awake condition. Positive iOmi values indicate that the neuron responds with higher firing rates to the omission than to the stimulus, while negative values indicate the opposite. **b.** Comparison of omission-sensitive (red) with omission-insensitive (blue) neurons shows an increasing omission selectivity towards AC, and further in the awake state. This is indicated by a larger separation between the curves, in particular for values > 0, indicating greater responses to omissions than stimuli.

Next, I compared the omission-sensitive (Fig. 25b, red) neurons to their complement, referred to as omission-insensitive (Fig. 25b, blue) neurons, in terms of the difference in activity to omissions and stimuli. In line with the definition of these groups of cells, I find the omission-sensitive neurons have a larger difference than omission-insensitive neurons, thus relatively responding more to omissions ($p = 0.028$ and $p = 0.016$ for

anaesthetized rats and mice respectively and p = 1.7x10-8 for awake mice, Wilcoxon sum of ranks tests). While the difference is negative under urethane anaesthesia, i.e. greater responses to stimuli than to omissions, in both species (Fig. 25b), this relation reverses for the omission-selective neurons in the awake mouse (Fig. 25b, right, red). In all comparisons above, both omission and stimulus responses were referenced to the activity in the pre-omission period, to focus on relative changes within cells instead of absolute firing rates.

In summary, the degree of omission-selectivity in the neural responses was comparable between species in the AC and increased in the awake compared with the anaesthetized state in the mouse. While omission-selectivity differed in omission-sensitive and omission-insensitive populations in all conditions, the difference was most pronounced in the awake state.

4.2.2.6. Omission-sensitive neurons latencies of omission- and sound response

In order to explore the omission responses further, I measured and compared the peak latency for the omission and sound evoked activity (paired Wilcoxon test with Holm-Bonferroni correction, $p<0.05$; Fig. 26). Response latencies for omitted tones, stimuli and after-omission stimuli, are shown in Fig. 26 for the three recorded conditions. The neurons show very similar latencies for the omission- and stimuli-evoked responses in both anaesthetized preparations, while the latency of the omission responses is larger than the latency of the stimuli-evoked responses in the awake mouse AC ($p<0.001$). This is probably caused by multiple factors, including differences in the profile of the responses to the stimulus (peaking closer to the sound onset) and the omission (more sustained responses), overall larger firing rates, and reduced stimulus adaptation in the awake condition, which would contribute to faster responses. A real and genuine omission response should be time-locked to the period when the stimulus is expected to happen (but it is omitted). These latency data support the notion that the source of the omission response (i.e. putative prediction) could differ from the stimulus response (forward response) as posited by predictive (Rao and Ballard, 1999).

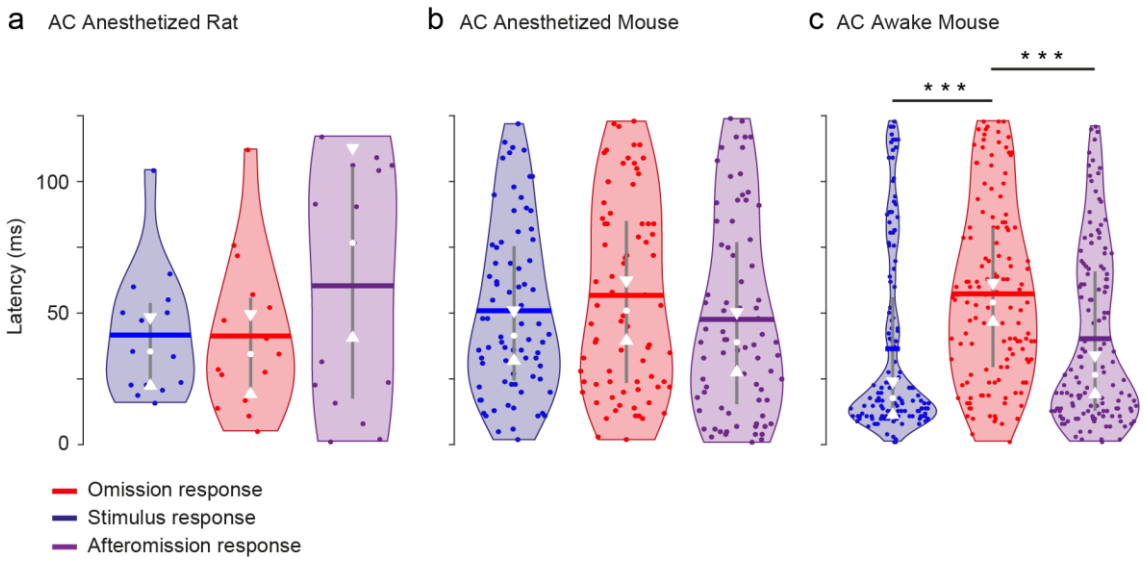

Figure 26. Distribution of response peak latencies (ms) of omission-sensitive neurons in the AC of the anaesthetized rat (**a**), anaesthetized mouse (**b**) and awake mouse (**c**). The blue, red and purple violin plots depict the distribution of the sound stimuli, omission and after-omission latencies (see Fig. 24 for the meaning of the violin plot symbols). Asterisks denote statistical significance between stimuli and omission latencies (***$p < 0.001$; paired Wilcoxon with Holm-Bonferroni correction).

4.2.2.7. Comparison between omission- and deviant responses

Responses to unexpected changes in tone properties, so called deviants, are closely related to the omission responses, as the latter can be considered a special case of a deviant. Their properties have long been studied under the topic of stimulus-specific adaptation, often considered a special case of predictive coding, where a certain degree of adaptation occurs for the repeated standard stimulus. Here the deviant stimulus leads to a larger response, in higher auditory areas even larger than it would in isolation (Malmierca et al., 2009; Nieto-Diego and Malmierca, 2016; Parras et al., 2017; Carbajal and Malmierca, 2018; Casado-Román et al., 2020). A natural question is whether the classical deviant responses co-occur with omission responses.

To address this question, I compare here (Fig. 27) the neural response for omission-sensitive neurons to deviant tones in the anaesthetized and awake mouse AC neurons (targeting A1). In the awake data set, the deviant and omission conditions were presented for a subset of 126 (out of a total of 393) cells, while in the anaesthetized set they were presented for all 350 cells, of which 55, and 76 were omission-sensitive, respectively. As

usual, the deviant response (Fig. 27a, left column, orange) was larger than the standard response (Fig. 27a, left column, blue; p=1.4x10-9, one-sided Wilcoxon signed ranks test), which in the anaesthetized condition was nearly completely adapted. The omission response was less precisely timed than the deviant response but was significantly larger than the pre-omission period (Fig. 27a, left, red). In this condition, both omission-sensitive and omission-insensitive neurons responded similarly to omission and deviant stimuli, as evidenced by the overlap of the cumulative distributions of the difference between deviant and omission responses (Fig. 27a, middle and right; p=0.15, Wilcoxon rank sum test between the two populations on omission - deviant responses). The curves intersect the ordinate at 0, indicating that responses to deviants were on average larger than to omissions.

On the other hand, the omission-sensitive neurons (Fig. 27b) also showed a very strong response to the deviant, and a clearer response to the standard than in the anaesthetized condition, likely due to reduced stimulus adaptation. In addition, the awake preparation shows a clear sustained response to the omission, with an overall rate similar to the deviant response (p=0.36). In this condition, omission-sensitive neurons respond to omissions with larger firing rates than to deviants (p=0.0017), which is not the case for omission-insensitive neurons (Fig. 27b, middle) This is also indicated by the 'dent' in the cumulative distribution of the difference between omission and deviant responses for the omission-sensitive neurons (Fig. 27b, right, red).

These response properties in the AC show that omission-sensitive neurons can also have a response to deviant sounds, however, in the awake state the omission response of the omission-sensitive neurons becomes comparable in size and more specific to omissions.

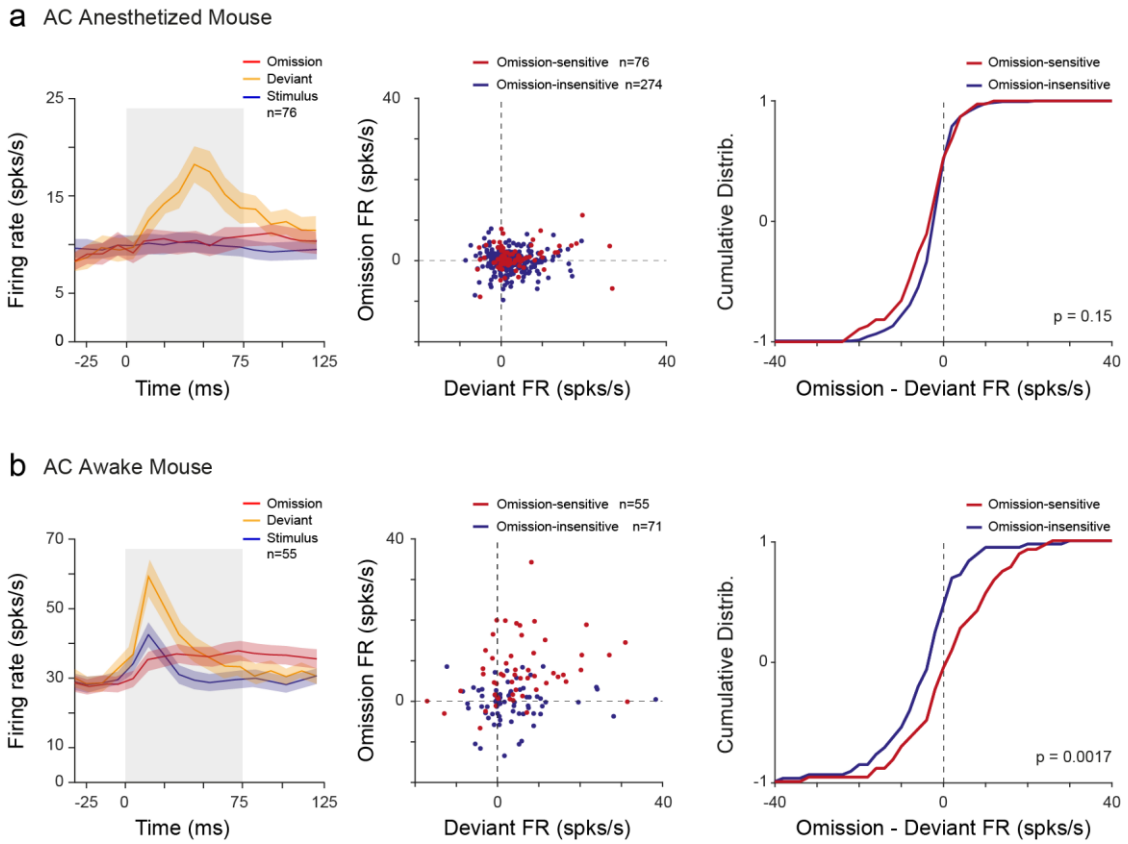

Figure 27. a. In the AC in the anaesthetized mouse, omission sensitive neurons show a strong response to deviants (orange, left), which substantially exceeds the omission (red) and standard stimulus (blue) responses (p=0.00018 and p=1.4x10-9), Wilcoxon signed ranks test (one sided) between deviant responses relative to omission or standard responses, n=76). The relative responses of Omission-sensitive (red) and Omission-insensitive (blue) neurons to omissions and deviant stimuli are statistically indistinguishable (middle), indicated by the overlapping cumulative distributions of difference between omission and deviant responses (right column, p=0.15, Wilcoxon rank sum test between the two populations on omission - deviant responses). Shaded areas in the left column indicate one SEM. All responses are relative to the pre-omission baseline period. **b.** In the AC of the awake mouse, the responses are generally larger and the Omission response becomes comparable in overall rate to the deviant response (p=0.36) while the deviant response is ~91% larger than the stimulus response (p=2.7x10-7). Many cells, in particular from the Omission-sensitive (red) group show Omission responses that are larger than the deviant response (middle, red dots above diagonal). In the awake state, Omission-sensitive neurons show a clear and significant separation in the difference between omission and deviant responses (p=0.0017).

4.2.2.8. Omission-sensitivity dynamics depend on brain state

Next, I analysed whether the response of omission-sensitive neurons show is dependent on the history of stimulation, and how this interacts with the state of the animal. First, I considered the neural responses as a function of the overall stimulation sequence. As expected, the stimulus response exhibited a fast decay, within just two stimuli across both the anaesthetized (Fig. 28a left, blue) and the awake (Fig. 28a right, blue) condition. In the awake condition, a second time-scale of adaptation existed with a time-constant of ~5 s. The level of the omission responses (red) stayed relatively constant over the period of the whole sequence in both states. The iOmi index of omission selectivity (Fig. 28b) showed a slow increase, which was more pronounced in the awake case ($r = 0.39$, $p = 1.2x10\text{-}16$, Pearson correlation) than in the anaesthetized condition ($r=0.1$, $p=0.035$). This was probably mostly driven by the adaptation of the standard response, potentially signifying a build-up of predictions (Heilbron and Chait, 2018).

Secondly, I studied the omission-evoked responses in relation to the number of stimuli preceding the stimulus omission. In the anaesthetized case a significant decrease ($p = 0.02$, Kruskal Wallis ANOVA) is observed for the omission response (Fig. 28c left, red). The response to the first standard after the omission (purple) shows a similar, but non-significant dependence. Surprisingly no dependence with a decrease for shorter sequences of standards is present in the awake case (Fig. 28c right). Conversely the standard response instead shows a significant decrease ($p = 0.00074$). For the omission response no dependence is present, although the omission response is on a high level relative to the standards (firing rates are normalized to the average standard response here), which suggests that the omission response might already have reached a plateau level. This possibility is supported by the rapid adaptation of the standard response after the omission (Fig. 28d), which is very salient in the anaesthetized case and completes after just two standard stimuli, and even after just one in the awake case. In the latter, this behaviour is only apparent if a shorter time window (30 ms) is used for the analysis (Fig. 28d right, inset), which matches the brief, driven response (see Fig. 28b right).

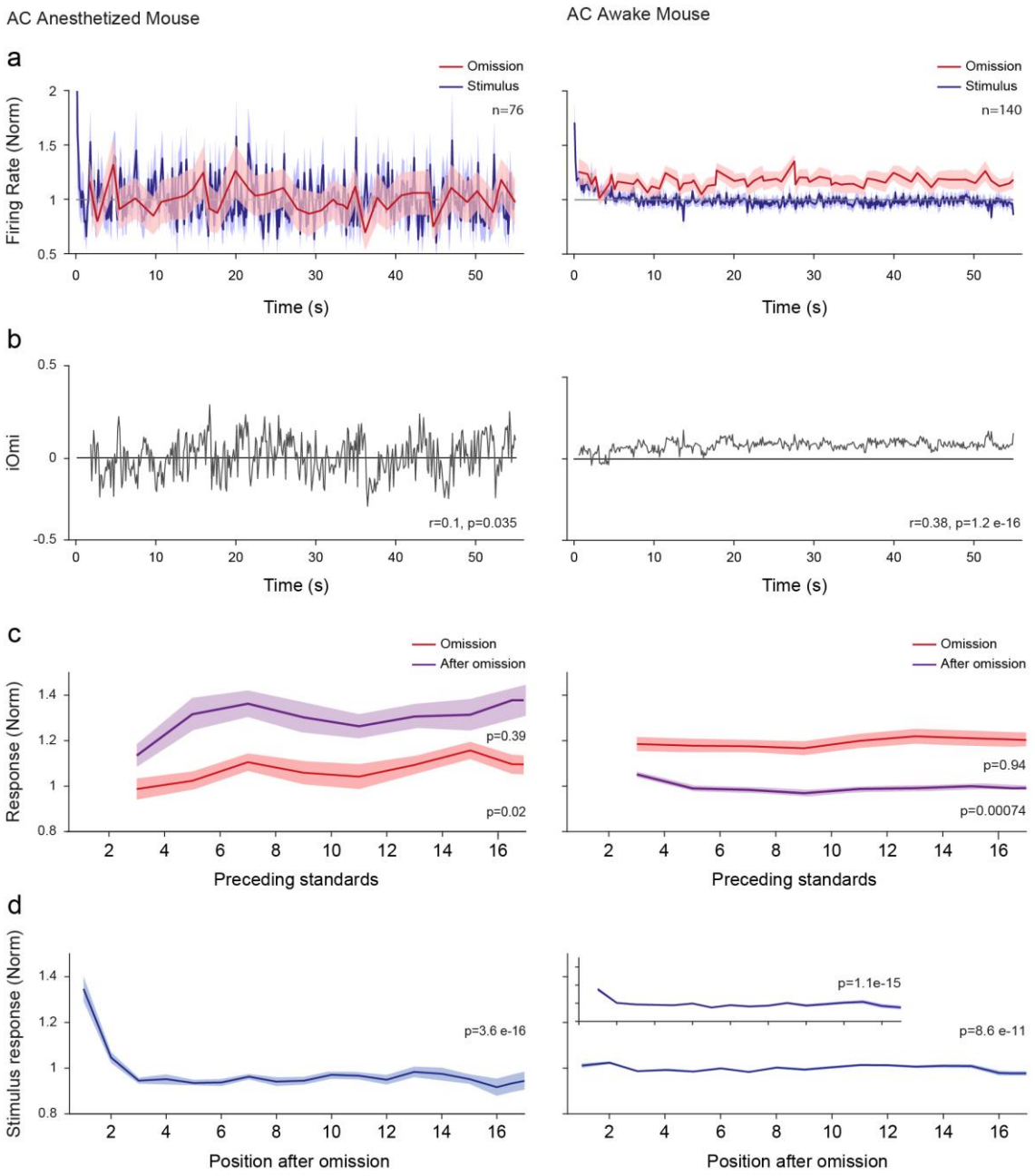

Figure 28. a. Responses of the omission sensitive cells to the standard stimulus (blue) adapt in both the anaesthetized (left) and awake (right) state. Adaptation occurs more rapidly in the anaesthetized state, reaching baseline already after ~1 s, while in the awake state two time-scales of adaptation are apparent, one very fast (1-2 stimuli, i.e. ~125-250 ms) and the second with a time-constant of ~5 s. The omission response stays relatively constant over the entire period in both conditions but is consistently larger in the awake case (p=1.2x10-22, Wilcoxon signed rank test between awake and anesthetized). **b.** The index of omission sensitivity in relation to the standard responses - iOmi - consequently increases over time in the awake case (r = 0.\38, p = 1.2x10-16, Pearson correlation), while this correlation is weaker and only borderline significant in the anaesthetized case (r = 0.1, p = 0.035). **c.** In the anaesthetized state the omission response exhibited a significant dependence on the number

of standards preceding it (p=0.02, Kruskal-Wallis Analysis of Variance). In the awake state, the omission response already starts at a high level and has no significant dependence on the number of preceding standards, possibly indicating that the dependence has already plateaued. The after-omission response shows a fast and significant decay to a plateau level. **d.** The response to the standard following an omission decayed quickly, within 2 stimuli under anaesthesia and just 1 stimulus in the awake (see inset for 20 ms analysis window, p-values based on Kruskal Wallis ANOVA). Using our standard analysis window (5-120 ms) the effect is also significant, but less pronounced, due to the brevity of the response (see Fig. 23b right).

In summary, the omission-sensitivity shows a significant slow increase over prolonged stimulation, particularly under awake conditions. A dependence on the number of preceding standards is found in anesthetised animals, but not in awake ones. The latter might indicate that the omission response has already reached a plateau, which cannot be resolved presently, as I would need to present even shorter sequences of standards (1-2).

4.2.2.9. Histological distribution of omission sensitive neurons

We analysed the distribution of omission-sensitive neurons across layers (Fig. 29a-c). In the AC of anaesthetized rats, the proportions of omission-sensitive neurons were 7.1%, 35%, and 22% for supragranular, granular and infragranular layers, respectively (Fig. 29a, burgundy bars relative to gray).

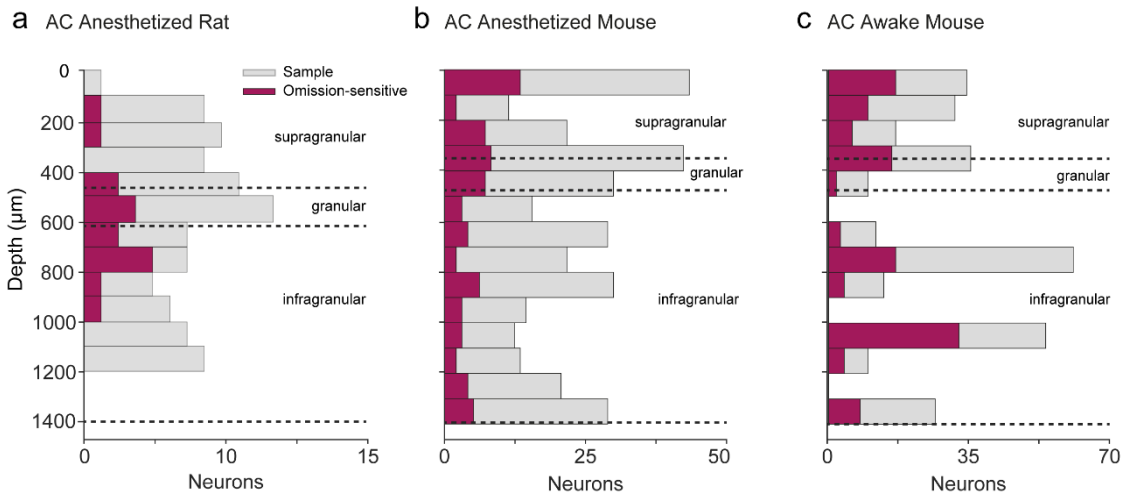

Figure 29. (**a**) Anaesthetized rat, (**b**) anaesthetized mouse and (**c**) awake mouse. Horizontal lines indicate the boundaries between supragranular (SG),

granular (G) and infragranular (IG) layers. While the fraction of omission-sensitive neurons (burgundy bars) relative to the total sample (gray bars) is low in supragranular layers in anaesthetized rats, for awake mice there is a tendency towards a higher proportion of omission-sensitive neurons is in the supragranular layers. Note that depth AC is 1400 µm thick in mice because of the oblique trajectory of the recording electrodes to the pial surface while in rat it is 1200 µm because of the orthogonal trajectory.

In the AC of anaesthetized mice, these proportions were 26% of the neurons in the supragranular layers were omission-sensitive, 30% in the granular and 19% in the infragranular (Fig. 29b, burgundy bars). For AC neurons in awake mice, these proportions are 40%, 38% and 34% for the supragranular, granular and infragranular layers (Fig. 29c, burgundy bars). I performed a bootstrapping analysis on all three recording sets, but only found a significant reduction relative to the distribution of expected counts in the supragranular layer ($p=0.003$, based on 300000 independent draws, and $p<0.05$ significance bound), although there appears to be a tendency for a higher fraction of omission-sensitive cells in supragranular layers in awake mice compared with the anaesthetized mice. However, additional research with higher density probes will be required to fully address this question.

Finally, I investigated the location of omission sensitive neurons in subfields of the AC (Fig. 30) and the IC in anaesthetized rat (Fig. 31). Location data was only available in the rat, as the recordings in the mouse were only targeted towards A1. Each recording was assigned to a dorsoventral and rostrocaudal coordinate, as I did for the previous analysis (see Fig. 22). Omission-sensitive neurons found in this study were located mostly towards the caudal areas of the AC, within the limits of A1, PAF and SRAF (Fig. 30a). In the IC, electrolytic lesions let us to observe that omission sensitive neurons were located in the cortices (Fig. 31).

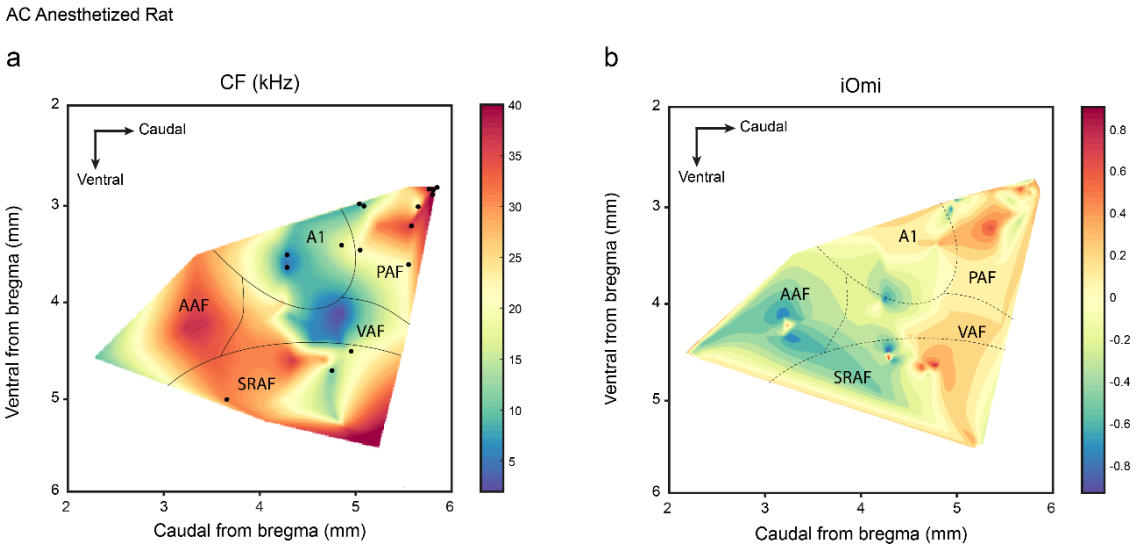

Figure 30. Distribution of omission-sensitive neurons and responses in AC fields. **a.** Distribution of characteristic frequencies across the rat AC fields. The frequency gradients were used to delineate the different auditory cortical fields. Black dots indicate the location of omission-sensitive neurons. **b.** Distribution of iOmi across the rat AC fields. Note how high iOmi neurons tend to be found in PAF and the caudal areas of VAF and SRAF.

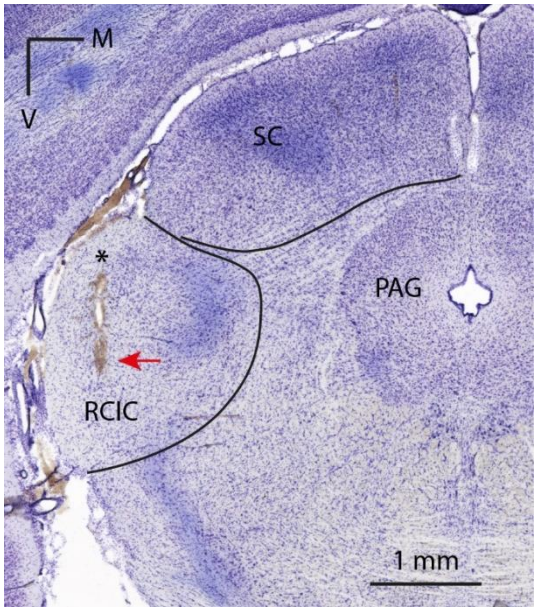

Figure 31. Histological location of recordings in IC. Coronal section showing the recording track (asterisk) and electrolytic lesion (red arrow) in the Rostral Cortex of IC (RCIC), performed with the recording tungsten electrode after recording from one neuron. Scale bar = 1 mm. Aq, aqueduct; PAG, periaqueductal gray; RCIC, rostral cortex of the IC; SC, superior colliculus; M, medial; V, ventral.

5. General Discussion and Final Remarks

The results of my thesis empirically support the main assumptions of the predictive coding theory. First, I describe the effect of ACh in the nMM and its modulation of the precision of the prediction error index. Second, I report evidence of genuine prediction/prediction errors in auditory neurons as omission responses that are widely considered as a pure prediction error signal.

The results obtained under the omission paradigm demonstrate the existence of auditory neurons that are sensitive to the omission of an expected sound. Omission responses in human studies are primarily observed at rather high presentation rates (Yabe et al., 1997; May and Tiitinen, 2010), corresponding to the presently used SOAs. On the basis of single unit recordings, my study demonstrates clear omission responses at the spiking level in the auditory system and, thus identifies a potential neuronal correlate for those omission responses previously recorded using non-invasive techniques such as EEG/MEG in human studies (Raij et al., 1997; Yabe et al., 1997; Friston, 2008; Friston and Kiebel, 2009; May and Tiitinen, 2010; Todorovic et al., 2011; Bendixen et al., 2012; Wacongne et al., 2012; Lieder et al., 2013; Cornella et al., 2015; Chennu et al., 2016; de Lange et al., 2018; Barron et al., 2020; Dercksen et al., 2020, 2022; Mori et al., 2021).

I demonstrate that robust neural activity emerges during the omission of a sound in a regular sequence of repetitive stimuli occurring at 125ms SOA in anaesthetized and awake rodents. I identified several key properties of the omission responses. These results demonstrate omission responses depend on different parameters, including repetition rate, brain state, and brain region. According to these findings, omission responses occur, as early as the midbrain level, and become stronger and more reliable at the cortical level. While they are clearly present under anesthesia, they become more pronounced in the awake condition. The omission responses are likely the earliest neuronal correlate underlying the salient perception of omitted stimuli in humans, and provide additional support for a hierarchical predictive coding framework (Friston, 2005; Den Ouden et al., 2009; Malmierca et al., 2009; Chao et al., 2018; Pérez-González et al., 2021).

These responses are consistent with prediction error signals, as these omissions result in the violation of an expected stimulus when it should have occurred. As in other sensory systems, where omission responses have been best explained by a deviation between

expected and actual visual stimuli (Fiser et al., 2016), my results are consistent with a predictive coding framework, in which sensory input is compared to an internal model of the environment to detect deviations from expectations. Since bottom-up inputs cannot account for omission responses, these results are consistent with the hypothesis that prediction is a hierarchical process encompassing subcortical and cortical neuronal circuitries and has been observed in two different species and two different brain states. Altogether, these findings are in agreement with a recent study that has combined 9.4T fMRI and high-density ECoG with a local-global auditory sequence paradigm to assess the hierarchical depth of auditory sequence processing in the marmoset brain (Malmierca and Ryugo, 2012). These authors demonstrate that the neural responses to omission cannot be explained by any modulation of feedforward propagation and should contain specific information of upcoming predictions (Malmierca and Ryugo, 2012; Choy Buentello et al., 2015). Hence, omission responses allowed us to study top-down prediction signals decoupled from bottom-up input signals, i.e., without sensory input. Such a perspective supports the notion of an endogenous neural activity that could reflect the genesis of predictions (Kraemer et al., 2005; Wang et al., 2018).

These results are strongly relevant as they report empirical evidence of predictive processing at the neuronal level. Nevertheless, the precise neural circuits underlying omission responses as a prediction or prediction error remain to be clarified. Since the auditory pathway is hierarchically organized, at each processing level neurons integrate information from multiple neurons at the level below, thus encoding increasingly abstract information over ever larger temporal and spatial scales. But the cortex is reciprocally connected, so neurons also receive input from the level above (Felleman and Van Essen, 1991; Carbajal and Malmierca, 2018).

Traditionally, it was assumed that higher levels only modulate lower levels by prioritizing the processing of some sensory inputs over others. But under the predictive coding view, following the proposal by (Mumford, 1992), the information at higher levels informs and potentially drives neurons at lower levels by signalling a prior or ‘best guess’ of their activity, defined as “prior belief”. At the lower level, the difference between the predicted and actual activity elicits a prediction error that is propagated back to the level above, where it is used to generate a new and improved “posterior belief” (Rao and Ballard, 1999; Friston, 2005; Bastos et al., 2012).

Under this framework, a strict cortical asymmetry exists between backward connections, carrying predictions, and forward connection, carrying prediction errors. Since forward connections originate in superficial, layer II/III, pyramidal neurons, and backward connections originate in deep, layer V/VI, pyramidal neurons (Felleman and Van Essen, 1991), this asymmetry has a straightforward anatomical consequence: prediction neurons reside in deep layers, and error neurons in superficial layers. Other models propose different organizations, some related with the functional asymmetry between forward and backward connections, and locating prediction and error neurons differently (Spratling, 2008a, 2008b, 2010), see Figure 32.

However, all the different hypotheses assume that predictions and errors are computed by separate neurons in different cortical layers and then, prediction and error responses are assumed to have distinct laminar profiles. That means that we cannot address, at this point, omission responses as error- or prediction units.

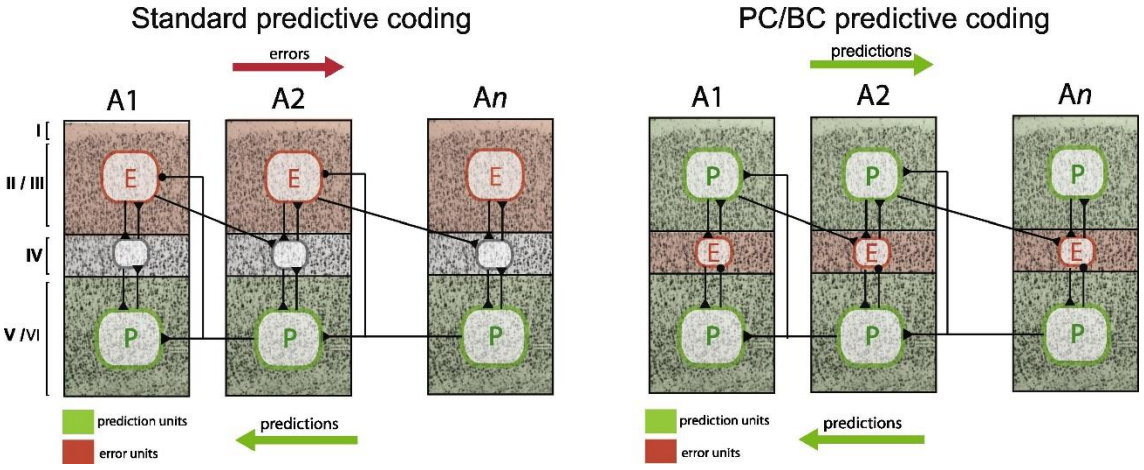

Figure 32. Different arrangements of error and expectation neurons in the AC implied by different formulations of Predictive Coding (PC). Columns denote hierarchically arranged cortical columns corresponding to primary (A1), secondary (A2) and higher order (An) auditory areas. In standard PC (left), errors flow upward and predictions downward; error units are therefore identified with superficial layers (II/III) and expectation units with deep layers (V/VI). Prediction units at higher levels can suppress error units at lower levels via top-down inhibitory connections (black circles). In Biased Competition models of PC (Spratling, 2008a, Spratling, 2008b; right), expectations flow upward and downward, error is computed at input layer IV,

prediction units suppress error units only via intracolumnar inhibition, and top-down connections are fully excitatory (black arrows). Adapted from Heilbron and Chait, 2018.

Predictive coding assumes that prediction errors are modulated by precision, i.e., the synaptic gain of the inputs that carry the prediction errors. I show that ACh modulates nMM by decreasing the standard- or deviant- tones response. One remarkable result is that the effects of ACh drive this nMM modulation on iPE but not iRS. For a further analysis of this, I also calculated the precision (inverse of the variance) of the prediction error for neurons showing decreased or increased iMM during ACh injection. In both cases, the precision was diminished revealing a clear role of ACh in prediction error modulation.

These results address another important assumption of predictive coding theory. This is that, at the same time, that prediction errors are driven through the different processing stations, they are weighted by post-synaptic gain. Interestingly the results are paradoxical in that ACh has been suggested to increase this postsynaptic gain, but in our results, ACh decreases the precision. There may be two main reasons to explain this paradoxical effect. First, we have carried out the experiments in an anaesthetized preparation, i.e. without attention, and second, the microiontophoretic injection of ACh may not mimic the natural release of ACh.

I also show that ACh exerts a global and distributed effect on AC neurons that is layer specific but field unspecific. Together, these findings reveal how ACh modulates prediction error signals differentially in the AC, likely gating these signals beyond the AC to frontal, higher cognitive regions.

These results aligns with different studies that proposes neuromodulators such as ACh as strong candidates for this task (Yu and Dayan, 2002; Bentley et al., 2004; Herrero et al., 2008; Ayala et al., 2016). It also supports earlier circuit level theories that have proposed ACh as a key element for learning and memory processes by changing the cortex to “read-out” to “read-in” mode. This process is modulated by enhancing the sensory-evoked afferent responses and suppressing the internal cortical processing (Hasselmo and McGaughy, 2004; Moran et al., 2013).

More specifically, ACh increases nMM in the AC reducing the firing rate in response to either 'deviants' or 'standards'. Previous studies shows a different effect in the IC, as ACh decreases nMM by increasing the responses to the 'standard' tones (Ayala and Malmierca, 2015a). These divergent effects may be explained by the different connectivity of both auditory areas (Fig. 33). While the AC receives its cholinergic input from the basal forebrain (BF), the IC is innervated by the pedunculopontine (PPT) and laterodorsal tegmental (LDT) regions in the brainstem. This intersection of auditory and cholinergic nuclei creates an intricate network involving ascending and descending projections that ultimately modulate the processing of auditory deviance detection.

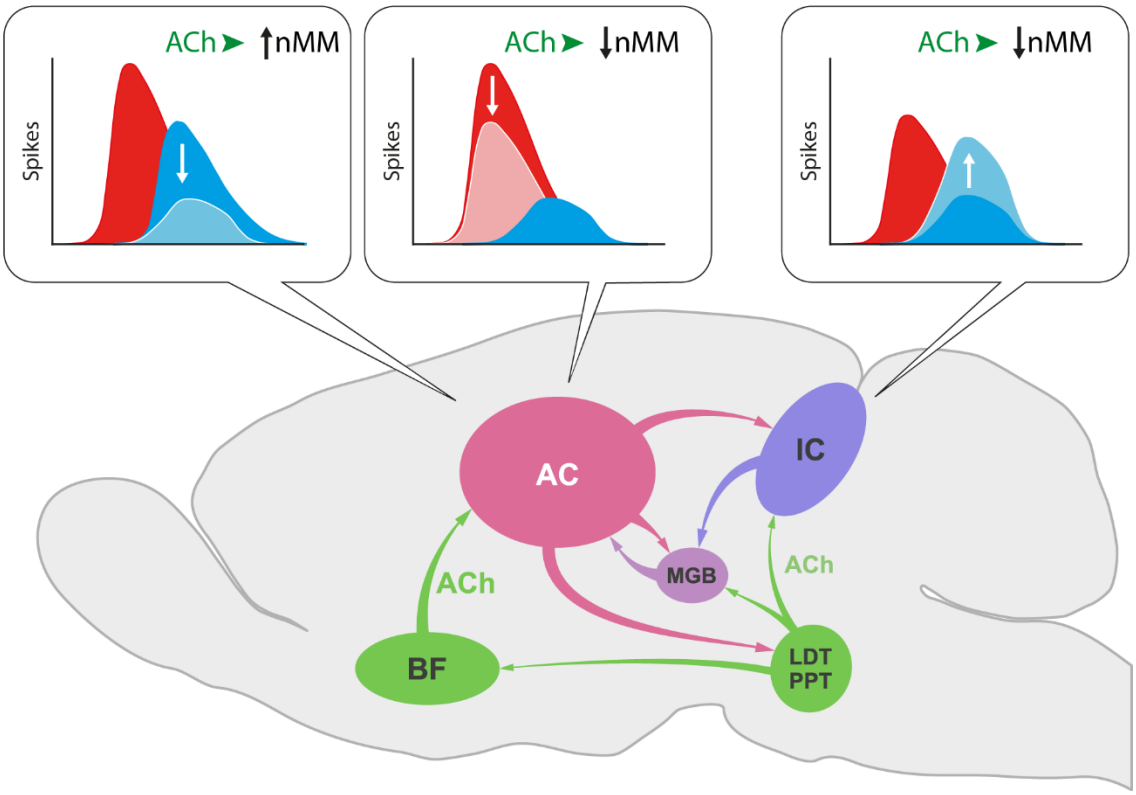

Figure 33. Effect of ACh on nMM in auditory midbrain and cortex. ACh increases nMM in the AC reducing the firing rate in response to either 'deviants' or 'standards', while it shows a different effect in the IC, as ACh decreases nMM by increasing the responses to the 'standard' tones (Ayala and Malmierca, 2015a).

6. Conclusions

Thus, considering the results of both studies, I conclude that:

I. A subset of neurons in the auditory brain respond to omitted tones in an otherwise regular pattern of standard tones.

II. Omission responses were found at different presentation rates but are more evident and have a higher probability of appearance at faster repetition rates of 125ms.

III. Omission responses are present at the level of the inferior colliculus at anaesthetized animals that increases as ascending in the auditory pathway hierarchical areas.

IV. Omission responses are significantly greater for random – rather than periodic presentations in the auditory cortex of awake mice.

V. Acetylcholine modulates neuronal mismatch responses in the auditory cortex of anaesthetized rats. This modulation is driven by decreasing standard- or deviant tone responses.

VI. Acetylcholine can scale or reduce prediction error but not repetition suppression.

VII. Acetylcholine minimizes the precision of the prediction error in the auditory cortex.

7. Bibliography

Adams RA, Stephan KE, Brown HR, Frith CD, Friston KJ (2013) The computational anatomy of psychosis. Front psychiatry 4 Available at: https://pubmed.ncbi.nlm.nih.gov/23750138/ [Accessed May 26, 2023].

Allen Institute for Brain Science (2011) Allen Reference Atlas. Mouse Brain [brain atlas] Available at: http://atlas.brain-map.org/atlas?atlas=1&plate=100960228#atlas=1&plate=100960069&resolution=8.38&x=6782&y=4142&zoom=-3&z=6.

Antunes FM, Malmierca MS (2011) Effect of auditory cortex deactivation on stimulus-specific adaptation in the medial geniculate body. J Neurosci 31:17306–17316.

Antunes FM, Nelken I, Covey E, Malmierca MS (2010) Stimulus-specific adaptation in the auditory thalamus of the anesthetized rat. PLoS One 5 Available at: https://pubmed.ncbi.nlm.nih.gov/21124913/ [Accessed February 25, 2022].

Ayala YA, Malmierca Dr. MS (2013) Stimulus-specific adaptation and deviance detection in the inferior colliculus. Front Neural Circuits 6 Available at: https://pubmed.ncbi.nlm.nih.gov/23335883/ [Accessed February 25, 2022].

Ayala YA, Malmierca MS (2015a) Cholinergic Modulation of Stimulus-Specific Adaptation in the Inferior Colliculus. J Neurosci 35:12261–12272 Available at: https://www.jneurosci.org/content/35/35/12261 [Accessed May 9, 2023].

Ayala YA, Malmierca MS (2015b) Cholinergic modulation of stimulus-specific adaptation in the inferior colliculus. J Neurosci 35:12261–12272.

Ayala YA, Pérez-González D, Malmierca MS (2016) Stimulus-specific adaptation in the inferior colliculus: The role of excitatory, inhibitory and modulatory inputs. Biol Psychol 116:10–22 Available at: https://pubmed.ncbi.nlm.nih.gov/26159810/ [Accessed March 20, 2022].

Barron HC, Auksztulewicz R, Friston K (2020) Prediction and memory: A predictive coding account. Prog Neurobiol 192 Available at: https://pubmed.ncbi.nlm.nih.gov/32446883/ [Accessed March 16, 2022].

Bartha-Doering L, Deuster D, Giordano V, Am Zehnhoff-Dinnesen A, Dobel C (2015) A systematic review of the mismatch negativity as an index for auditory sensory memory: From basic research to clinical and developmental perspectives. Psychophysiology 52:1115–1130 Available at: https://pubmed.ncbi.nlm.nih.gov/26096130/ [Accessed May 23, 2023].

Bastos AM, Usrey WM, Adams RA, Mangun GR, Fries P, Friston KJ (2012) Canonical Microcircuits for Predictive Coding. Neuron 76:695–711 Available at: /pmc/articles/PMC3777738/ [Accessed July 5, 2021].

Bendixen A, SanMiguel I, Schröger E (2012) Early electrophysiological indicators for predictive processing in audition: A review. Int J Psychophysiol 83:120–131.

Bendixen A, Schröger E, Winkler I (2009) I heard that coming: Event-related potential evidence for stimulus-driven prediction in the auditory system. J Neurosci 29:8447–8451 Available at: /pmc/articles/PMC6665649/ [Accessed July 5, 2021].

Bentley P, Husain M, Dolan RJ (2004) Effects of cholinergic enhancement on visual stimulation, spatial attention, and spatial working memory. Neuron 41:969–982 Available at: https://pubmed.ncbi.nlm.nih.gov/15046728/ [Accessed May 29, 2023].

Braga A, Schönwiesner M (2022) Neural Substrates and Models of Omission Responses and Predictive Processes. Front Neural Circuits 16 Available at: /pmc/articles/PMC8844463/ [Accessed February 25, 2022].

Carbajal G V., Malmierca MS (2018) The Neuronal Basis of Predictive Coding Along the Auditory Pathway: From the Subcortical Roots to Cortical Deviance Detection. Trends Hear 22 Available at: https://pubmed.ncbi.nlm.nih.gov/30022729/ [Accessed February 25, 2022].

Carbajal G V, Malmierca MS (2020) Novelty Processing in the Auditory System: Detection, Adaptation or Expectation? In: The Senses: A Comprehensive Reference, 2nd Editio. (Fritzsch B, Gothe B, eds), pp 749–776. Elsevier. Available at: https://linkinghub.elsevier.com/retrieve/pii/B9780128093245241540.

Casado-Román L, Carbajal G V., Pérez-González D, Malmierca MS (2020) Prediction

error signaling explains neuronal mismatch responses in the medial prefrontal cortex. PLoS Biol 18 Available at: https://pubmed.ncbi.nlm.nih.gov/33347436/ [Accessed February 25, 2022].

Chao ZC, Takaura K, Wang L, Fujii N, Dehaene S (2018) Large-Scale Cortical Networks for Hierarchical Prediction and Prediction Error in the Primate Brain. Neuron 100:1252-1266.e3 Available at: https://pubmed.ncbi.nlm.nih.gov/30482692/ [Accessed February 28, 2022].

Chennu S, Noreika V, Gueorguiev D, Shtyrov Y, Bekinschtein TA, Henson R (2016) Silent expectations: Dynamic causal modeling of cortical prediction and attention to sounds that weren't. J Neurosci 36:8305–8316 Available at: https://pubmed.ncbi.nlm.nih.gov/27511005/ [Accessed July 5, 2021].

Choy Buentello D, Bishop DC, Oliver DL (2015) Differential distribution of GABA and glycine terminals in the inferior colliculus of rat and mouse. J Comp Neurol 523:2683–2697 Available at: https://pubmed.ncbi.nlm.nih.gov/25976159/ [Accessed March 20, 2022].

Clark A (2013) Whatever next? Predictive brains, situated agents, and the future of cognitive science. Behav Brain Sci 36:181–204 Available at: https://pubmed.ncbi.nlm.nih.gov/23663408/ [Accessed May 26, 2023].

Cornella M, Bendixen A, Grimm S, Leung S, Schröger E, Escera C (2015) Spatial auditory regularity encoding and prediction: Human middle-latency and long-latency auditory evoked potentials. Brain Res 1626:21–30 Available at: https://pubmed.ncbi.nlm.nih.gov/25912975/ [Accessed February 25, 2022].

de Lange FP, Heilbron M, Kok P (2018) How Do Expectations Shape Perception? Trends Cogn Sci 22:764–779 Available at: https://pubmed.ncbi.nlm.nih.gov/30122170/ [Accessed March 16, 2022].

Den Ouden HEM, Friston KJ, Daw ND, McIntosh AR, Stephan KE (2009) A dual role for prediction error in associative learning. Cereb Cortex 19:1175–1185 Available at: www.vislab.ucl.ac.uk/Cogent/index.html [Accessed February 25, 2022].

Den Ouden HEM, Kok P, de Lange FP (2012) How prediction errors shape perception,

attention, and motivation. Front Psychol 3 Available at: https://pubmed.ncbi.nlm.nih.gov/23248610/ [Accessed February 25, 2022].

Dercksen TT, Widmann A, Scharf F, Wetzel N (2022) Sound omission related brain responses in children. Dev Cogn Neurosci 53 Available at: https://pubmed.ncbi.nlm.nih.gov/34923314/ [Accessed February 25, 2022].

Dercksen TT, Widmann A, Schröger E, Wetzel N (2020) Omission related brain responses reflect specific and unspecific action-effect couplings. Neuroimage 215 Available at: https://pubmed.ncbi.nlm.nih.gov/32289452/ [Accessed February 25, 2022].

Duque D, Malmierca MS (2015) Stimulus-specific adaptation in the inferior colliculus of the mouse: anesthesia and spontaneous activity effects. Brain Struct Funct 220:3385–3398 Available at: https://pubmed.ncbi.nlm.nih.gov/25115620/ [Accessed March 20, 2022].

Escera C, Malmierca MS (2014) The auditory novelty system: An attempt to integrate human and animal research. Psychophysiology 51:111–123 Available at: https://pubmed.ncbi.nlm.nih.gov/24423134/ [Accessed July 5, 2021].

Feldman H, Friston KJ (2010) Attention, uncertainty, and free-energy. Front Hum Neurosci 4 Available at: https://pubmed.ncbi.nlm.nih.gov/21160551/ [Accessed May 26, 2023].

Felleman DJ, Van Essen DC (1991) Distributed hierarchical processing in the primate cerebral cortex. Cereb Cortex 1:1–47 Available at: https://academic.oup.com/cercor/article/1/1/1/408896 [Accessed June 13, 2023].

Fields C, Friston K, Glazebrook JF, Levin M (2022) A free energy principle for generic quantum systems. Prog Biophys Mol Biol 173:36–59 Available at: https://pubmed.ncbi.nlm.nih.gov/35618044/ [Accessed May 26, 2023].

Fiser A, Mahringer D, Oyibo HK, Petersen A V., Leinweber M, Keller GB (2016) Experience-dependent spatial expectations in mouse visual cortex. Nat Neurosci 19:1658–1664.

Fisher DJ, Campbell DJ, Abriel SC, Ells EML, Rudolph ED, Tibbo PG (2018) Auditory Mismatch Negativity and P300a Elicited by the “Optimal” Multi-feature Paradigm in Early Schizophrenia. Clin EEG Neurosci 49:238–247 Available at: https://pubmed.ncbi.nlm.nih.gov/29502452/ [Accessed May 23, 2023].

Fishman YI (2014) The mechanisms and meaning of the mismatch negativity. Brain Topogr 27:500–526 Available at: https://link.springer.com/article/10.1007/s10548-013-0337-3 [Accessed July 5, 2021].

Fishman YI, Steinschneider M (2012) Searching for the mismatch negativity in primary auditory cortex of the awake monkey: deviance detection or stimulus specific adaptation? J Neurosci 32:15747–15758 Available at: https://pubmed.ncbi.nlm.nih.gov/23136414/ [Accessed June 12, 2023].

Fonken YM, Mukerji A, Jimenez R, Lin J, Brunner P, Schalk G, Knight RT (2019) Unexpected sound omissions are signaled in human posterior superior temporal gyrus: an intracranial study. bioRxiv:733212 Available at: https://www.biorxiv.org/content/10.1101/733212v1 [Accessed March 18, 2022].

Friston K (2002) Functional integration and inference in the brain. Prog Neurobiol 68:113–143.

Friston K (2005) A theory of cortical responses. Philos Trans R Soc B Biol Sci 360:815–836 Available at: https://pubmed.ncbi.nlm.nih.gov/15937014/ [Accessed July 5, 2021].

Friston K (2008) Hierarchical Models in the Brain. Cit Frist K 4:1000211 Available at: www.ploscompbiol.org [Accessed March 16, 2022].

Friston K (2010) The free-energy principle: a unified brain theory? Nat Rev Neurosci 2010 112 11:127–138 Available at: https://www.nature.com/articles/nrn2787 [Accessed May 26, 2023].

Friston K (2012) Predictive coding, precision and synchrony. Cogn Neurosci 3:238–239.

Friston K, Kiebel S (2009) Cortical circuits for perceptual inference. Neural Networks

22:1093–1104 Available at: /pmc/articles/PMC2796185/ [Accessed July 5, 2021].

Friston K, Kilner J, Harrison L (2006) A free energy principle for the brain. J Physiol Paris 100:70–87.

Friston K, Moran RJ, Nagai Y, Taniguchi T, Gomi H, Tenenbaum J (2021) World model learning and inference. Neural Networks 144:573–590.

Friston K, Schwartenbeck P, FitzGerald T, Moutoussis M, Behrens T, Dolan RJ (2014) The anatomy of choice: dopamine and decision-making. Philos Trans R Soc Lond B Biol Sci 369 Available at: https://pubmed.ncbi.nlm.nih.gov/25267823/ [Accessed May 26, 2023].

Friston KJ, Shiner T, FitzGerald T, Galea JM, Adams R, Brown H, Dolan RJ, Moran R, Stephan KE, Bestmann S (2012) Dopamine, Affordance and Active Inference. PLOS Comput Biol 8:e1002327 Available at: https://journals.plos.org/ploscompbiol/article?id=10.1371/journal.pcbi.1002327 [Accessed May 26, 2023].

Friston KJ, Stephan KE (2007) Free-energy and the brain. Synthese 159:417–458 Available at: https://link.springer.com/article/10.1007/s11229-007-9237-y [Accessed May 26, 2023].

Fritz JB, Elhilali M, David S V., Shamma SA (2007) Does attention play a role in dynamic receptive field adaptation to changing acoustic salience in A1? Hear Res 229:186–203 Available at: https://pubmed.ncbi.nlm.nih.gov/17329048/ [Accessed May 23, 2023].

Garrido MI, Friston KJ, Kiebel SJ, Stephan KE, Baldeweg T, Kilner JM (2008) The functional anatomy of the MMN: a DCM study of the roving paradigm. Neuroimage 42:936–944 Available at: https://pubmed.ncbi.nlm.nih.gov/18602841/ [Accessed February 25, 2022].

Garrido MI, Kilner JM, Stephan KE, Friston KJ (2009) The mismatch negativity: A review of underlying mechanisms. Clin Neurophysiol 120:453–463 Available at: https://pubmed.ncbi.nlm.nih.gov/19181570/ [Accessed June 28, 2021].

Goris J, Braem S, Nijhof AD, Rigoni D, Deschrijver E, Van de Cruys S, Wiersema JR, Brass M (2018) Sensory Prediction Errors Are Less Modulated by Global Context in Autism Spectrum Disorder. Biol Psychiatry Cogn Neurosci Neuroimaging 3:667–674.

Grimm S, Escera C (2012) Auditory deviance detection revisited: evidence for a hierarchical novelty system. Int J Psychophysiol 85:88–92 Available at: https://pubmed.ncbi.nlm.nih.gov/21669238/ [Accessed June 12, 2023].

Hara K, Harris RA (2002) The anesthetic mechanism of urethane: the effects on neurotransmitter-gated ion channels. Anesth Analg 94:313–318 Available at: https://pubmed.ncbi.nlm.nih.gov/11812690/ [Accessed March 3, 2022].

Hasselmo ME, McGaughy J (2004) High acetylcholine levels set circuit dynamics for attention and encoding and low acetylcholine levels set dynamics for consolidation. Prog Brain Res 145:207–231 Available at: https://pubmed.ncbi.nlm.nih.gov/14650918/ [Accessed May 29, 2023].

Heilbron M, Chait M (2018) Great Expectations: Is there Evidence for Predictive Coding in Auditory Cortex? Neuroscience 389:54–73 Available at: https://pubmed.ncbi.nlm.nih.gov/28782642/ [Accessed February 25, 2022].

Heldmann M, Münte TF, Paracka L, Beyer F, Brüggemann N, Saryyeva A, Rasche D, Krauss JK, Tronnier VM (2017) Human subthalamic nucleus - Automatic auditory change detection as a basis for action selection. Neuroscience 355:141–148 Available at: https://pubmed.ncbi.nlm.nih.gov/28504196/ [Accessed May 23, 2023].

Herrero JL, Roberts MJ, Delicato LS, Gieselmann MA, Dayan P, Thiele A (2008) Acetylcholine contributes through muscarinic receptors to attentional modulation in V1. Nat 2008 4547208 454:1110–1114 Available at: https://www.nature.com/articles/nature07141 [Accessed May 26, 2023].

Hohwy J (2017) Priors in perception: Top-down modulation, Bayesian perceptual learning rate, and prediction error minimization. Conscious Cogn 47:75–85 Available at: https://pubmed.ncbi.nlm.nih.gov/27663763/ [Accessed May 26, 2023].

Horváth J, Müller D, Weise A, Schröger E (2010) Omission mismatch negativity builds up late. Neuroreport 21:537–541.

Hudac CM, DesChamps TD, Arnett AB, Cairney BE, Ma R, Webb SJ, Bernier RA (2018) Early enhanced processing and delayed habituation to deviance sounds in autism spectrum disorder. Brain Cogn 123:110–119 Available at: https://pubmed.ncbi.nlm.nih.gov/29550506/ [Accessed May 23, 2023].

Hullfish J, Sedley W, Vanneste S (2019) Prediction and perception: Insights for (and from) tinnitus. Neurosci Biobehav Rev 102:1–12.

Jääskeläinen IP, Ahveninen J, Bonmassar G, Dale AM, Ilmoniemi RJ, Levänen S, Lin FH, May P, Melcher J, Stufflebeam S, Tiitinen H, Belliveau JW (2004) Human posterior auditory cortex gates novel sounds to consciousness. Proc Natl Acad Sci U S A 101:6809–6814 Available at: https://pubmed.ncbi.nlm.nih.gov/15096618/ [Accessed May 19, 2023].

Jacobsen T, Horenkamp T, Schröger E (2003a) Preattentive memory-based comparison of sound intensity. Audiol Neurootol 8:338–346 Available at: https://pubmed.ncbi.nlm.nih.gov/14566104/ [Accessed May 28, 2023].

Jacobsen T, Schröger E (2001) Is there pre-attentive memory-based comparison of pitch? Psychophysiology 38:723–727 Available at: https://pubmed.ncbi.nlm.nih.gov/11446587/ [Accessed May 28, 2023].

Jacobsen T, Schröger E, Horenkamp T, Winkler I (2003b) Mismatch negativity to pitch change: Varied stimulus proportions in controlling effects of neural refractoriness on human auditory event-related brain potentials. Neurosci Lett 344:79–82 Available at: https://pubmed.ncbi.nlm.nih.gov/12782332/ [Accessed May 28, 2023].

Jiang Y, Komatsu M, Chen Y, Xie R, Zhang K, Xia Y, Gui P, Liang Z, Wang L (2022) Constructing the hierarchy of predictive auditory sequences in the marmoset brain. Elife 11 Available at: https://elifesciences.org/articles/74653 [Accessed February 25, 2022].

Kirino E, Hayakawa Y, Inami R, Inoue R, Aoki S (2019) Simultaneous fMRI-EEG-DTI

recording of MMN in patients with schizophrenia. PLoS One 14 Available at: https://pubmed.ncbi.nlm.nih.gov/31071097/ [Accessed May 30, 2023].

Koelsch S, Heinke W, Sammler D, Olthoff D (2006) Auditory processing during deep propofol sedation and recovery from unconsciousness. Clin Neurophysiol 117:1746–1759 Available at: https://pubmed.ncbi.nlm.nih.gov/16807099/ [Accessed May 23, 2023].

Koelsch S, Vuust P, Friston K (2019) Predictive Processes and the Peculiar Case of Music. Trends Cogn Sci 23:63–77 Available at: https://doi.org/10.1016/j.tics.2018.10.006.

Kraemer DJM, Macrae CN, Green AE, Kelley WM (2005) Musical imagery: sound of silence activates auditory cortex. Nature 434:158 Available at: https://pubmed.ncbi.nlm.nih.gov/15758989/ [Accessed February 28, 2022].

Kreitschmann-Andermahr I, Rosburg T, Meier T, Volz HP, Nowak H, Sauer H (1999) Impaired sensory processing in male patients with schizophrenia—a magnetoencephalographic study of auditory mismatch detection. Schizophr Res 35:121–129.

Kriegeskorte N, Simmons WK, Bellgowan PS, Baker CI (2009) Circular analysis in systems neuroscience: The dangers of double dipping. Nat Neurosci 12:535–540.

Lieder F, Daunizeau J, Garrido MI, Friston KJ, Stephan KE (2013) Modelling trial-by-trial changes in the mismatch negativity. PLoS Comput Biol 9 Available at: https://pubmed.ncbi.nlm.nih.gov/23436989/ [Accessed March 16, 2022].

Malmierca MS, Cristaudo S, Pérez-González D, Covey E (2009) Stimulus-specific adaptation in the inferior colliculus of the anesthetized rat. J Neurosci 29:5483–5493 Available at: https://pubmed.ncbi.nlm.nih.gov/19403816/ [Accessed February 28, 2022].

Malmierca MS, Niño-Aguillón BE, Nieto-Diego J, Porteros Á, Pérez-González D, Escera C (2019) Pattern-sensitive neurons reveal encoding of complex auditory regularities in the rat inferior colliculus. Neuroimage.

Malmierca MS, Ryugo DK (2012) Auditory System. In: The Mouse Nervous System, pp 607–645. Elsevier. Available at: https://linkinghub.elsevier.com/retrieve/pii/B978012369497310024X [Accessed March 21, 2022].

May P, Tiitinen H, Ilmoniemi RJ, Nyman G, Taylor JG, Näätänen R (1999) Frequency change detection in human auditory cortex. J Comput Neurosci 6:99–120 Available at: https://pubmed.ncbi.nlm.nih.gov/10333158/ [Accessed May 19, 2023].

May PJC, Tiitinen H (2010) Mismatch negativity (MMN), the deviance-elicited auditory deflection, explained. Psychophysiology 47:66–122 Available at: https://pubmed.ncbi.nlm.nih.gov/19686538/ [Accessed July 5, 2021].

Miasnikov AA, Chen JC, Weinberger NM (2008) Specific auditory memory induced by nucleus basalis stimulation depends on intrinsic acetylcholine. Neurobiol Learn Mem 90:443–454 Available at: https://pubmed.ncbi.nlm.nih.gov/18573347/ [Accessed May 29, 2023].

Minks E, Jurák P, Chládek J, Chrastina J, Halámek J, Shaw DJ, Bareš M (2014) Mismatch negativity-like potential (MMN-like) in the subthalamic nuclei in Parkinson's disease patients. J Neural Transm 121:1507–1522 Available at: https://pubmed.ncbi.nlm.nih.gov/24809684/ [Accessed May 23, 2023].

Moran RJ, Campo P, Symmonds M, Stephan KE, Dolan RJ, Friston KJ (2013) Free energy, precision and learning: the role of cholinergic neuromodulation. J Neurosci 33:8227–8236 Available at: https://pubmed.ncbi.nlm.nih.gov/23658161/ [Accessed May 26, 2023].

Mori Y, Hoshino H, Osakabe Y, Wada T, Kanno K, Shiga T, Itagaki S, Miura I, Yabe H (2021) Omission mismatch negativity of speech sounds reveals a functionally impaired temporal window of integration in schizophrenia. Clin Neurophysiol 132:1144–1150 Available at: https://pubmed.ncbi.nlm.nih.gov/33774379/ [Accessed February 28, 2022].

Morlet D, Fischer C (2014) MMN and novelty P3 in coma and other altered states of consciousness: a review. Brain Topogr 27:467–479 Available at:

https://pubmed.ncbi.nlm.nih.gov/24281786/ [Accessed May 23, 2023].

Mumford D (1992) On the computational architecture of the neocortex II The role of cortico-cortical loops. Biol Cybern 66:241–251.

Näätänen R (1990) The role of attention in auditory information processing as revealed by event-related potentials and other brain measures of cognitive function. Behav Brain Sci 13:201–233.

Näätänen R (1992). (1992) Attention and brain function. Hillsdale, NJ: Erlbaum.

Näätänen R, Alho K (1995) Generators of electrical and magnetic mismatch responses in humans. Brain Topogr 7:315–320 Available at: https://pubmed.ncbi.nlm.nih.gov/7577329/ [Accessed May 19, 2023].

Näätänen R, Astikainen P, Ruusuvirta T, Huotilainen M (2010) Automatic auditory intelligence: An expression of the sensory–cognitive core of cognitive processes. Brain Res Rev 64:123–136.

Näätänen R, Gaillard AWK, Mäntysalo S (1978) Early selective-attention effect on evoked potential reinterpreted. Acta Psychol (Amst) 42:313–329 Available at: https://pubmed.ncbi.nlm.nih.gov/685709/ [Accessed February 25, 2022].

Näätänen R, Michie PT (1979) Early selective-attention effects on the evoked potential: a critical review and reinterpretation. Biol Psychol 8:81–136 Available at: https://pubmed.ncbi.nlm.nih.gov/465623/ [Accessed May 19, 2023].

Näätänen R, Paavilainen P, Rinne T, Alho K (2007) The mismatch negativity (MMN) in basic research of central auditory processing: A review. Clin Neurophysiol 118:2544–2590.

Näätänen R, Winkler I (1999) The concept of auditory stimulus representation in cognitive neuroscience. Psychol Bull 125:826–859.

Nashida T, Yabe H, Sato Y, Hiruma T, Sutoh T, Shinozaki N, Kaneko S (2000) Automatic auditory information processing in sleep. Sleep 23:821–828 Available at: https://pubmed.ncbi.nlm.nih.gov/11007449/ [Accessed May 23, 2023].

Nieto-Diego J, Malmierca MS (2016) Topographic Distribution of Stimulus-Specific Adaptation across Auditory Cortical Fields in the Anesthetized Rat. PLoS Biol 14:e1002397 Available at: http://www.ncbi.nlm.nih.gov/pubmed/26950883 [Accessed June 14, 2019].

Parr T, Benrimoh DA, Vincent P, Friston KJ (2018) Precision and False Perceptual Inference. Front Integr Neurosci 12 Available at: https://pubmed.ncbi.nlm.nih.gov/30294264/ [Accessed May 26, 2023].

Parr T, Friston KJ (2019) Attention or salience? Curr Opin Psychol 29:1–5.

Parras GG, Nieto-Diego J, Carbajal G V., Valdés-Baizabal C, Escera C, Malmierca MS (2017) Neurons along the auditory pathway exhibit a hierarchical organization of prediction error. Nat Commun 8 Available at: www.nature.com/naturecommunications [Accessed June 13, 2019].

Paxinos G, Watson C, Diego S, Boston L, York N (1997) The Rat Brainin Stereotaxic Coordinates Academic Press.

Pérez-González D, Parras GG, Morado-Díaz CJ, Aedo-Sánchez C, Carbajal G V., Malmierca MS (2021) Deviance detection in physiologically identified cell types in the rat auditory cortex. Hear Res 399 Available at: https://pubmed.ncbi.nlm.nih.gov/32482383/ [Accessed February 25, 2022].

Polley DB, Read HL, Storace DA, Merzenich MM (2007) Multiparametric auditory receptive field organization across five cortical fields in the albino rat. J Neurophysiol 97:3621–3638 Available at: https://pubmed.ncbi.nlm.nih.gov/17376842/ [Accessed June 21, 2022].

Quaedflieg CW, Münte S, Kalso E, Sambeth A (2014) Effects of remifentanil on processing of auditory stimuli: a combined MEG/EEG study. J Psychopharmacol 28:39–48 Available at: https://pubmed.ncbi.nlm.nih.gov/24257810/ [Accessed May 23, 2023].

Raij T, McEvoy L, Mäkelä JP, Hari R (1997) Human auditory cortex is activated by omission of auditory stimuli. Brain Res 745:134–143 Available at: https://pubmed.ncbi.nlm.nih.gov/9037402/ [Accessed July 5, 2021].

Ranganath C, Rainer G (2003) Neural mechanisms for detecting and remembering novel events. Nat Rev Neurosci 4:193–202 Available at: https://pubmed.ncbi.nlm.nih.gov/12612632/ [Accessed May 23, 2023].

Rao RPNN, Ballard DH (1999) Predictive coding in the visual cortex: a functional interpretation of some extra-classical receptive-field effects. Nat Neurosci 2:79–87 Available at: http://neurosci.nature.com [Accessed July 5, 2021].

Rodriguez RA, Bussière M, Froeschl M, Nathan HJ (2014) Auditory-evoked potentials during coma: do they improve our prediction of awakening in comatose patients? J Crit Care 29:93–100 Available at: https://pubmed.ncbi.nlm.nih.gov/24125771/ [Accessed May 23, 2023].

Ruhnau P, Herrmann B, Schröger E (2012) Finding the right control: The mismatch negativity under investigation. Clin Neurophysiol 123:507–512.

Rüsseler J, Altenmüller E, Nager W, Kohlmetz C, Münte TF (2001) Event-related brain potentials to sound omissions differ in musicians and non-musicians. 308:33–36 Available at: www.elsevier.com/locate/neulet [Accessed February 25, 2022].

SanMiguel I, Saupe K, Schröger E (2013a) I know what is missing here: Electrophysiological prediction error signals elicited by omissions of predicted "what" but not "when." Front Hum Neurosci 7 Available at: https://pubmed.ncbi.nlm.nih.gov/23908618/ [Accessed July 5, 2021].

SanMiguel I, Widmann A, Bendixen A, Trujillo-Barreto N, Schröger E (2013b) Hearing silences: human auditory processing relies on preactivation of sound-specific brain activity patterns. J Neurosci 33:8633–8639 Available at: https://pubmed.ncbi.nlm.nih.gov/23678108/ [Accessed June 22, 2022].

Schröger E, Kotz SA, SanMiguel I (2015) Bridging prediction and attention in current research on perception and action. Brain Res 1626:1–13 Available at: https://pubmed.ncbi.nlm.nih.gov/26348988/ [Accessed February 27, 2022].

Schröger E, Wolff C (1996) Mismatch response of the human brain to changes in sound location. Neuroreport 7:3005–3008 Available at: https://pubmed.ncbi.nlm.nih.gov/9116228/ [Accessed May 28, 2023].

Schwartz S, Shinn-Cunningham B, Tager-Flusberg H (2018) Meta-analysis and systematic review of the literature characterizing auditory mismatch negativity in individuals with autism. Neurosci Biobehav Rev 87:106–117 Available at: https://pubmed.ncbi.nlm.nih.gov/29408312/ [Accessed May 23, 2023].

Sculthorpe LD, Ouellet DR, Campbell KB (2009) MMN elicitation during natural sleep to violations of an auditory pattern. Brain Res 1290:52–62.

Sedley W, Gander PE, Kumar S, Kovach CK, Oya H, Kawasaki H, Howard MA, Griffiths TD (2016) Neural signatures of perceptual inference. Elife 5.

Solomon SS, Tang H, Sussman E, Kohn A (2021) Limited Evidence for Sensory Prediction Error Responses in Visual Cortex of Macaques and Humans. Cereb Cortex (New York, NY) 31:3136 Available at: /pmc/articles/PMC8599921/ [Accessed June 5, 2023].

Spratling MW (2008a) Predictive coding as a model of biased competition in visual attention. Vision Res 48:1391–1408.

Spratling MW (2008b) Reconciling predictive coding and biased competition models of cortical function. Front Comput Neurosci 2 Available at: https://pubmed.ncbi.nlm.nih.gov/18978957/ [Accessed June 13, 2023].

Spratling MW (2010) Predictive coding as a model of response properties in cortical area V1. J Neurosci 30:3531–3543 Available at: https://pubmed.ncbi.nlm.nih.gov/20203213/ [Accessed June 13, 2023].

Stefanics G, Astikainen P, Czigler I (2015) Visual mismatch negativity (vMMN): A prediction error signal in the visual modality. Front Hum Neurosci 8 Available at: /pmc/articles/PMC4302941/ [Accessed July 5, 2021].

Stekelenburg JJ, Vroomen J (2015) Predictive coding of visual-auditory and motor-auditory events: An electrophysiological study. Brain Res 1626:88–96 Available at: https://pubmed.ncbi.nlm.nih.gov/25641042/ [Accessed May 9, 2023].

Strauss M, Sitt JD, King JR, Elbaz M, Azizi L, Buiatti M, Naccache L, Van Wassenhove V, Dehaene S (2015) Disruption of hierarchical predictive coding

during sleep. Proc Natl Acad Sci U S A 112:E1353–E1362 Available at: https://pubmed.ncbi.nlm.nih.gov/25737555/ [Accessed June 22, 2022].

Suda Y, Tada M, Matsuo T, Kawasaki K, Saigusa T, Ishida M, Mitsui T, Kumano H, Kirihara K, Suzuki T, Matsumoto K, Hasegawa I, Kasai K, Uka T (2022) Prediction-Related Frontal-Temporal Network for Omission Mismatch Activity in the Macaque Monkey. Front Psychiatry 13:557954 Available at: www.frontiersin.org.

Sussman E, Winkler I, Wang W (2003) MMN and attention: competition for deviance detection. Psychophysiology 40:430–435 Available at: https://pubmed.ncbi.nlm.nih.gov/12946116/ [Accessed May 23, 2023].

Tandon R (1999) Cholinergic aspects of schizophrenia. Br J Psychiatry Suppl 174:7–11 Available at: https://pubmed.ncbi.nlm.nih.gov/10211133/ [Accessed May 9, 2023].

Tervaniemi M, Saarinen J, Paavilainen P, Danilova N, Näätänen R (1994) Temporal integration of auditory information in sensory memory as reflected by the mismatch negativity. Biol Psychol 38:157–167 Available at: https://pubmed.ncbi.nlm.nih.gov/7873700/ [Accessed November 12, 2021].

Todd J, Harms L, Schal l U, Michie PT (2013) Mismatch negativity: translating the potential. Front psychiatry 4 Available at: https://pubmed.ncbi.nlm.nih.gov/24391602/ [Accessed May 23, 2023].

Todorovic A, Ede F van, Maris E, Lange FP de (2011) Prior Expectation Mediates Neural Adaptation to Repeated Sounds in the Auditory Cortex: An MEG Study. J Neurosci 31:9118 Available at: /pmc/articles/PMC6623501/ [Accessed November 2, 2021].

Trautmann EM, Stavisky SD, Lahiri S, Ames KC, Kaufman MT, O'Shea DJ, Vyas S, Sun X, Ryu SI, Ganguli S, Shenoy K V. (2019) Accurate Estimation of Neural Population Dynamics without Spike Sorting. Neuron 103:292-308.e4 Available at: https://pubmed.ncbi.nlm.nih.gov/31171448/ [Accessed February 28, 2022].

Tsolaki AC, Kosmidou V, Kompatsiaris I (Yiannis), Papadaniil C, Hadjileontiadis L, Adam A, Tsolaki M (2017) Brain source localization of MMN and P300 ERPs in

mild cognitive impairment and Alzheimer's disease: a high-density EEG approach. Neurobiol Aging 55:190–201 Available at: https://pubmed.ncbi.nlm.nih.gov/28461101/ [Accessed May 23, 2023].

Tsukano H, Horie M, Hishida R, Takahashi K, Takebayashi H, Shibuki K (2016) Quantitative map of multiple auditory cortical regions with a stereotaxic fine-scale atlas of the mouse brain. Sci Rep 6 Available at: https://pubmed.ncbi.nlm.nih.gov/26924462/ [Accessed February 28, 2022].

Ulanovsky N, Las L, Nelken I (2003) Processing of low-probability sounds by cortical neurons. Nat Neurosci 6:391–398 Available at: https://pubmed.ncbi.nlm.nih.gov/12652303/ [Accessed July 5, 2021].

van Laarhoven T, Stekelenburg JJ, Eussen MLJM, Vroomen J (2020) Atypical visual-auditory predictive coding in autism spectrum disorder: Electrophysiological evidence from stimulus omissions. Autism 24:1849–1859 Available at: https://pubmed.ncbi.nlm.nih.gov/32519561/ [Accessed May 30, 2023].

Voigts J, Siegle J, Pritchett DL, Moore CI (2013) The flexDrive: An ultra-light implant for optical control and highly parallel chronic recording of neuronal ensembles in freely moving mice. Front Syst Neurosci 7 Available at: /pmc/articles/PMC3652307/ [Accessed June 22, 2022].

Wacongne C, Changeux JP, Dehaene S (2012) A neuronal model of predictive coding accounting for the mismatch negativity. J Neurosci 32:3665–3678 Available at: /pmc/articles/PMC6703454/ [Accessed July 5, 2021].

Wacongne C, Labyt E, van Wassenhove V, Bekinschtein T, Naccache L, Dehaene S (2011) Evidence for a hierarchy of predictions and prediction errors in human cortex. Proc Natl Acad Sci 108:20754–20759 Available at: https://pubmed.ncbi.nlm.nih.gov/22147913/ [Accessed February 25, 2022].

Wang M, Li R, Li J, Zhang J, Chen X, Zeng S, Liao X (2018) Frequency selectivity of echo responses in the mouse primary auditory cortex. Sci Rep 8 Available at: https://pubmed.ncbi.nlm.nih.gov/29311673/ [Accessed February 28, 2022].

Winkler I (2007) Interpreting the Mismatch Negativity. J Psychophysiol 21:147–163

Available at: /record/2008-04140-004 [Accessed February 28, 2022].

Winkler I, Karmos G, Näätänen R (1996) Adaptive modeling of the unattended acoustic environment reflected in the mismatch negativity event-related potential. Brain Res 742:239–252.

Yabe H, Tervaniemi M, Reinikainen K, Näätänen R (1997) Temporal window of integration revealed by MMN to sound omission. Neuroreport 8:1971–1974 Available at: https://pubmed.ncbi.nlm.nih.gov/9223087/ [Accessed July 5, 2021].

Yu A, Dayan P (2003) Expected and unexpected uncertainty: ACh and NE in the neocortex. In: Advances in Neural Information Processing Systems.

Yu AJ, Dayan P (2002) Acetylcholine in cortical inference. Neural Netw 15:719–730 Available at: https://pubmed.ncbi.nlm.nih.gov/12371522/ [Accessed May 29, 2023].

Yu AJ, Dayan P (2005) Uncertainty, neuromodulation, and attention. Neuron 46:681–692 Available at: https://pubmed.ncbi.nlm.nih.gov/15944135/ [Accessed May 29, 2023].

Yuille A, Kersten D (2006) Vision as Bayesian inference: analysis by synthesis? Trends Cogn Sci 10:301–308 Available at: https://pubmed.ncbi.nlm.nih.gov/16784882/ [Accessed February 25, 2022].

MECANISMOS FUNCIONALES QUE MEDIAN LA ADAPTACIÓN NEURONAL EN EL CEREBRO AUDITIVO:

LA MODULACIÓN COLINÉRGICA Y LAS RESPUESTAS A LA OMISIÓN

1. Introducción

Nuestro entorno está en permanente cambio y entenderlo es crucial para la supervivencia de todos los seres vivos, incluidos nosotros, los humanos. Pensemos en un restaurante abarrotado de gente. Al sentarnos a la mesa, nuestros sentidos se ven bombardeados por múltiples estímulos. Las conversaciones se solapan y se mezclan, el ruido de platos y cubiertos crea una sinfonía de ruidos, y el aroma y las fragancias de los distintos alimentos inundan el ambiente. En medio de este caos sensorial, nuestro cerebro debe navegar y dar sentido a la escena que nos rodea. A pesar de todo esto, somos capaces de centrarnos en una conversación concreta en nuestra mesa, distinguiendo las voces de nuestros amigos del resto de conversaciones que nos rodean. Incluso, se puede percibir de fondo la sutileza de la melodía de una canción que nos resulta familiar. En este escenario tan desafiante, el cerebro se encarga de aislar e interpretar objetos auditivos individuales, como voces o música, dentro de un complejo paisaje auditivo.

Una de las funciones clave del sistema auditivo es transformar esta compleja escena auditiva en representaciones significativas que sean biológicamente relevantes como, por ejemplo, una bandeja llena de copas de cristal que caen al suelo y se rompen en mil pedazos, advirtiéndonos del peligro de cortarnos en nuestro escenario. Debido a la capacidad limitada de procesamiento de nuestros sistemas sensoriales, nuestro cerebro se ve obligado a generar interpretaciones significativas a partir de un volumen excesivo de entradas sensoriales fragmentadas, ruidosas e inciertas. Por tanto, nuestro cerebro debe filtrar los sonidos irrelevantes y extraer la información significativa de la sobrecarga sensorial, lo que nos permite entablar conversaciones y disfrutar del ambiente del restaurante.

La mayoría de los sonidos que llegan a nuestro sistema sensorial se caracterizan por ser repetitivos, lo que los convierte también en predecibles. El hecho de que sean predecibles implica que puedan tener poca relevancia funcional, dejando así como información crítica la reflejada por estímulos poco frecuentes. La capacidad del sistema auditivo para filtrar automáticamente estos estímulos predecibles y destacar sonidos únicos e impredecibles se conoce como *detección de la novedad* (Grimm and Escera, 2012; Escera and Malmierca, 2014). En otras palabras, la detección de la novedad es un proceso clave que da lugar a mecanismos internos muy afinados capaces de discriminar entre sonidos familiares y novedosos.

1.1. El MMN como biomarcador principal de detección de novedades

El trabajo pionero del Prof. Risto Näätänen (1978) describió el denominado *potencial de disparidad* (MMN, *Mistmatch Negativity* en la nomenclatura anglosajona), registrado sobre el cuero cabelludo humano (Näätänen et al., 1978, 2007; Näätänen, 1990, 1992) mediante técnicas de electroencefalografía (EEG). El MMN forma parte de la familia de los *potenciales evocados* (*Event Related Potentials*, ERP), que reflejan la capacidad del cerebro para detectar cambios en la escena auditiva, es decir, la detección de novedades. La ocurrencia del MMN puede desencadenarse por cualquier alteración en la entrada auditiva a través de un paradigma tradicional de *estímulo discrepante* (paradigma "*oddball*"). En él, se presentan estímulos auditivos infrecuentes (denominados estímulos discrepantes, impredecibles, con un 10% de probabilidad de aparición) que se intercalan aleatoriamente en una sucesión de estímulos regulares (denominados estímulos estándar, predecibles, con un 90% de probabilidad de aparición) (Näätänen, 1992). Como resultado, la amplitud del MMN es proporcional a la diferencia entre las respuestas cuando un tono se presenta como estándar o se presenta como discrepante, alcanzando su amplitud máxima entre 100 y 220 ms después del inicio del tono discrepante (Näätänen et al., 1978).

El MMN se ha medido ampliamente en diferentes estados cerebrales: Durante el sueño (Nashida et al., 2000; Sculthorpe et al., 2009; Strauss et al., 2015), bajo anestesia (Koelsch et al., 2006; Quaedflieg et al., 2014), o incluso en estados comatosos (Morlet and Fischer, 2014; Rodriguez et al., 2014). En la actualidad, se cree que el mecanismo computacional subyacente a la detección de la novedad constituye la base de procesos cognitivos de orden superior (Näätänen et al., 2010), como la atención (Sussman et al., 2003; Fritz et al., 2007) o la memoria (Ranganath and Rainer, 2003; Bartha-Doering et al., 2015).

Por todo ello, el MMN se ha utilizado ampliamente como biomarcador en pacientes con trastornos del neurodesarrollo, neurodegenerativos y psiquiátricos que suelen presentar una disminución significativa del MMN como se ha visto en la esquizofrenia (Garrido et al., 2009; Todd et al., 2013; Fisher et al., 2018), en la enfermedad de Parkinson (Minks et al., 2014; Heldmann et al., 2017), en trastornos del espectro autista (Goris et al., 2018; Hudac et al., 2018; Schwartz et al., 2018) o en la enfermedad de Alzheimer (Tsolaki et al., 2017; Jiang et al., 2022), entre otros.

1.2. Del cuero cabelludo humano a neuronas individuales en animales

Debido al uso tan extendido y por tanto, a la relevancia del MMN, muchos estudios han intentado explorar este fenómeno a nivel neuronal utilizando los mismos paradigmas que se utilizan en electrofisiología humana (Ulanovsky et al., 2003; Malmierca et al., 2009; Antunes et al., 2010; Ayala and Malmierca Dr., 2013; Escera and Malmierca, 2014; Duque and Malmierca, 2015; Nieto-Diego and Malmierca, 2016; Carbajal and Malmierca, 2018). Estos trabajos describen un mecanismo por el que muchas neuronas del sistema auditivo muestran una respuesta al estímulo estándar gradualmente disminuida que puede ser reactivada por un sonido discrepante inesperado (Fig. 2a). Este mecanismo se denomina *adaptación específica al estímulo* (*stimulus-specific adaptation*, SSA) y ha sido propuesto como correlato neuronal del MMN debido a sus propiedades comunes (Ulanovsky et al., 2003).

Teorías como la *hipótesis de la adaptación* (May and Tiitinen, 2010) o *la hipótesis del ajuste del modelo o del rastro de memoria* (Winkler, 2007) han tratado de explicar la detección de novedades bajo diferentes perspectivas.

La hipótesis de la adaptación intenta dar explicación a la detección de la novedad, en particular al MMN, basándose en un mecanismo fisiológico de adaptación sináptica. Esta teoría se postula en contra de la existencia de un auténtico proceso de detección de novedades, argumentando que el estímulo estándar induce la SSA debido a mecanismos pasivos como la depresión sináptica en las neuronas de la corteza auditiva (May et al., 1999; Ulanovsky et al., 2003; Jääskeläinen et al., 2004). De esta forma, los canales de frecuencia de las neuronas de la corteza auditiva que no han sido estimulados y que sintonizan tonos de otras frecuencias (en nuestro caso, los discrepantes) han permanecido frescos, manteniendo su capacidad de respuesta (May and Tiitinen, 2010; Fishman, 2014).

Por otra parte, la interpretación cognitiva clásica del MMN (la hipótesis del ajuste del modelo o de la huella de memoria) propone que al repetir la presentación de un estímulo se crea una huella sensorial o memoria de ese estímulo y, por tanto, de la regularidad. Este rastro de memoria se codifica principalmente en fuentes temporales de la corteza auditiva (Näätänen and Michie, 1979; Näätänen, 1990), permitiendo entonces la detección de diferencias sensoriales entre el rastro de memoria generado por la repetición del tono estándar y la entrada real (Näätänen and Alho, 1995). Esta hipótesis interpreta el MMN

como el resultado de toda actividad neuronal que implica los recursos cognitivos para procesar los estímulos discrepantes (Winkler et al., 1996; Näätänen and Winkler, 1999).

Ambas teorías presentan ciertas limitaciones a la hora de explicar el fenómeno de detección de novedades. El hecho de que el MMN aparezca en ausencia de atención o percepción consciente del estímulo discrepante sugiere que es un proceso automático que no depende únicamente del ajuste de modelos internos basados en la atención o la percepción consciente. En segundo lugar, la SSA se ha observado no sólo para estímulos simples, sino también para estímulos complejos, como los sonidos del habla y la música (Koelsch et al., 2019; Malmierca et al., 2019). Así también, la hipótesis de la adaptación por sí sola tiene dificultades para explicar la especificidad y selectividad de la SSA en diferentes dominios sensoriales o la debida a estímulos complejos.

Además, tanto el MMN como la SSA se han observado en múltiples niveles de la vía auditiva, incluidas ciertas áreas subcorticales. Esto indica que múltiples procesos neuronales contribuyen a estos fenómenos más allá de los simples mecanismos de adaptación o ajuste de modelos, conduciendo a la necesidad de un enfoque diferente para comprender cómo se genera el MMN y, por tanto, de teorías más atractivas, como describimos a continuación.

1.3. Codificación predictiva: La solución salomónica como teoría unificadora

En las últimas décadas, la teoría de la codificación predictiva ha ido posicionándose como una teoría muy explicativa e integradora de la función neuronal. Esta trata de explicar cómo el cerebro comprende e interpreta el mundo que nos rodea (Friston, 2002, 2012). Según esta teoría, el cerebro extrae continuamente regularidades del entorno con las que genera predicciones o expectativas y construir así, un modelo interno.

A continuación, estas predicciones se comparan con la entrada sensorial y cualquier discrepancia o error de predicción se utiliza para actualizar y refinar este modelo existente (Fig. 3). Dentro este marco conceptual, la respuesta MMN es considerada como una señal de error de predicción neurofisiológica (Friston, 2005; Winkler, 2007; Garrido et al., 2008, 2009; Den Ouden et al., 2012; Stefanics et al., 2015; Parras et al., 2017; Casado-Román et al., 2020) como resultado de la comparación entre la entrada sensorial real ascendente (bottom-up) y una traza de memoria, la llamada predicción, codificada en la actividad descendente (top-down) (Yuille and Kersten, 2006; Antunes and Malmierca,

2011; Carbajal and Malmierca, 2018, 2020). Así, un error de predicción se produce cuando la entrada sensorial real no coincide con el modelo interno.

Esta teoría es probablemente una de las más controvertidas y a su vez también influyente y acreditada de la función neuronal, ya que desafía los puntos de vista tradicionales de la percepción y la cognición de una manera elegante y convincente (Heilbron and Chait, 2018). La codificación predictiva goza de apoyo empírico, especialmente a partir de estudios sobre la SSA, que ha sido descrita a lo largo de las diferentes estaciones de procesamiento de la vía auditiva (Parras et al., 2017; Casado-Román et al., 2020) (Fig. 4). Estos estudios propusieron un nuevo enfoque para entender la detección de novedades a nivel neuronal, apoyando la teoría de la codificación predictiva. En estos estudios las respuestas neuronales se desmembraron en dos componentes: *supresión por repetición* y de *error de predicción,* utilizando los controles de no repetición que ya habían sido introducidos previamente en estudios del MMN (Schröger and Wolff, 1996; Jacobsen and Schröger, 2001; Jacobsen et al., 2003b, 2003a). De esta forma, la diferencia entre las respuestas evocadas por los estímulos discrepante y estándar pasa a denominarse *desajuste neuronal* (nMM).

1.4. En busca de la fidelidad: la precisión de los errores de predicción

Como hemos mencionado anteriormente, la teoría de la codificación predictiva apuesta por un procesamiento jerárquico activo que compara las predicciones descendentes y los errores de predicción ascendentes. En lugar de procesar toda la información, un procesamiento predictivo se limitaría a integrar las señales de error de predicción (Clark, 2013). De esta forma, a medida que las expectativas se actualizan, la cantidad de errores de predicción que hay que codificar disminuye progresivamente. Por lo tanto, la reducción de los errores de predicción refleja un procesamiento optimizado de la información, que es precisamente el principio fundamental de la codificación predictiva: La minimización de los errores de predicción (Friston et al., 2006; Friston, 2010; Fields et al., 2022).

Una forma en la que un sistema perceptivo podría minimizar los errores de predicción es adoptando un modelo generativo y jerárquico dentro de su red neuronal. Este modelo implica la comparación continua de las entradas sensoriales ascendentes con las predicciones descendentes en múltiples niveles de procesamiento, que están fuertemente

interconectados. Las creencias previas ("*prior beliefs*", en la nomenclatura de la codificación predictiva, (Parr and Friston, 2019a)) se actualizarán en cada estación de procesamiento en función de los errores de predicción recibidos desde el nivel inferior. Las creencias posteriores ("*posterior beliefs*", en la nomenclatura de la codificación predictiva, (Parr and Friston, 2019a) de un nivel se convierten en las expectativas del nivel inmediatamente inferior. Así, cualquier error de predicción se envía al nivel inmediatamente superior para actualizar la creencia previa (Friston and Stephan, 2007; Hohwy, 2017). Este ciclo de actualización de predicciones mediante la integración de los errores de predicción continúa hasta que éstos se reducen, ajustándose a las expectativas de los niveles inferiores. Así, la percepción es el resultado de una jerarquía de comparaciones activas, donde cada nivel restringe el procesamiento de sus niveles interrelacionados. Esto implica la convergencia de las expectativas y de la información sensorial a través de niveles conectados, permitiendo que la percepción emerja con un uso mínimo de recursos de procesamiento (Carbajal and Malmierca, 2020).

Este proceso podría parecer finito, pero no lo es. El sistema nervioso está continuamente procesando errores de predicción ya que el entorno está cambiando constantemente, pero también puede estarlo debido a un posible funcionamiento errático de nuestro propio sistema nervioso. En situaciones patológicas como, por ejemplo, la pérdida de audición o el hecho de trabajar en un entorno ruidoso, pueden provocar errores de predicción. Como consecuencia de esto, no todas las señales de error de predicción deben considerarse de igual forma. Aquí es, donde el concepto de *precisión* desempeña un papel fundamental en la formación de las predicciones y sus actualizaciones (Fig. 5). Las actualizaciones se examinan discriminando la incertidumbre del error de predicción. Mientras que las señales sinápticas se propagan a lo largo de la jerarquía de procesamiento, se les va dando diferentes pesos dependiendo de lo precisas que se espera que sean (Friston, 2008; Parr et al., 2018; Parr and Friston, 2019b). Si el cerebro espera un alto nivel de precisión, las señales de error de predicción se amplificarán haciéndose más influyentes en la actualización de las creencias previas y, por el contrario, cuando se espera una baja precisión, las señales de error de predicción se atenuarán para evitar imprecisiones y reforzar así estas creencias previas.

Por tanto, la magnitud de la señal de error de predicción depende no sólo del tamaño del desajuste entre la señal y la predicción, sino también de la precisión de la predicción. En otras palabras, la precisión de una predicción refleja el nivel de confianza o certeza que

el cerebro le asigna, o lo que es lo mismo, la precisión esperada se refiere al grado de amplificación que la ganancia postsináptica aplica al error de predicción, ajustado su impacto en los niveles superiores de procesamiento. Esto permite que los errores de predicción más precisos y fiables contribuyan más al aprendizaje que los menos precisos y por tanto menos fiables (Friston and Kiebel, 2009).

En la literatura científica (Friston, 2005, 2008), la predicción se ha representado matemáticamente como una distribución de probabilidad gaussiana relativa a una característica perceptiva. En esa distribución, la moda representa la predicción más probable, mientras que la inversa de la varianza define la confianza en esa predicción, lo que se define como precisión. Describimos pues, una predicción como la suma de la expectativa en sí y la fiabilidad esperada de esa expectativa. La percepción, por tanto, es el resultado de una media ponderada entre la entrada sensorial (procesamiento ascendente) y la predicción (procesamiento descendente), donde la fiabilidad viene determinado por la precisión (Sedley et al., 2016).

Como decíamos anteriormente, los errores de predicción se modulan a través de la regulación de la ganancia postsináptica impulsada por sistemas neuromoduladores (Friston, 2008; Feldman and Friston, 2010; Parr et al., 2018; Parr and Friston, 2019b). Un ajuste adecuado de la precisión es crucial para el correcto funcionamiento del sistema perceptivo, de manera que unos receptores neuronales alterados podrían conducir a una modulación errónea de la precisión, lo que daría lugar a signos y síntomas de trastornos neuropsiquiátricos y enfermedades neurodegenerativas, como las alucinaciones auditivas, la esquizofrenia o la enfermedad de Alzheimer (Tandon, 1999; Adams et al., 2013; Hullfish et al., 2019; Friston et al., 2021).

Originalmente, Yu y Dayan (2002) propusieron los sistemas colinérgico y dopaminérgico como los responsables de esta modulación (Yu and Dayan, 2002, 2003, 2005). También los estudios de Moran (Moran et al., 2013) y de Friston (Friston et al., 2012, 2014), muestran la acción natural de neurotransmisores como la acetilcolina y la dopamina, que podrían estar jugando un papel fundamental en el equilibrio de la precisión. El marco de Yu y Dayan (2002) propone que la acetilcolina (ACh) modula la incertidumbre asociada a las señales descendentes y modula la interacción entre el procesamiento descendente y ascendente en la determinación de las representaciones neuronales apropiadas para las entradas en las representaciones de alto nivel. En él, describen cómo la modulación

colinérgica conduce a una percepción apropiada (Yu and Dayan, 2002). Miasnikov y sus colegas (Miasnikov et al., 2008) demostraron que la "memoria" sensorial depende de la modulación colinérgica en el dominio auditivo. Otros estudios han analizado las respuestas simuladas y empíricas sobre el papel de la señalización colinérgica en la percepción y la atención (Moran et al., 2013). Sus resultados encajan con la narrativa y marcos tanto teóricos como empíricos previos que apoyan que la ACh potencia las señales ascendentes en respuesta a la incertidumbre (Yu and Dayan, 2002, 2003; Bentley et al., 2004).

En resumen, existen numerosas pruebas teóricas y empíricas del papel que juega la ACh en la promoción de la influencia de las entradas sensoriales en la percepción y la atención.

1.5. El sonido del silencio: respuestas neuronales a la omisión de estímulos auditivos

Aunque existe una gran cantidad de datos que demuestran el procesamiento predictivo a lo largo de las diferentes modalidades sensoriales (para una revisión véase (Bendixen et al., 2012), en la actualidad se desconoce cómo se generan las predicciones y cuál es su código de representación neuronal una vez formuladas.

Se ha argumentado que las respuestas de omisión proporcionarían pruebas empíricas y concluyentes del proceso predictivo, ya que se produce en ausencia de entrada sensorial (Wacongne et al., 2011, 2012; Heilbron and Chait, 2018; Braga and Schönwiesner, 2022). Se ha observado, cómo la omisión de un tono en una secuencia de estímulos regulares puede provocar una respuesta neuronal. Esta respuesta no se transmite a lo largo de la vía aferente como consecuencia de una entrada sensorial, sino que refleja una expectativa interna de que un estímulo debería ocurrir (Braga and Schönwiesner, 2022). De ahí que las predicciones puedan estudiarse examinando la respuesta neuronal ante la omisión de un sonido esperado. Esto es importante porque confirma que el MMN no es simplemente un proceso pasivo que conduce a la adaptación sináptica al estimular continuamente las mismas vías aferentes (Parras et al., 2017; Casado-Román et al., 2020). Por lo tanto, las respuestas de omisión podrían ser una herramienta crucial e infravalorada para desentrañar los mecanismos subyacentes del procesamiento predictivo, especialmente en modelos animales. Así, ya que la actividad neuronal evocada por el estímulo discrepante refleja la diferencia entre una señal sensorial y la predicción descendente, la omisión de

un estímulo esperado refleja la señal de predicción pura (Bendixen et al., 2009; Den Ouden et al., 2009; Todorovic et al., 2011; Wacongne et al., 2011, 2012; Cornella et al., 2015; Schröger et al., 2015).

En estudios realizados en humanos (Fig. 6) se ha visto como por la omisión de un estímulo auditivo esperado se produce una respuesta de MMN (Tervaniemi et al., 1994; Raij et al., 1997; Yabe et al., 1997; Horváth et al., 2010; May and Tiitinen, 2010; Wacongne et al., 2011, 2012; Heilbron and Chait, 2018; Fonken et al., 2019). Más concretamente, estas omisiones suelen evocar una respuesta negativa temprana (oN1) que alcanza un pico máximo de respuesta entre los 45 y 100 ms con respecto al inicio de la omisión (SanMiguel et al., 2013a, 2013b; Stekelenburg and Vroomen, 2015; van Laarhoven et al., 2020).

Este tipo de estudios ha dado lugar a hallazgos intrigantes. En primer lugar, los mecanismos neuronales que subyacen a las respuestas de omisión parecen implicar generadores similares a los de las respuestas de MMN convencionales. Estos generadores incluyen áreas de la corteza auditiva (Kraemer et al., 2005; Raij et al., 1997; Suda et al., 2022) al igual que regiones frontotemporales (Suda et al., 2022; Yabe et al., 1997), sugiriendo que existe un sustrato neural compartido para la detección tanto de estímulos discrepantes como de omisiones. Además, los estudios sobre las respuestas a la omisión tienen el potencial de proporcionar información sobre trastornos que están caracterizados por presentar un procesamiento auditivo alterado, como la esquizofrenia (Kreitschmann-Andermahr et al., 1999; Kirino et al., 2019; Mori et al., 2021) o los trastornos del espectro autista (van Laarhoven et al., 2020) (Fig. 7). Sin embargo y, a pesar de su relevancia, la evidencia de las respuestas de omisión de un estímulo auditivo a nivel neuronal sigue siendo esquiva.

2. Hipótesis

Se han podido observar procesos predictivos a lo largo de la vía auditiva que apoyan la hipótesis de la codificación predictiva (Parras et al., 2017; Casado-Román et al., 2020). En estos estudios, se registró la actividad de neuronas individuales en el colículo inferior, el cuerpo geniculado medial, la corteza auditiva y la corteza prefrontal. La estimulación se realizó bajo el paradigma *oddball* y los controles de no repetición que permitieron discriminar los componentes de la respuesta de error de predicción y los debidos a efectos adaptación (Fig. 8a, b). En ellos demostraron, no solo que los errores de predicción están presentes en regiones subcorticales, sino que además, los errores de predicción están organizados jerárquicamente y aumentan a medida que se difunden hacia áreas temporales y prefrontales (Casado-Román et al., 2020). Estos estudios demuestran que, en células auditivas individuales, los errores de predicción son un componente fundamental para la detección de novedades. Además, los errores de predicción están modulados por la precisión. Se ha propuesta la acetilcolina como uno de los candidatos para esta modulación (Yu and Dayan, 2003, 2005). En 2015, Ayala y Malmierca demostraron que la aplicación de ACh en neuronas del colículo inferior provocaba una reducción en la SSA debido a un aumento de la respuesta al tono repetido (Ayala and Malmierca, 2015). Sin embargo, el efecto de la ACh sobre las respuestas nMM en las neuronas de la corteza auditiva aún se desconoce.

Además, estudios previos han demostrado que el MMN se puede generar como consecuencia de la omisión de un estímulo esperado mediante el paradigma *oddball* clásico (Rüsseler et al., 2001; Dercksen et al., 2020; Horváth et al., 2010 Bendixen et al., 2009). En 1997, Yabe y sus colegas estudiaron el MMN provocado por esta omisión al mantener la velocidad de presentación del estímulo (SOA, *stimulus onset asynchrony* en la nomenclatura anglosajona) constante y alta. Estos autores mostraron una respuesta MMN muy clara sólo cuando el SOA era inferior a 150 ms, lo que permite hacer una estimación de la duración de la ventana de integración temporal (Yabe et al., 1997).

A nivel neuronal, las respuestas de omisión han podido observarse en la corteza visual (Fiser et al., 2016; Solomon et al., 2021), pero actualmente, resultados que apoyen la teoría de la codificación predictiva a nivel neuronal y auditivo en modelos animales, son muy limitados.

Teniendo en cuenta las observaciones anteriores, propongo las siguientes hipótesis:

I. Las proyecciones colinérgicas regulan la precisión del error de predicción cambiando y reajustando la precisión en las neuronas de la corteza auditiva.

II. La vía auditiva posee neuronas específicas que codifican la omisión de un estímulo esperado, es decir, las neuronas pueden responder incluso en ausencia de una entrada sensorial.

3. Objetivos

Partiendo de mi hipótesis, me propongo los siguientes objetivos:

I. Determinar si las entradas colinérgicas afectan a las señales de error de predicción en las neuronas de la corteza auditiva.

II. Determinar si las neuronas auditivas pueden codificar la omisión de un estímulo esperado.

Para responder a las preguntas derivadas de estos objetivos hemos realizado dos tipos de experimentos complementarios:

I. Inyecciones de acetilcolina mediante técnicas de microiontoforésis en neuronas de la corteza auditiva mientras se registra la actividad neuronal bajo el paradigma *oddball* y empleando paradigmas de no repetición: *cascade* y *many standards.*

II. Registro de neuronas individuales en el colículo inferior y en la corteza auditiva bajo el paradigma *oddball* empleando como estímulo discrepante la omisión del mismo.

4. Resumen de resultados

4.1. Estudio I

En este primer estudio, hemos analizado la influencia de la modulación colinérgica sobre el CSI (índice comúnmente utilizado en estudios de SSA) y el error de predicción en la corteza auditiva de rata anestesiada. Para ello, hemos registrado un total de 113 neuronas antes, durante y después de la inyección de acetilcolina mediante técnicas de microiontoforésis. Realizamos registros en todas las subdivisiones de la corteza auditiva: A1, campo auditivo anterior (AAF), campo auditivo ventral (VAF), campo auditivo posterior (PAF) y campo auditivo suprarrenal (SRAF) y las profundidades de registro oscilaron entre 120-1191 µm incluyendo neuronas de todas las capas en ratas anestesiadas con uretano.

Registramos el mapa de frecuencia (*frequency response area*, FRA) y analizamos la distribución topográfica de la frecuencia característica (CF) de cada neurona para poder asignar cada una de ellas a una subdivisión específica de la corteza auditiva. Para ello, a cada registro se le asignó unas coordenadas dorso-ventral y rostro-caudal relativas al bregma siguiendo estudios previos (Polley et al., 2007; Nieto-Diego and Malmierca, 2016; Parras et al., 2017). Este análisis nos permitió agrupar los datos de todos los animales (Fig. 9a) y construir un mapa sintético de la frecuencia característica de la corteza auditiva de la rata (Fig. 9). De forma similar a estos trabajos previos, encontramos una zona de inversión de alta frecuencia entre VAF (caudal) y AAF (rostral), una zona de inversión de baja frecuencia entre A1 y PAF (dorso-caudal), y una inversión de alta frecuencia entre VAF y SRAF (ventral). Así, pudimos definir de forma fiable los campos corticales auditivos lemniscales (A1, AAF y VAF) y no lemniscales (SRAF, PAF) (Fig. 9).

A continuación, calculamos el CSI antes, durante y después de la inyección de ACh y pudimos observar la modulación de los CSI en todas las neuronas de forma individual (Fig. 10 y Fig. 11). La ACh produjo un aumento significativo del valor de CSI en el 25,9% de las neuronas registradas mientras que el 43,5% de las neuronas no se vieron afectadas y el 30,6% mostró una disminución significativa de su CSI (puntos morados, grises y naranjas respectivamente) (Fig. 12a). El valor promedio de CSI durante la inyección de ACh (CSI = 0,54 ± 0,27) fue similar al de la condición control (CSI = 0,57 ± 0,23; prueba

de Wilcoxon Signed Rank, p=0,359; Fig. 12b). A continuación, analizamos el efecto de la ACh sobre la respuesta a los estímulos discrepantes y estándar por separado. Estos resultados muestran que la ACh produjo una disminución significativa en la media de la tasa de disparo en respuesta a los tonos discrepantes (11,75 ±17,46 Hz) en comparación con la condición de control (16,51 ±16,19 Hz; prueba de Wilcoxon Signed Rank, p < 0,001). Este efecto de disminución también se observó en la media de la tasa de disparo en respuesta a los tonos estándar (4,58 ±6,38 vs 3,97 ±9,90 Hz, control vs ACh; prueba de Wilcoxon Signed Rank, p = 0,001) (Fig. 12c).

Con el objetivo de describir mejor estos cambios en el CSI, estudiamos las diferencias entre control y efecto en las diferentes subdivisiones de la corteza auditiva. Para ello, estudiamos las respuestas de los tonos estándar, tonos discrepantes y el CSI. Este último no mostró diferencias significativas entre campos debido a la aplicación de ACh (Fig. 13, primera fila). Sin embargo, sí hubo diferencias significativas para estímulo estándar en AAF (p=0.001) (Fig. 13, segunda fila) y para el estímulo discrepante en AAF, VAF y SRAF p=0.011, p=0.026 y p=0.009, respectivamente; prueba de Wilcoxon Signed Rank con la corrección de Holm-Bonferroni) (Fig. 13, última fila).

De forma paralela, calculamos el índice SI, también comúnmente utilizado en estudios de SSA, que refleja los cambios de manera independientemente para las respuestas a las frecuencias individuales del paradigma *oddball* (f1 y f2) (Fig. 14). Los resultados mostraron que era más probable que la ACh causara una disminución en el SI en todos los campos AC excepto en AAF, donde el SI aumentó (Fig. 14a). A continuación, representamos el efecto de la ACh en las diferentes capas de la corteza auditiva. Este análisis demostró que las unidades que experimentan una disminución del SI son más frecuentes alrededor de la capa granular (capa IV), mientras que las unidades que experimentan un aumento del SI se encuentran con más frecuencia en las capas infragranulares (Fig. 14b).

En los análisis del SI, comprobamos que la ACh produjo un aumento significativo del valor SI en el 27% en las frecuencias registradas (Fig. 15a, puntos morados), mientras que el 31% (Fig. 15a, puntos naranjas) mostró una disminución significativa de su SI y el 42% de las frecuencias no se vieron afectadas por la ACh (Fig. 15a, puntos grises). El valor medio de SI (SI = 0,55 ± 0,31, condición control) se redujo durante la inyección de ACh (SI = 0,40 ± 0,50) aunque no significativamente (Wilcoxon Signed Rank test,

p=0,086; Fig. 15b). Al separar las neuronas en función de si el SI sufría un descenso o un aumento, pudimos observar cómo la ACh afectaba a estos dos grupos de forma diferente, disminuyendo la respuesta al estímulo discrepante o al estímulo estándar para neuronas que veían disminuido o aumentado su SI respectivamente (Fig. 15c, d).

Por último, hemos calculado los índices de discrepancia neuronal o *neuronal mismatch* (nMM): índice de disparidad (*mismatch index*, iMM), índice de error de predicción (*prediction error index*, iPE) e índice de supresión por repetición (*repetition suppession index*, iRS) para ambos grupos (SI disminuido o aumentado por la ACh, Fig. 16a, b). El resultado principal de este análisis es que la modulación ejercida por la ACh sobre el iMM es la consecuencia de la modulación sobre el error de predicción en ambos casos (Fig. 16c, d; violines rojos) y no de la supresión por repetición (Fig. 16c, d; violines azules). Curiosamente en ambos casos, la precisión (inversa de la varianza) del error de predicción, disminuye con la aplicación de ACh (Fig. 16e, f).

4.2. Estudio II

En nuestro segundo trabajo, estudiamos las respuestas neuronales de la vía auditiva a la omisión de un estímulo esperado dentro de una secuencia repetitiva de frecuencia fija, lo que significaría, una expectativa violada. Para ello, registramos la actividad neuronal en el colículo inferior (CI) y la corteza auditiva de ratas anestesiadas con uretano (CA) y la corteza auditiva de ratones despiertos (CA) en respuesta a un conjunto de secuencias de tonos puros.

Las secuencias correspondían a un paradigma de estímulo discrepante en el que éste era la omisión del estímulo (Fig. 16). Registramos neuronas individuales exponiéndolas a un conjunto de seis secuencias, con frecuencias e intensidades fijas elegidas dentro de su área de respuesta en frecuencia (*frequency response area*, FRA). Las secuencias diferían en su velocidad de presentación (SOA: 125, 250 o 500 ms) y en ellas, el estímulo omitido fue presentado tras un número variable de tonos estándar (aleatorio) o un número fijo (periódico) manteniendo siempre un 10% de aparición de la omisión. Registramos la actividad espontánea de cada neurona antes de iniciar cada secuencia y durante 2,5-10,0 s (equivalente a ≥ 20 estímulos respectivamente para cada SOA) como control de la actividad evocada (Fig. 18).

Definimos las respuestas a la omisión como una actividad elevada y localizada temporalmente en los periodos de silencio cuando un estímulo se omitía. Como criterio estadístico establecimos que esta actividad neuronal debía ser significativamente mayor que (i) la actividad espontánea de la neurona, previa a toda la secuencia de estimulación y (ii) la actividad neuronal registrada justo antes de cada omisión (ventanas temporales de -25 a 5, -75 a 5 y -195 a 5 ms, mientras que las ventanas de respuesta consideradas fueron de 5 a 120, 5 a 150 y 5 a 225 ms, respectivamente; simulación Montecarlo para una prueba bilateral con corrección Benjamini-Hochberg para comparaciones múltiples, $p<0,05$).

Como resultado, pudimos clasificar como *respuestas de omisión* al 2,2 % (16/713 secuencias), el 10,9 % (119/1092 secuencias) y el 15,1 % (1373/9075 secuencias) de las respuestas de CI y CA de ratas anestesiadas y ratones despiertos respectivamente.

A continuación, comparamos la actividad evocada por las omisiones con la evocada por los estímulos, ambos referidos a la actividad espontánea, para todas las velocidades de

presentación y omisiones presentadas aleatoria o periódicamente (prueba t pareada con corrección de Bonferroni, p<0,05; Fig. 20). Con ello pudimos observar que, en todos los casos de rata anestesiada, la respuesta producida por la omisión fue similar a la respuesta evocada por el estímulo. Sin embargo, en corteza auditiva de ratón despierto y a velocidades de presentación rápidas, 125 ms, la respuesta evocada por la omisión, bien fuese presentada de forma aleatoria o periódica, fue significativamente mayor que la evocada por el estímulo, mostrando, a su vez, un interesante significativo de la respuesta a la omisión cuando era presentada de forma aleatoria (Fig. 20c; primera fila, barras verticales rojas). Además, cuando estas omisiones fueron aleatorias, la diferencia en respuesta a la omisión y al estímulo, se mantuvo para velocidades de presentación más lentas de 250 y 500 ms.

Para cuantificar la comparación entre la actividad provocada por el sonido (StimFR) y la provocada por la omisión (OmiFR), calculamos un índice de omisión [iOmi = (Omi FR - Stim FR)/(Omi FR + Stim FR)] (Fig. 21a-c). El iOmi varía de -0,9 a 0,6 en CI, y de -1 a 1 y -0,7 a 1 en CA de animales anestesiados y despiertos respectivamente. Los valores negativos y positivos de iOmi muestran secuencias que exhiben una mayor respuesta al sonido o a la omisión, respectivamente. La media de iOmi nos da una idea del poder de detección de omisiones de las neuronas de cada área auditiva, siendo negativa para las neuronas CI y volviéndose positiva y ligeramente superior a medida que asciendo por la vía auditiva y pasando de las neuronas de CA de animales anestesiados a las de animales despiertos (iOmi = -0.0084, 0.0771 y 0.1594 respectivamente; Fig. 21a-c). Aquellas respuestas de omisión cuyo iOmi > 0,33 las denominamos "respuestas selectivas de omisión", ya que este valor del índice corresponde a una diferencia del doble (Fiser et al., 2016). Así, un total de 30/119 (25,21%) y 311/1373 (22,65%) en CA de animales anestesiados y despiertos son respuestas selectivas a la omisión. Todas las respuestas de CI muestran un iOmi < 0,20, excepto una única respuesta que muestra un iOmi de 0,54.

A continuación, analizamos la distribución de iOmi a través de las capas de CA tanto para animales anestesiados como despiertos (Fig. 22c-d). Para ratas anestesiadas, la proporción de respuestas de omisión sobre el total de neuronas registradas fue de 10,73% (44/410), 10,04% (23/229) y 10,36% (40/386) para las capas supragranular, granular e infragranular, respectivamente. Para ratones despiertos, estas proporciones son ligeramente mayores; así, el 14,97% (417/2786) de las secuencias de nuestra muestra de AC se localizaron en las capas supragranulares, el 16,45% (272/1653) en las granulares

y el 14,75% (684/4636) en las infragranulares. Finalmente, al representar estos índices en al mapa topográfico de la corteza auditiva en el caso de la rata anestesiada, pudimos observar un gradiente rostro-caudal del iOmi donde los índices positivos estaban localizados en PAF y las áreas más caudales de VAF y SRAF (Fig. 22).

Los resultados expuestos anteriormente son muy reveladores, ya que nos permitieron identificar las respuestas de omisión y algunos de los detalles por los que se rigen. Sin embargo, este análisis pude dar lugar los problemas resultantes de un análisis circular (en el que las hipótesis distorsionan los resultados). En dicho caso, el análisis estadístico no es «riguroso» ya está sesgado e invalida los resultados obtenidos. En particular, el uso de del mismo conjunto de datos para inferir los resultados y para validar el modelo (el proceso llamado «*double-dipping*» en la terminología anglosajona), invalida completamente los resultados estadísticos obtenidos (que asumen la independencia entre ambos conjuntos de datos). El Dr. Nikolaus Kriegeskorte y sus colegas (2009) nos describen este problema de manera muy elegante en el contexto de las neurociencias. Estos autores nos ofrecen varios ejemplos de las «trampas» que nos pone la estadística y algunas ideas (más bien políticas) sobre cómo evitarlo (mucho más común de lo que parece en las ciencias en la frontera de «las ciencias naturales y sociales» como es el caso de las neurociencias. Por todo ello, y para evitar estos inconvenientes del análisis circular estudiamos más a fondo los datos llevándolos a una representación neuronal. Así pues, realizamos los análisis estadísticos empleando la mitad de los datos y utilizamos la otra mitad para su representación gráfica. A su vez, realizamos registros en neuronas de CA de ratones anestesiados con uretano para vincular las dos especies animales.

Entonces, promediamos todas las condiciones (secuencias) registradas para cada neurona independientemente de si mostraban respuestas significativas a la omisión o no para obtener un único valor de respuesta por neurona. De esta forma, encontramos de forma respuestas de omisión consistentes (Fig. 23a, líneas rojas) a velocidades de 125 ms. Pudimos observar estas respuestas a nivel neuronal en todas las áreas registradas y las denominamos *neuronas sensibles a la omisión* (n= 8, n=15 para CI y CA de rata anestesiada y n=76, n=140 para CA de ratón anestesiado y despierto; véase Fig. 23b y Fig. 24 para los análisis en corteza auditiva). Al hacer este análisis global de respuesta, no pudimos observar las diferencias significativas entre omisiones presentadas de forma aleatoria o periódica.

Analizamos también el iOmi a nivel neuronal que mostró el mismo incremento de animal anestesiado a despierto, aunque de menor magnitud, que observamos previamente a nivel de secuencias (Fig. 25). Por último, analizamos las latencias de las respuestas evocadas por la omisión y por el estímulo (Fig. 26) y comparamos las respuestas a la omisión con las respuestas a un estímulo discrepante clásico (Fig. 27). En la corteza auditiva del ratón anestesiado (Fig. 27a), las neuronas sensibles a la omisión muestran una fuerte respuesta a los estímulos discrepantes (en naranja, izquierda), que supera sustancialmente las respuestas a la omisión (en rojo) y al estímulo estándar (azul). En el ratón despierto, las estas neuronas muestran una separación clara y significativa en la diferencia entre estas respuestas ($p=0,0017$; Fig. 27b). A continuación, describimos la sensibilidad a la omisión en función de la estimulación previa, observando que la respuesta a la omisión muestra un aumento significativo y lento durante la estimulación, en particular en animales despiertos (Fig. 28).

En último lugar, analizamos la distribución de las neuronas sensibles a la omisión a lo largo de las capas de la corteza auditiva (Fig. 29a-c). Aquí observamos que la fracción de estas neuronas (barras burdeos) en relación a la muestra total (barras grises), es baja en las capas supragranulares en ratas anestesiadas, mientras que en ratones despiertos se muestra una tendencia de mayor proporción de éstas en las capas supragranulares.

5. Conclusiones

Así pues, considerando los resultados de ambos estudios, concluyo que:

I. Un subconjunto de neuronas del cerebro auditivo responde a los tonos omitidos en un patrón, por lo demás regular, de tonos estándar.

II. Las respuestas de omisión se encontraron a diferentes velocidades de presentación siendo más evidentes y presentando una mayor probabilidad de aparición a velocidades de repetición más rápidas de 125 ms.

III. Las respuestas de omisión están presentes a nivel del colículo inferior en animales anestesiados y aumentan de forma ascendente a lo largo de la jerarquía auditiva.

IV. Las respuestas de omisión son significativamente mayores para presentaciones aleatorias que periódicas en la corteza auditiva de los ratones despiertos.

V. La acetilcolina modula las respuestas de desajuste neuronal en la corteza auditiva de ratas anestesiadas. Esta modulación es impulsada por la disminución de las respuestas del tono estándar o del discrepante.

VI. La acetilcolina puede escalar o reducir el error de predicción, pero no la supresión por repetición.

VII. La acetilcolina minimiza la precisión del error de predicción en la corteza auditiva.

6. Bibliografía

Adams RA, Stephan KE, Brown HR, Frith CD, Friston KJ (2013) The computational anatomy of psychosis. Front psychiatry 4 Available at: https://pubmed.ncbi.nlm.nih.gov/23750138/ [Accessed May 26, 2023].

Antunes FM, Malmierca MS (2011) Effect of auditory cortex deactivation on stimulus-specific adaptation in the medial geniculate body. J Neurosci 31:17306–17316.

Antunes FM, Nelken I, Covey E, Malmierca MS (2010) Stimulus-specific adaptation in the auditory thalamus of the anesthetized rat. PLoS One 5 Available at: https://pubmed.ncbi.nlm.nih.gov/21124913/ [Accessed February 25, 2022].

Ayala YA, Malmierca Dr. MS (2013) Stimulus-specific adaptation and deviance detection in the inferior colliculus. Front Neural Circuits 6 Available at: https://pubmed.ncbi.nlm.nih.gov/23335883/ [Accessed February 25, 2022].

Ayala YA, Malmierca MS (2015) Cholinergic Modulation of Stimulus-Specific Adaptation in the Inferior Colliculus. J Neurosci 35:12261–12272 Available at: https://www.jneurosci.org/content/35/35/12261 [Accessed May 9, 2023].

Bartha-Doering L, Deuster D, Giordano V, Am Zehnhoff-Dinnesen A, Dobel C (2015) A systematic review of the mismatch negativity as an index for auditory sensory memory: From basic research to clinical and developmental perspectives. Psychophysiology 52:1115–1130 Available at: https://pubmed.ncbi.nlm.nih.gov/26096130/ [Accessed May 23, 2023].

Bendixen A, SanMiguel I, Schröger E (2012) Early electrophysiological indicators for predictive processing in audition: A review. Int J Psychophysiol 83:120–131.

Bendixen A, Schröger E, Winkler I (2009) I heard that coming: Event-related potential evidence for stimulus-driven prediction in the auditory system. J Neurosci 29:8447–8451 Available at: /pmc/articles/PMC6665649/ [Accessed July 5, 2021].

Bentley P, Husain M, Dolan RJ (2004) Effects of cholinergic enhancement on visual stimulation, spatial attention, and spatial working memory. Neuron 41:969–982 Available at: https://pubmed.ncbi.nlm.nih.gov/15046728/ [Accessed May 29, 2023].

Braga A, Schönwiesner M (2022) Neural Substrates and Models of Omission Responses and Predictive Processes. Front Neural Circuits 16 Available at:

/pmc/articles/PMC8844463/ [Accessed February 25, 2022].

Carbajal G V., Malmierca MS (2018) The Neuronal Basis of Predictive Coding Along the Auditory Pathway: From the Subcortical Roots to Cortical Deviance Detection. Trends Hear 22 Available at: https://pubmed.ncbi.nlm.nih.gov/30022729/ [Accessed February 25, 2022].

Carbajal G V, Malmierca MS (2020) Novelty Processing in the Auditory System: Detection, Adaptation or Expectation? In: The Senses: A Comprehensive Reference, 2nd Editio. (Fritzsch B, Gothe B, eds), pp 749–776. Elsevier. Available at: https://linkinghub.elsevier.com/retrieve/pii/B9780128093245241540.

Casado-Román L, Carbajal G V., Pérez-González D, Malmierca MS (2020) Prediction error signaling explains neuronal mismatch responses in the medial prefrontal cortex. PLoS Biol 18 Available at: https://pubmed.ncbi.nlm.nih.gov/33347436/ [Accessed February 25, 2022].

Cornella M, Bendixen A, Grimm S, Leung S, Schröger E, Escera C (2015) Spatial auditory regularity encoding and prediction: Human middle-latency and long-latency auditory evoked potentials. Brain Res 1626:21–30 Available at: https://pubmed.ncbi.nlm.nih.gov/25912975/ [Accessed February 25, 2022].

Den Ouden HEM, Friston KJ, Daw ND, McIntosh AR, Stephan KE (2009) A dual role for prediction error in associative learning. Cereb Cortex 19:1175–1185 Available at: www.vislab.ucl.ac.uk/Cogent/index.html [Accessed February 25, 2022].

Den Ouden HEM, Kok P, de Lange FP (2012) How prediction errors shape perception, attention, and motivation. Front Psychol 3 Available at: https://pubmed.ncbi.nlm.nih.gov/23248610/ [Accessed February 25, 2022].

Duque D, Malmierca MS (2015) Stimulus-specific adaptation in the inferior colliculus of the mouse: anesthesia and spontaneous activity effects. Brain Struct Funct 220:3385–3398 Available at: https://pubmed.ncbi.nlm.nih.gov/25115620/ [Accessed March 20, 2022].

Escera C, Malmierca MS (2014) The auditory novelty system: An attempt to integrate human and animal research. Psychophysiology 51:111–123 Available at: https://pubmed.ncbi.nlm.nih.gov/24423134/ [Accessed July 5, 2021].

Feldman H, Friston KJ (2010) Attention, uncertainty, and free-energy. Front Hum Neurosci 4 Available at: https://pubmed.ncbi.nlm.nih.gov/21160551/ [Accessed May 26, 2023].

Fields C, Friston K, Glazebrook JF, Levin M (2022) A free energy principle for generic quantum systems. Prog Biophys Mol Biol 173:36–59 Available at: https://pubmed.ncbi.nlm.nih.gov/35618044/ [Accessed May 26, 2023].

Fiser A, Mahringer D, Oyibo HK, Petersen A V., Leinweber M, Keller GB (2016) Experience-dependent spatial expectations in mouse visual cortex. Nat Neurosci 19:1658–1664.

Fisher DJ, Campbell DJ, Abriel SC, Ells EML, Rudolph ED, Tibbo PG (2018) Auditory Mismatch Negativity and P300a Elicited by the "Optimal" Multi-feature Paradigm in Early Schizophrenia. Clin EEG Neurosci 49:238–247 Available at: https://pubmed.ncbi.nlm.nih.gov/29502452/ [Accessed May 23, 2023].

Fishman YI (2014) The mechanisms and meaning of the mismatch negativity. Brain Topogr 27:500–526 Available at: https://link.springer.com/article/10.1007/s10548-013-0337-3 [Accessed July 5, 2021].

Fonken YM, Mukerji A, Jimenez R, Lin J, Brunner P, Schalk G, Knight RT (2019) Unexpected sound omissions are signaled in human posterior superior temporal gyrus: an intracranial study. bioRxiv:733212 Available at: https://www.biorxiv.org/content/10.1101/733212v1 [Accessed March 18, 2022].

Friston K (2002) Functional integration and inference in the brain. Prog Neurobiol 68:113–143.

Friston K (2005) A theory of cortical responses. Philos Trans R Soc B Biol Sci 360:815–836 Available at: https://pubmed.ncbi.nlm.nih.gov/15937014/ [Accessed July 5, 2021].

Friston K (2008) Hierarchical Models in the Brain. Cit Frist K 4:1000211 Available at: www.ploscompbiol.org [Accessed March 16, 2022].

Friston K (2010) The free-energy principle: a unified brain theory? Nat Rev Neurosci 2010 112 11:127–138 Available at: https://www.nature.com/articles/nrn2787 [Accessed May 26, 2023].

Friston K (2012) Predictive coding, precision and synchrony. Cogn Neurosci 3:238–239.

Friston K, Kiebel S (2009) Cortical circuits for perceptual inference. Neural Networks 22:1093–1104 Available at: /pmc/articles/PMC2796185/ [Accessed July 5, 2021].

Friston K, Kilner J, Harrison L (2006) A free energy principle for the brain. J Physiol Paris 100:70–87.

Friston K, Moran RJ, Nagai Y, Taniguchi T, Gomi H, Tenenbaum J (2021) World model learning and inference. Neural Networks 144:573–590.

Friston K, Schwartenbeck P, FitzGerald T, Moutoussis M, Behrens T, Dolan RJ (2014) The anatomy of choice: dopamine and decision-making. Philos Trans R Soc Lond B Biol Sci 369 Available at: https://pubmed.ncbi.nlm.nih.gov/25267823/ [Accessed May 26, 2023].

Friston KJ, Shiner T, FitzGerald T, Galea JM, Adams R, Brown H, Dolan RJ, Moran R, Stephan KE, Bestmann S (2012) Dopamine, Affordance and Active Inference. PLOS Comput Biol 8:e1002327 Available at: https://journals.plos.org/ploscompbiol/article?id=10.1371/journal.pcbi.1002327 [Accessed May 26, 2023].

Friston KJ, Stephan KE (2007) Free-energy and the brain. Synthese 159:417–458 Available at: https://link.springer.com/article/10.1007/s11229-007-9237-y [Accessed May 26, 2023].

Fritz JB, Elhilali M, David S V., Shamma SA (2007) Does attention play a role in dynamic receptive field adaptation to changing acoustic salience in A1? Hear Res 229:186–203 Available at: https://pubmed.ncbi.nlm.nih.gov/17329048/ [Accessed May 23, 2023].

Garrido MI, Friston KJ, Kiebel SJ, Stephan KE, Baldeweg T, Kilner JM (2008) The functional anatomy of the MMN: a DCM study of the roving paradigm. Neuroimage 42:936–944 Available at: https://pubmed.ncbi.nlm.nih.gov/18602841/ [Accessed February 25, 2022].

Garrido MI, Kilner JM, Stephan KE, Friston KJ (2009) The mismatch negativity: A review of underlying mechanisms. Clin Neurophysiol 120:453–463 Available at: https://pubmed.ncbi.nlm.nih.gov/19181570/ [Accessed June 28, 2021].

Goris J, Braem S, Nijhof AD, Rigoni D, Deschrijver E, Van de Cruys S, Wiersema JR, Brass M (2018) Sensory Prediction Errors Are Less Modulated by Global Context in Autism Spectrum Disorder. Biol Psychiatry Cogn Neurosci Neuroimaging 3:667–674.

Grimm S, Escera C (2012) Auditory deviance detection revisited: evidence for a hierarchical novelty system. Int J Psychophysiol 85:88–92 Available at: https://pubmed.ncbi.nlm.nih.gov/21669238/ [Accessed June 12, 2023].

Heilbron M, Chait M (2018) Great Expectations: Is there Evidence for Predictive Coding in Auditory Cortex? Neuroscience 389:54–73 Available at: https://pubmed.ncbi.nlm.nih.gov/28782642/ [Accessed February 25, 2022].

Heldmann M, Münte TF, Paracka L, Beyer F, Brüggemann N, Saryyeva A, Rasche D, Krauss JK, Tronnier VM (2017) Human subthalamic nucleus - Automatic auditory change detection as a basis for action selection. Neuroscience 355:141–148 Available at: https://pubmed.ncbi.nlm.nih.gov/28504196/ [Accessed May 23, 2023].

Hohwy J (2017) Priors in perception: Top-down modulation, Bayesian perceptual learning rate, and prediction error minimization. Conscious Cogn 47:75–85 Available at: https://pubmed.ncbi.nlm.nih.gov/27663763/ [Accessed May 26, 2023].

Horváth J, Müller D, Weise A, Schröger E (2010) Omission mismatch negativity builds up late. Neuroreport 21:537–541.

Hudac CM, DesChamps TD, Arnett AB, Cairney BE, Ma R, Webb SJ, Bernier RA (2018) Early enhanced processing and delayed habituation to deviance sounds in autism spectrum disorder. Brain Cogn 123:110–119 Available at: https://pubmed.ncbi.nlm.nih.gov/29550506/ [Accessed May 23, 2023].

Hullfish J, Sedley W, Vanneste S (2019) Prediction and perception: Insights for (and from) tinnitus. Neurosci Biobehav Rev 102:1–12.

Jääskeläinen IP, Ahveninen J, Bonmassar G, Dale AM, Ilmoniemi RJ, Levänen S, Lin FH, May P, Melcher J, Stufflebeam S, Tiitinen H, Belliveau JW (2004) Human posterior auditory cortex gates novel sounds to consciousness. Proc Natl Acad Sci U S A 101:6809–6814 Available at: https://pubmed.ncbi.nlm.nih.gov/15096618/ [Accessed May 19, 2023].

Jacobsen T, Horenkamp T, Schröger E (2003a) Preattentive memory-based comparison of sound intensity. Audiol Neurootol 8:338–346 Available at: https://pubmed.ncbi.nlm.nih.gov/14566104/ [Accessed May 28, 2023].

Jacobsen T, Schröger E (2001) Is there pre-attentive memory-based comparison of pitch? Psychophysiology 38:723–727 Available at: https://pubmed.ncbi.nlm.nih.gov/11446587/ [Accessed May 28, 2023].

Jacobsen T, Schröger E, Horenkamp T, Winkler I (2003b) Mismatch negativity to pitch change: Varied stimulus proportions in controlling effects of neural refractoriness on human auditory event-related brain potentials. Neurosci Lett 344:79–82 Available at: https://pubmed.ncbi.nlm.nih.gov/12782332/ [Accessed May 28, 2023].

Jiang Y, Komatsu M, Chen Y, Xie R, Zhang K, Xia Y, Gui P, Liang Z, Wang L (2022) Constructing the hierarchy of predictive auditory sequences in the marmoset brain. Elife 11 Available at: https://elifesciences.org/articles/74653 [Accessed February 25, 2022].

Kirino E, Hayakawa Y, Inami R, Inoue R, Aoki S (2019) Simultaneous fMRI-EEG-DTI recording of MMN in patients with schizophrenia. PLoS One 14 Available at: https://pubmed.ncbi.nlm.nih.gov/31071097/ [Accessed May 30, 2023].

Koelsch S, Heinke W, Sammler D, Olthoff D (2006) Auditory processing during deep propofol sedation and recovery from unconsciousness. Clin Neurophysiol 117:1746–1759 Available at: https://pubmed.ncbi.nlm.nih.gov/16807099/ [Accessed May 23, 2023].

Koelsch S, Vuust P, Friston K (2019) Predictive Processes and the Peculiar Case of Music. Trends Cogn Sci 23:63–77 Available at: https://doi.org/10.1016/j.tics.2018.10.006.

Kreitschmann-Andermahr I, Rosburg T, Meier T, Volz HP, Nowak H, Sauer H (1999) Impaired sensory processing in male patients with schizophrenia—a magnetoencephalographic study of auditory mismatch detection. Schizophr Res 35:121–129.

Kriegeskorte N, Simmons WK, Bellgowan PS, Baker CI (2009) Circular analysis in systems neuroscience: The dangers of double dipping. Nat Neurosci 12:535–540.

Malmierca MS, Cristaudo S, Pérez-González D, Covey E (2009) Stimulus-specific adaptation in the inferior colliculus of the anesthetized rat. J Neurosci 29:5483–5493 Available at: https://pubmed.ncbi.nlm.nih.gov/19403816/ [Accessed February 28, 2022].

Malmierca MS, Niño-Aguillón BE, Nieto-Diego J, Porteros Á, Pérez-González D, Escera C (2019) Pattern-sensitive neurons reveal encoding of complex auditory regularities in the rat inferior colliculus. Neuroimage.

May P, Tiitinen H, Ilmoniemi RJ, Nyman G, Taylor JG, Näätänen R (1999) Frequency change detection in human auditory cortex. J Comput Neurosci 6:99–120 Available at: https://pubmed.ncbi.nlm.nih.gov/10333158/ [Accessed May 19, 2023].

May PJC, Tiitinen H (2010) Mismatch negativity (MMN), the deviance-elicited auditory deflection, explained. Psychophysiology 47:66–122 Available at: https://pubmed.ncbi.nlm.nih.gov/19686538/ [Accessed July 5, 2021].

Miasnikov AA, Chen JC, Weinberger NM (2008) Specific auditory memory induced by nucleus basalis stimulation depends on intrinsic acetylcholine. Neurobiol Learn Mem 90:443–454 Available at: https://pubmed.ncbi.nlm.nih.gov/18573347/ [Accessed May 29, 2023].

Minks E, Jurák P, Chládek J, Chrastina J, Halámek J, Shaw DJ, Bareš M (2014) Mismatch negativity-like potential (MMN-like) in the subthalamic nuclei in Parkinson's disease patients. J Neural Transm 121:1507–1522 Available at: https://pubmed.ncbi.nlm.nih.gov/24809684/ [Accessed May 23, 2023].

Moran RJ, Campo P, Symmonds M, Stephan KE, Dolan RJ, Friston KJ (2013) Free energy, precision and learning: the role of cholinergic neuromodulation. J Neurosci 33:8227–8236 Available at: https://pubmed.ncbi.nlm.nih.gov/23658161/ [Accessed May 26, 2023].

Mori Y, Hoshino H, Osakabe Y, Wada T, Kanno K, Shiga T, Itagaki S, Miura I, Yabe H (2021) Omission mismatch negativity of speech sounds reveals a functionally impaired temporal window of integration in schizophrenia. Clin Neurophysiol 132:1144–1150 Available at: https://pubmed.ncbi.nlm.nih.gov/33774379/ [Accessed February 28, 2022].

Morlet D, Fischer C (2014) MMN and novelty P3 in coma and other altered states of

consciousness: a review. Brain Topogr 27:467–479 Available at: https://pubmed.ncbi.nlm.nih.gov/24281786/ [Accessed May 23, 2023].

Näätänen R (1990) The role of attention in auditory information processing as revealed by event-related potentials and other brain measures of cognitive function. Behav Brain Sci 13:201–233.

Näätänen R (1992). (1992) Attention and brain function. Hillsdale, NJ: Erlbaum.

Näätänen R, Alho K (1995) Generators of electrical and magnetic mismatch responses in humans. Brain Topogr 7:315–320 Available at: https://pubmed.ncbi.nlm.nih.gov/7577329/ [Accessed May 19, 2023].

Näätänen R, Astikainen P, Ruusuvirta T, Huotilainen M (2010) Automatic auditory intelligence: An expression of the sensory–cognitive core of cognitive processes. Brain Res Rev 64:123–136.

Näätänen R, Gaillard AWK, Mäntysalo S (1978) Early selective-attention effect on evoked potential reinterpreted. Acta Psychol (Amst) 42:313–329 Available at: https://pubmed.ncbi.nlm.nih.gov/685709/ [Accessed February 25, 2022].

Näätänen R, Michie PT (1979) Early selective-attention effects on the evoked potential: a critical review and reinterpretation. Biol Psychol 8:81–136 Available at: https://pubmed.ncbi.nlm.nih.gov/465623/ [Accessed May 19, 2023].

Näätänen R, Paavilainen P, Rinne T, Alho K (2007) The mismatch negativity (MMN) in basic research of central auditory processing: A review. Clin Neurophysiol 118:2544–2590.

Näätänen R, Winkler I (1999) The concept of auditory stimulus representation in cognitive neuroscience. Psychol Bull 125:826–859.

Nashida T, Yabe H, Sato Y, Hiruma T, Sutoh T, Shinozaki N, Kaneko S (2000) Automatic auditory information processing in sleep. Sleep 23:821–828 Available at: https://pubmed.ncbi.nlm.nih.gov/11007449/ [Accessed May 23, 2023].

Nieto-Diego J, Malmierca MS (2016) Topographic Distribution of Stimulus-Specific Adaptation across Auditory Cortical Fields in the Anesthetized Rat. PLoS Biol 14:e1002397 Available at: http://www.ncbi.nlm.nih.gov/pubmed/26950883 [Accessed June 14, 2019].

Parr T, Benrimoh DA, Vincent P, Friston KJ (2018) Precision and False Perceptual Inference. Front Integr Neurosci 12 Available at: https://pubmed.ncbi.nlm.nih.gov/30294264/ [Accessed May 26, 2023].

Parr T, Friston KJ (2019a) Generalised free energy and active inference. Biol Cybern 113:495–513 Available at: https://doi.org/10.1007/s00422-019-00805-w [Accessed June 15, 2023].

Parr T, Friston KJ (2019b) Attention or salience? Curr Opin Psychol 29:1–5.

Parras GG, Nieto-Diego J, Carbajal G V., Valdés-Baizabal C, Escera C, Malmierca MS (2017) Neurons along the auditory pathway exhibit a hierarchical organization of prediction error. Nat Commun 8 Available at: www.nature.com/naturecommunications [Accessed June 13, 2019].

Polley DB, Read HL, Storace DA, Merzenich MM (2007) Multiparametric auditory receptive field organization across five cortical fields in the albino rat. J Neurophysiol 97:3621–3638 Available at: https://pubmed.ncbi.nlm.nih.gov/17376842/ [Accessed June 21, 2022].

Quaedflieg CW, Münte S, Kalso E, Sambeth A (2014) Effects of remifentanil on processing of auditory stimuli: a combined MEG/EEG study. J Psychopharmacol 28:39–48 Available at: https://pubmed.ncbi.nlm.nih.gov/24257810/ [Accessed May 23, 2023].

Raij T, McEvoy L, Mäkelä JP, Hari R (1997) Human auditory cortex is activated by omission of auditory stimuli. Brain Res 745:134–143 Available at: https://pubmed.ncbi.nlm.nih.gov/9037402/ [Accessed July 5, 2021].

Ranganath C, Rainer G (2003) Neural mechanisms for detecting and remembering novel events. Nat Rev Neurosci 4:193–202 Available at: https://pubmed.ncbi.nlm.nih.gov/12612632/ [Accessed May 23, 2023].

Rodriguez RA, Bussière M, Froeschl M, Nathan HJ (2014) Auditory-evoked potentials during coma: do they improve our prediction of awakening in comatose patients? J Crit Care 29:93–100 Available at: https://pubmed.ncbi.nlm.nih.gov/24125771/ [Accessed May 23, 2023].

Rüsseler J, Altenmüller E, Nager W, Kohlmetz C, Münte TF (2001) Event-related brain

potentials to sound omissions differ in musicians and non-musicians. 308:33–36 Available at: www.elsevier.com/locate/neulet [Accessed February 25, 2022].

SanMiguel I, Saupe K, Schröger E (2013a) I know what is missing here: Electrophysiological prediction error signals elicited by omissions of predicted "what" but not "when." Front Hum Neurosci 7 Available at: https://pubmed.ncbi.nlm.nih.gov/23908618/ [Accessed July 5, 2021].

SanMiguel I, Widmann A, Bendixen A, Trujillo-Barreto N, Schröger E (2013b) Hearing silences: human auditory processing relies on preactivation of sound-specific brain activity patterns. J Neurosci 33:8633–8639 Available at: https://pubmed.ncbi.nlm.nih.gov/23678108/ [Accessed June 22, 2022].

Schröger E, Kotz SA, SanMiguel I (2015) Bridging prediction and attention in current research on perception and action. Brain Res 1626:1–13 Available at: https://pubmed.ncbi.nlm.nih.gov/26348988/ [Accessed February 27, 2022].

Schröger E, Wolff C (1996) Mismatch response of the human brain to changes in sound location. Neuroreport 7:3005–3008 Available at: https://pubmed.ncbi.nlm.nih.gov/9116228/ [Accessed May 28, 2023].

Schwartz S, Shinn-Cunningham B, Tager-Flusberg H (2018) Meta-analysis and systematic review of the literature characterizing auditory mismatch negativity in individuals with autism. Neurosci Biobehav Rev 87:106–117 Available at: https://pubmed.ncbi.nlm.nih.gov/29408312/ [Accessed May 23, 2023].

Sculthorpe LD, Ouellet DR, Campbell KB (2009) MMN elicitation during natural sleep to violations of an auditory pattern. Brain Res 1290:52–62.

Sedley W, Gander PE, Kumar S, Kovach CK, Oya H, Kawasaki H, Howard MA, Griffiths TD (2016) Neural signatures of perceptual inference. Elife 5.

Solomon SS, Tang H, Sussman E, Kohn A (2021) Limited Evidence for Sensory Prediction Error Responses in Visual Cortex of Macaques and Humans. Cereb Cortex (New York, NY) 31:3136 Available at: /pmc/articles/PMC8599921/ [Accessed June 5, 2023].

Stefanics G, Astikainen P, Czigler I (2015) Visual mismatch negativity (vMMN): A prediction error signal in the visual modality. Front Hum Neurosci 8 Available at:

/pmc/articles/PMC4302941/ [Accessed July 5, 2021].

Stekelenburg JJ, Vroomen J (2015) Predictive coding of visual-auditory and motor-auditory events: An electrophysiological study. Brain Res 1626:88–96 Available at: https://pubmed.ncbi.nlm.nih.gov/25641042/ [Accessed May 9, 2023].

Strauss M, Sitt JD, King JR, Elbaz M, Azizi L, Buiatti M, Naccache L, Van Wassenhove V, Dehaene S (2015) Disruption of hierarchical predictive coding during sleep. Proc Natl Acad Sci U S A 112:E1353–E1362 Available at: https://pubmed.ncbi.nlm.nih.gov/25737555/ [Accessed June 22, 2022].

Sussman E, Winkler I, Wang W (2003) MMN and attention: competition for deviance detection. Psychophysiology 40:430–435 Available at: https://pubmed.ncbi.nlm.nih.gov/12946116/ [Accessed May 23, 2023].

Tandon R (1999) Cholinergic aspects of schizophrenia. Br J Psychiatry Suppl 174:7–11 Available at: https://pubmed.ncbi.nlm.nih.gov/10211133/ [Accessed May 9, 2023].

Tervaniemi M, Saarinen J, Paavilainen P, Danilova N, Näätänen R (1994) Temporal integration of auditory information in sensory memory as reflected by the mismatch negativity. Biol Psychol 38:157–167 Available at: https://pubmed.ncbi.nlm.nih.gov/7873700/ [Accessed November 12, 2021].

Todd J, Harms L, Schal l U, Michie PT (2013) Mismatch negativity: translating the potential. Front psychiatry 4 Available at: https://pubmed.ncbi.nlm.nih.gov/24391602/ [Accessed May 23, 2023].

Todorovic A, Ede F van, Maris E, Lange FP de (2011) Prior Expectation Mediates Neural Adaptation to Repeated Sounds in the Auditory Cortex: An MEG Study. J Neurosci 31:9118 Available at: /pmc/articles/PMC6623501/ [Accessed November 2, 2021].

Tsolaki AC, Kosmidou V, Kompatsiaris I (Yiannis), Papadaniil C, Hadjileontiadis L, Adam A, Tsolaki M (2017) Brain source localization of MMN and P300 ERPs in mild cognitive impairment and Alzheimer's disease: a high-density EEG approach. Neurobiol Aging 55:190–201 Available at: https://pubmed.ncbi.nlm.nih.gov/28461101/ [Accessed May 23, 2023].

Ulanovsky N, Las L, Nelken I (2003) Processing of low-probability sounds by cortical neurons. Nat Neurosci 6:391–398 Available at:

https://pubmed.ncbi.nlm.nih.gov/12652303/ [Accessed July 5, 2021].

van Laarhoven T, Stekelenburg JJ, Eussen MLJM, Vroomen J (2020) Atypical visual-auditory predictive coding in autism spectrum disorder: Electrophysiological evidence from stimulus omissions. Autism 24:1849–1859 Available at: https://pubmed.ncbi.nlm.nih.gov/32519561/ [Accessed May 30, 2023].

Wacongne C, Changeux JP, Dehaene S (2012) A neuronal model of predictive coding accounting for the mismatch negativity. J Neurosci 32:3665–3678 Available at: /pmc/articles/PMC6703454/ [Accessed July 5, 2021].

Wacongne C, Labyt E, van Wassenhove V, Bekinschtein T, Naccache L, Dehaene S (2011) Evidence for a hierarchy of predictions and prediction errors in human cortex. Proc Natl Acad Sci 108:20754–20759 Available at: https://pubmed.ncbi.nlm.nih.gov/22147913/ [Accessed February 25, 2022].

Winkler I (2007) Interpreting the Mismatch Negativity. J Psychophysiol 21:147–163 Available at: /record/2008-04140-004 [Accessed February 28, 2022].

Winkler I, Karmos G, Näätänen R (1996) Adaptive modeling of the unattended acoustic environment reflected in the mismatch negativity event-related potential. Brain Res 742:239–252.

Yabe H, Tervaniemi M, Reinikainen K, Näätänen R (1997) Temporal window of integration revealed by MMN to sound omission. Neuroreport 8:1971–1974 Available at: https://pubmed.ncbi.nlm.nih.gov/9223087/ [Accessed July 5, 2021].

Yu A, Dayan P (2003) Expected and unexpected uncertainty: ACh and NE in the neocortex. In: Advances in Neural Information Processing Systems.

Yu AJ, Dayan P (2002) Acetylcholine in cortical inference. Neural Netw 15:719–730 Available at: https://pubmed.ncbi.nlm.nih.gov/12371522/ [Accessed May 29, 2023].

Yu AJ, Dayan P (2005) Uncertainty, neuromodulation, and attention. Neuron 46:681–692 Available at: https://pubmed.ncbi.nlm.nih.gov/15944135/ [Accessed May 29, 2023].

Yuille A, Kersten D (2006) Vision as Bayesian inference: analysis by synthesis? Trends Cogn Sci 10:301–308 Available at: https://pubmed.ncbi.nlm.nih.gov/16784882/ [Accessed February 25, 2022].

ANEXO I

COGNITIVE NEUROSCIENCE

Neuronal responses to omitted tones in the auditory brain: A neuronal correlate for predictive coding

Ana B. Lao-Rodríguez[1,2]†, Karol Przewrocki[3]†, David Pérez-González[1,2,4]†, Artoghrul Alishbayli[3], Evrim Yilmaz[3], Manuel S. Malmierca[1,2,5]*‡, Bernhard Englitz[3]*‡

Prediction provides key advantages for survival, and cognitive studies have demonstrated that the brain computes multilevel predictions. Evidence for predictions remains elusive at the neuronal level because of the complexity of separating neural activity into predictions and stimulus responses. We overcome this challenge by recording from single neurons from cortical and subcortical auditory regions in anesthetized and awake preparations, during unexpected stimulus omissions interspersed in a regular sequence of tones. We find a subset of neurons that responds reliably to omitted tones. In awake animals, omission responses are similar to anesthetized animals, but larger and more frequent, indicating that the arousal and attentional state levels affect the degree to which predictions are neuronally represented. Omission-sensitive neurons also responded to frequency deviants, with their omission responses getting emphasized in the awake state. Because omission responses occur in the absence of sensory input, they provide solid and empirical evidence for the implementation of a predictive process.

INTRODUCTION

Mismatch negativity (MMN) is a component of the auditory event–related potentials that is elicited when acoustic expectations are violated. It has been shown to correlate with behavioral and perceptual measures of deviance detection. Furthermore, the amplitude of the MMN response indexes the magnitude of the expectancy violation. The MMN response is widely considered as a neurophysiological correlate of a perceptual prediction error (*1*–*9*) that results from the comparison between the actual sensory (bottom-up) input and a memory trace, so-called prediction, encoded in top-down activity (*10*–*14*). A prediction error would arise when there is a mismatch between the internal prediction and the actual sensory input. A distinct aspect of the MMN is that the omission of an expected auditory stimulus (analogous to the deviant stimulus in an oddball paradigm) is often accompanied by elicitation of the omission MMN component in humans (*15*–*22*). This is important because it confirms that MMN is not simply a passive, bottom-up process that leads to synaptic adaptation to repeated stimuli due to a constant stimulation of the same afferent pathways (*8*, *23*). Previous studies have argued that the omission response provides conclusive, empirical evidence of the predictive process, as it occurs in the absence of sensory input (*19*, *20*).

Thus, predictions can be studied by examining the neuronal signature to the omission of an expected sound. Omission responses therefore might constitute a critical and underestimated test, particularly in animal models, which may be pivotal in uncovering the substrates of predictive processes. If stimulus-evoked neuronal activity indexes the difference between a sensory signal and its top-down prediction, then the omission of a predicted sensory signal should lead to neural activity, which reflects the pure prediction signal (*4*, *19*, *20*, *24*–*27*). A classic functional magnetic resonance imaging study has previously examined the topic of auditory imagery by introducing gaps of silence in familiar and unknown songs, showing neural activation of auditory cortex (AC) during the gaps of silence (*28*). However, empirical data at the single-neuron level in animal models to support the predictive coding hypothesis in this context are elusive.

We therefore aimed to investigate whether single neurons in different auditory areas respond to the omission of stimuli similar to the human MMN response. We used two rodent species that have proven to share a similar auditory system (*29*, *30*), which allow easy experimental manipulation in anesthetized or awake preparations. We found neural responses to the (silent) omission of a predictable pure tone in a subpopulation of neurons in the AC neurons under urethane anesthesia and in the awake state. In the latter, the proportion of AC neurons exhibiting omission responses was found to be substantially larger (~36% of recorded neurons, compared to 22% in anesthetized). These neurons responded to pure-tone stimuli but showed an even larger response when tones in a sequence of identical tones were omitted. We explored responses at different rates of tone trains and found that this distinct response to the omitted stimuli mostly occurred during rapid tone trains as in human MMN studies [stimulus onset asynchrony (SOA) $\leq$ 150 ms]. Omission selectivity increased during the sequence, primarily because of further adaptation of the response to the standard tone. In the awake state, omission responses became more distinct from deviant responses. Spatially, strong omission responses were more abundant in the caudal portions of the primary AC (A1), posterior auditory field (PAF), suprarhinal auditory field (SRAF), and ventral auditory field (VAF) in anesthetized rats.

[1]Cognitive and Auditory Neuroscience Laboratory (CANELAB), Institute of Neuroscience of Castilla y León, University of Salamanca, Salamanca, Spain. [2]Institute for Biomedical Research of Salamanca (IBSAL), Salamanca, Spain. [3]Computational Neuroscience Lab, Department of Neurophysiology, Donders Centre of Neuroscience, Nijmegen, Netherlands. [4]Department of Basic Psychology, Psychobiology and Methodology of Behavioral Sciences, University of Salamanca, Salamanca, Spain. [5]Department of Cell Biology and Pathology, University of Salamanca, Salamanca, Spain.
*Corresponding author. Email: msm@usal.es (M.S.M.); englitz@science.ru.nl (B.E.)
†These authors contributed equally to this work.
‡These authors contributed equally to this work.

RESULTS

Below, we first describe the quantitative characterization of omission-related responses and their dependence upon several experimental factors such as species, brain region, brain state, SOA, and sequence predictability. Then, we compare omission-related responses in relation to corresponding stimulus-bound (evoked) responses. Moreover, we investigate the latency of the responses, their sequence dependence, relation to pure-tone deviant responses, and their laminar and field specificity.

We tested whether neurons of the auditory pathway exhibit elevated responses to the omission of sounds within a fixed-rate, repetitive sequence, i.e., whether their response signifies a violated expectation of a regularly repeating sequence. For this purpose, we recorded neuronal activity in the AC of urethane-anesthetized rats (n = 77) and mice (n = 350) as well as awake mice (n = 393), and also from the inferior colliculus (IC) (n = 48; cf. Supplementary Materials) in urethane-anesthetized rats in response to a set of long pure-tone sound sequences. The sequences corresponded to an oddball paradigm (*31*) where the deviant was an omitted stimulus (Fig. 1 and fig. S1). We tested each neuron with a set of tone sequences, with fixed frequencies and intensities chosen to fall within its frequency response area. Sequences differed in their SOA (SOA: 125, 250, or 500 ms), in which the pre-activity and the analysis windows were chosen in accordance to the increasing SOAs to capture possible long latencies, and precise sequencing, either with a random number of tones before an omission or a fixed number (periodic). In a subset of the recordings in the mouse AC, we also presented classical oddball sequences of identical temporal structure with pure-tone deviants.

Omission responses were defined as a temporally localized elevation of spiking activity occurring during the periods of silence (omitted deviant; Fig. 1, asterisks in AC recording trace) when a stimulus was omitted (randomly or periodically, 10% probability in both cases) in a long sequence of tones (Fig. 1). Significance was assessed on a neuron level first before aggregating across neurons. This is essential as the classical theory of predictive coding (*14*) suggests that only a subset of neurons will respond to the omission of a predictable stimulus, likely signaling a prediction or prediction error (see Discussion for details), particularly inhibitory neurons (*19*–*21*). Specifically, we compared the neuronal activity recorded just before each omission trial (time windows of −25 to 5, −75 to 5, and −195 to 5 ms), with the window corresponding to the timing of the expected stimulus (5 to 120, 5 to 150, and 5 to 225 ms, respectively), using one-sided Wilcoxon signed-rank test at a

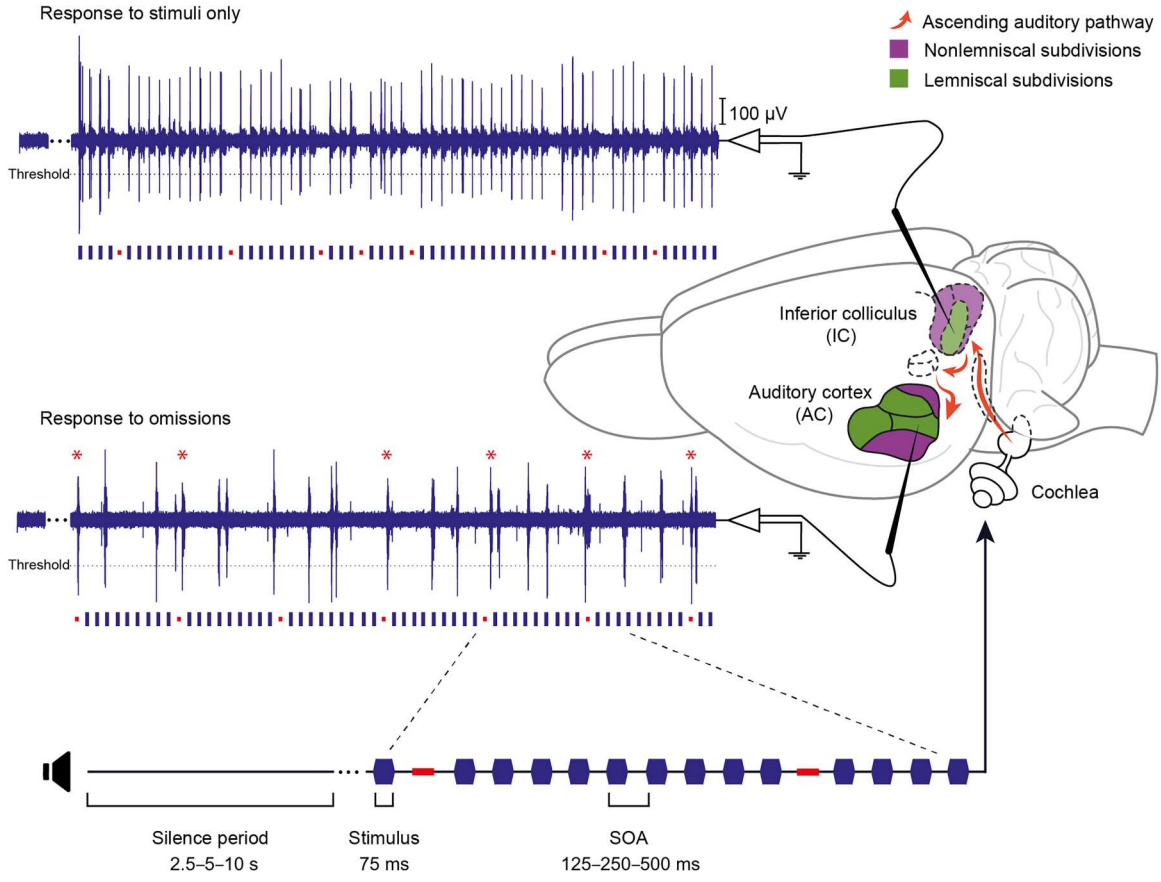

Fig. 1. Experimental setup and design for recording from the IC and AC. While stimulating with sequences of pure tones, neuronal activity was recorded using microelectrodes in the urethane-anesthetized rats (AC and IC) as well as urethane-anesthetized and awake mice (AC). The long tone sequence consisted of a repeating tone (standard probability: 90%) that was occasionally replaced by an omitted tone (average deviant probability: 10%). Traces correspond to actual recordings (from the IC and AC of urethane-anesthetized rats, respectively). Red stars indicate neuronal responses during an omitted tone. SOA denotes the amount of time between the start of one stimulus and the start of the following stimulus.

significance level of 0.05. We only checked for elevations in firing rate here, while we do not exclude that other neurons might show systematic reductions of their activity. To preempt a positive detection bias due to circular analysis ("double dipping") (*32*, *33*), we implemented split data analysis, i.e., half of the omission trials were used to assess whether a neuron showed a significant response, and the other half of the data were then used further on. In this way, random elevations of firing rate cannot systematically influence all subsequently analyzed measures. Following these criteria, 19.5% (15 of 77) and 21.7% (76 of 350) neurons from urethane-anesthetized rat and mice, respectively, as well as 35.6% (140 of 393) neurons from awake mice responded to omitted tones in 125 ms of SOA and are referred to as "omission-sensitive neurons." Data from the IC are only reported in the Supplementary Materials (cf. fig. S2), as the number of omission-sensitive neurons was too low for subsequent analyses.

Evidence of omission responses in AC neurons

Omission responses were originally found at an SOA of 125 ms in human electroencephalography (EEG) recordings (*16*). In the present experiments in rodents, we consistently find omission responses for this SOA (see Fig. 2A, red traces; representative neurons with significant omission responses, i.e., omission-sensitive neurons) under all three recording conditions. Omission responses in the AC of anesthetized rodents (Fig. 2A, left and middle) are salient in comparison to the preceding stimulus response, which is the last stimulus in the stimulation sequence before the omission. The omission response for the awake mouse AC neuron is very distinct, both in size and timing (Fig. 2A, right).

Next, we computed grand-average peristimulus time histograms (PSTHs) including all neurons showing significant omission responses (Fig. 2B; see Materials and Methods for details) for the three conditions. As in the individual cells, the omission responses are more robust as we progress from anesthetized to awake animals. Significantly, while positive omission responses are present in anesthetized rodents, AC populations (Fig. 2B, left and right), they are even more pronounced in the awake mouse preparation (Fig. 2B, right). The stimulus-evoked response (blue) shows less adaptation in awake mice (Fig. 2B, right) as opposed to cortical neurons in anesthetized rats and mice (Fig. 2B, left and middle). In awake mice, the onset responses to each stimulus are visible and the omission-evoked activity (red) is readily recognizable (Fig. 2B, right). The firing rate in response to sound stimulation is low in anesthetized rodents, except for the first stimulus after the omission, and it tends to increase during omitted tones (Fig. 2B, left and middle).

The shape of the responses to the stimulus typically had an onset component, both in individual examples and at the population level. Using the 115-ms analysis window that includes most of the evoked responses (see Materials and Methods), only in the case of the anesthetized animals the response to the stimulus after the omission was larger than the response to the stimulus previous to the omission ($P = 0.0125$ and $P < 0.0001$ for rats and mice, respectively; Wilcoxon test). However, when using a 30-ms analysis window encompassing only the onset component, we found that the response to the stimulus after the omission was larger than the response to the stimulus previous to the omission under all conditions (anesthetized rat: $P = 0.0496$, anesthetized mouse: $P = 0.0402$, awake mouse: $P < 0.001$; Wilcoxon test). Under the awake condition, as opposed to the responses to the stimuli, the omission responses tended to be more sustained and started from the expected time of occurrence of the omitted stimulus, often continuing to the subsequent stimulus presentation.

In summary, omission-evoked responses are strongly represented at 125 ms of SOA occurring both under anesthetized and awake states in the AC, with a substantial increase in magnitude in the awake state (for comparison with our smaller dataset from the IC, see fig. S2). At longer SOA (250 and 500 ms), we still detected a small subset of omission-sensitive neurons, but their average responses (based on the second half of the split data analysis) did not provide substantial evidence for reliable omission responses at these SOAs.

Table 1. Summary of firing rates.

Firing rates (spks/s)	AC anesthetized rat	AC anesthetized mouse	AC awake mouse
Mean			
Stimulus	1.0963	0.4046	2.0372
Omission	1.1347	1.0728	5.3385
After-omission	2.9421	3.1175	2.0246
Median			
Stimulus	0.8614	0.3840	1.4255
Omission	1.087	0.9116	3.2464
After-omission	1.1592	1.8439	1.8081
***P* values**			
Stimulus/pre-omission	0.0002	<0.0001	<0.0001
Omission/pre-omission	0.0001	<0.0001	<0.0001
After-omission/pre-omission	0.0001	<0.0001	<0.0001
Omission/stimulus	0.5765	0.0670	<0.0001
Stimulus/after-omission	0.0384	<0.0001	0.2756
Omission/after-omission	0.2769	0.0016	<0.0001

Comparison between sound and omission responses

Above, we identified putative omission-sensitive neurons using the split data approach on half of the omission trials. Below, we evaluate their response on the population level and compare them to responses to stimuli (not just the preceding one) and responses to stimuli after the omission. Each of these responses was referenced to the omission preceding activity to have a common local baseline, as we expect the spontaneous rate before the stimulation sequence to overestimate the within-sequence spontaneous rate (Wilcoxon test with Holm-Bonferroni correction, $P < 0.05$; Fig. 3). AC neurons from anesthetized rats and mice responded with similar firing rates to stimuli and omissions ($P = 0.577$ and $P = 0.067$, respectively; Fig. 3, A and B). On the other hand, awake mice AC neurons showed a significant enhancement of omission responses

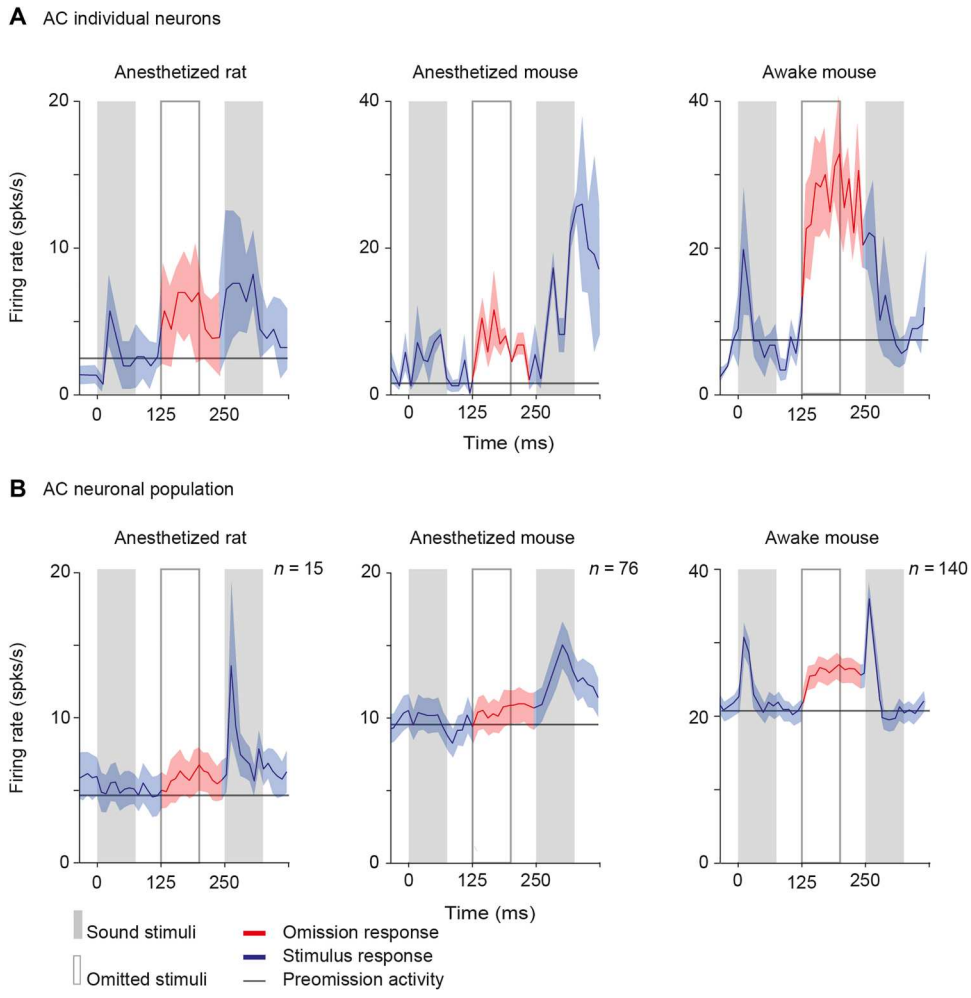

Fig. 2. Neurons in the AC show responses to the omission of a predictable sound. (**A**) Representative examples of omission responses in individual AC neurons. Neurons from the three recorded conditions are shown in the different columns (anesthetized rat, anesthetized mouse, and awake mouse; from left to right, respectively). Firing rates (spikes per second) and time (ms) are represented in vertical and horizontal axes. The duration of the stimuli and omitted tones (75 ms) is represented by vertical gray-shaded and white continuous line boxes, respectively. The responses have been computed as centered on the omitted tone whose response is occurring during the white vertical reference box. The red traces indicate responses during the omission analysis window. The preomission activity is also depicted as reference (gray horizontal line). Shaded areas indicate SEM. (**B**) Grand average of the responses of all the omission-sensitive neurons, per recorded condition, indicating the number of neurons included.

relative to stimulus responses ($P < 0.001$; Fig. 3C; cf. Table 1 for details).

We found that the response to the omission was particularly stronger than to the first stimulus after an omission under the awake condition, highlighting the omission response in the sequence ($P < 0.001$; Fig. 3C). The average firing rate in response to after-omission stimuli was significantly larger than the average response to the rest of stimuli in anesthetized rat and mouse neurons ($P = 0.038$ and $P < 0.001$), but not in awake mice AC neurons ($P = 0.276$), although it is also significant when using a 30-ms window, adapted to the brevity of the response (see above). The reduced average response to all stimuli (excluding after omissions) is probably due to an adaptation effect to the repeated stimuli (*7*, *34*), which is later released by the occurrence of the omission and subsequent after omission (see more details below in the "Omission-sensitivity dynamics depend on brain state" section).

Furthermore, we tested whether there were differences in the response to the omission under the periodic and random conditions (with a common, average probability for omissions of 10%), but there were no significant differences at the population level ($P = 0.93$, Wilcoxon test). As an occurrence of the omission in the periodic sequence is more predictable, we originally hypothesized a greater response under the random condition. The lack of a difference could be explained by the length of our shortest sequence under the random condition (*3*) in relation to the dynamics of response adaptation (see more details below in the "Omission-sensitivity dynamics depend on brain state" section and Discussion).

In summary, we find two important features regarding the omission firing rates: First, for omission-sensitive neurons, the firing rate during the omission is similar to the sound-evoked firing rate under the anesthetized condition (in both rat and mouse), but under the awake condition, the omission response is even larger than the

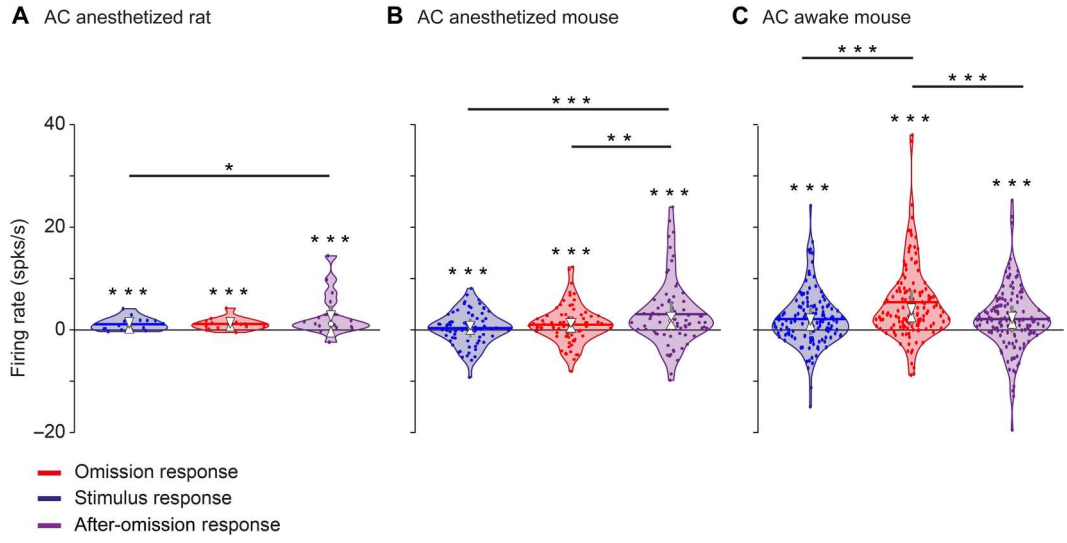

Fig. 3. The prevalence and strength of omission responses increase under awake condition. Firing rates of omission-sensitive neurons in the AC of the anesthetized rat (**A**), anesthetized mouse (**B**), and awake mouse (**C**). Sound-, omission-, and after-omission–evoked activities are represented by blue, red, and purple violin plots, respectively. In this and similar violin plots, the horizontal solid lines indicate the mean of the distribution, while the inner gray box indicates the interquartile range. Similarly, the white circles indicate the median and the white triangles show the 95% confidence interval for the median. Evoked firing rates have been baseline-corrected, relative to preomission activity. Asterisks directly over the violin plots indicate that the distribution is statistically different from 0 (Wilcoxon test with Holm-Bonferroni correction; see Table 1). Asterisks over horizontal lines indicate significantly different distributions (Wilcoxon test with Holm-Bonferroni correction; see Table 1). *$P < 0.05$, **$P < 0.01$, and ***$P < 0.001$.

sound-evoked activity over the analysis window. Second, the neural response of omission-sensitive neurons exhibits a timed rise at the start of the expected tone following an omission.

To quantify the comparison between sound- and omission-evoked activities, we computed an omission index (iOmi) at the cellular level [iOmi = (Omi FR − Stim FR)/(Omi FR + Stim FR)], for the omission-sensitive neurons, under the three recorded conditions, where the firing rate (FR) for stimuli was averaged from all stimulus presentations (Fig. 4A). Negative and positive iOmi values show neurons that exhibit a larger response to the sound or to the omission, respectively.

The average iOmi (Fig. 4A, vertical red dotted lines) quantifies the response selectivity to omissions for a group of neurons, here applied to the omission-sensitive neurons. Anesthetized rat AC neurons respond similarly on average to the stimulus and to the omission (iOmi = −0.089, $P = 0.661$, Wilcoxon test with Holm-Bonferroni correction; Fig. 4A, left), as well as anesthetized mouse AC neurons (iOmi = −0.006, $P = 0.836$; Fig. 4A, middle), while in awake mouse AC neurons, the average response to the omission is larger than to the stimulus (iOmi = 0.055, $P < 0.001$; Fig. 4A, right). Notably, the average iOmi is significantly larger in the awake mouse AC than in the anesthetized mouse AC ($P = 0.0013$, Wilcoxon rank sum).

Next, we compared the omission-sensitive (Fig. 4B, red) neurons to their complement, referred to as omission-insensitive (Fig. 4B, blue) neurons, in terms of the difference in activity to omissions and stimuli. In line with the definition of these groups of cells, we find that the omission-sensitive neurons have a larger difference than omission-insensitive neurons, thus relatively responding more to omissions ($P = 0.028$ and $P = 0.016$ for anesthetized rats and mice, respectively, and $P = 1.7 \times 10^{-8}$ for awake mice, Wilcoxon rank sum tests). While under urethane anesthesia, the difference is negative, i.e., greater responses to stimuli than to omissions, in both species (Fig. 4B); this relation reverses for the omission-selective neurons in the awake mouse (Fig. 4B, right, red). In all comparisons above, both omission and stimulus responses were referenced to the activity in the preomission period to focus on relative changes within cells instead of absolute firing rates.

In summary, the degree of omission selectivity in the neural responses was comparable between species in the AC and increased in the awake compared with the anesthetized state in the mouse. While omission selectivity differed in omission-sensitive and omission-insensitive populations under all conditions, the difference was most pronounced in the awake state.

Response latencies of omission and sound responses

To explore the omission responses further, we measured and compared the peak latency for the omission- and sound-evoked activity (paired Wilcoxon test with Holm-Bonferroni correction, $P < 0.05$; Fig. 5). Response latencies for omitted tones, stimuli, and after-omission stimuli are shown in Fig. 5 for the three recorded conditions. The neurons show very similar latencies for the omission- and stimuli-evoked responses in both anesthetized preparations (Fig. 5, A and B, and Table 2), while the latency of the omission responses is larger than the latency of the stimuli-evoked responses in the awake mouse AC ($P < 0.001$); this is probably caused by multiple factors, including differences in the profile of the responses to the stimulus (peaking closer to the sound onset) and the omission (more sustained responses), overall larger firing rates, and reduced stimulus adaptation under the awake condition, which would contribute to faster responses. A real and genuine omission response should be time-locked to the period when the stimulus is expected to happen (but it is omitted). These latency data support the notion that the source of the omission response (i.e., putative prediction)

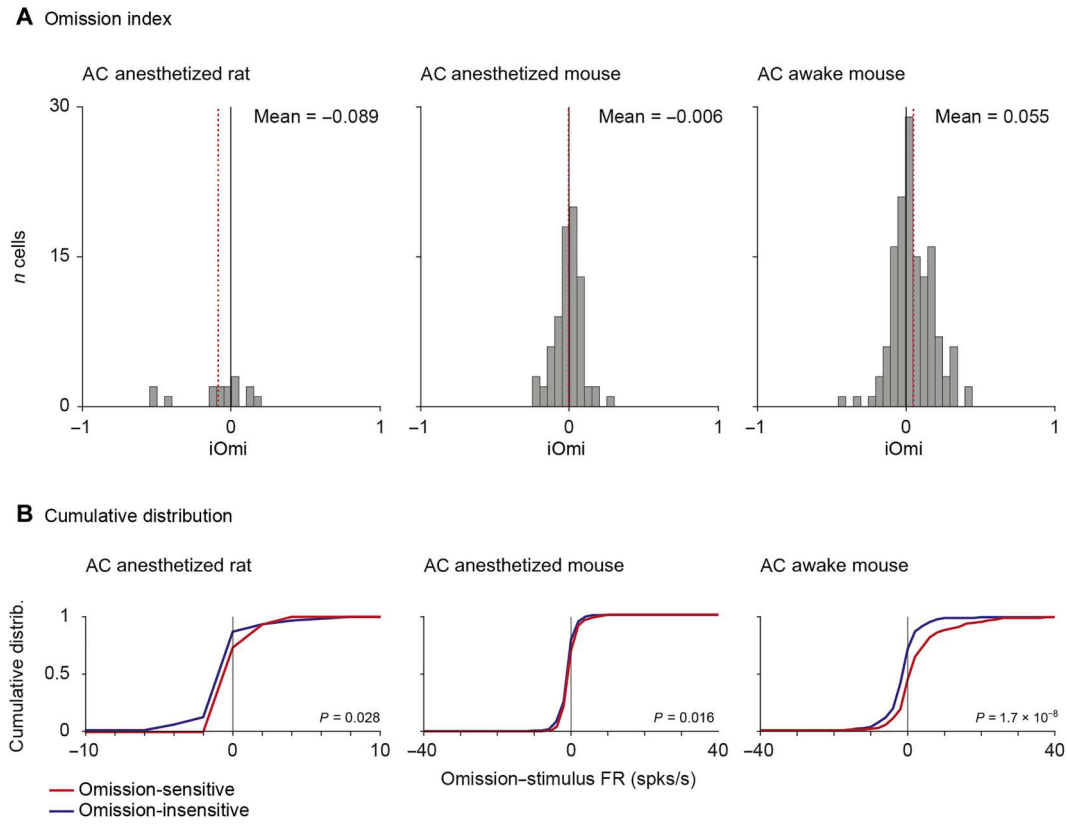

Fig. 4. Responses to omission become larger than stimulus responses under the awake condition. Distribution of iOmi between the recorded conditions. (**A**) iOmi for omission-sensitive neurons show progressively increasing values, from negative under the rat anesthetized condition, to positive values in the mouse preparations, being highest under the awake condition. Positive iOmi values indicate that the neuron responds with higher firing rates to the omission than to the stimulus, while negative values indicate the opposite. (**B**) Comparison of omission-sensitive (red) with omission-insensitive (blue) neurons shows increasing omission selectivity toward AC and further in the awake state. This is indicated by a larger separation between the curves, particularly for values >0, indicating greater responses to omissions than stimuli.

could differ from the stimulus response (forward response) as posited by predictive (*14*) coding (cf. Table 2 for details).

Comparison between omission and deviant responses

Responses to unexpected changes in tone properties, so called deviants, are very related to responses to omissions, as the latter can be considered a special case of a deviant. Their properties have long been studied under the topic of stimulus-specific adaptation—often considered a special case of predictive coding—where a certain degree of adaptation occurs for the repeated standard stimulus, while the deviant stimulus leads to a larger response, in higher auditory areas even larger than it would be in isolation (*7*, *8*, *10*, *23*, *34*). A natural question is whether the classical deviant responses co-occur with omission responses.

To address this question, we compare here the neural response for omission-sensitive neurons in the anesthetized and awake mouse AC (targeting A1). In the awake dataset, the deviant and omission conditions were presented for a subset of 126 (of a total of 393) cells, while in the anesthetized set, they were presented for all 350 cells, of which 55 and 76 were omission-sensitive, respectively. As usual, the deviant response (Fig. 6A, left column, orange) was larger than the standard response ($P = 1.4 \times 10^{-9}$, one-sided Wilcoxon signed-rank test; Fig. 6A, left column, blue), which, under the anesthetized condition, was nearly completely adapted. The omission response was less precisely timed than the deviant response, but was significantly larger than the preomission period (Fig. 6A, left, red). Under this condition, both omission-sensitive and omission-insensitive neurons responded similarly to omission and deviant stimuli, as evidenced by the overlap of the cumulative distributions of the difference between deviant and omission responses ($P = 0.15$, Wilcoxon rank sum test between the two populations on omission-deviant responses; Fig. 6A, middle and right). The curves intersect the ordinate at 0, indicating that responses to deviants were, on average, larger than to omissions.

On the other hand, the omission-sensitive neurons (Fig. 6B) also showed a very strong response to the deviant and a clearer response to the standard than under the anesthetized condition, likely because of reduced stimulus adaptation. In addition, the awake preparation shows a clear sustained response to the omission, with an overall rate similar to the deviant response ($P = 0.36$). Under this condition, omission-sensitive neurons respond to omissions with larger firing rates than to deviants ($P = 0.0017$), which is not the case for omission-insensitive neurons (Fig. 6B, middle). This is also indicated by the "dent" in the cumulative distribution of the difference between omission and deviant responses for the omission-sensitive neurons (Fig. 6B, right, red). These response

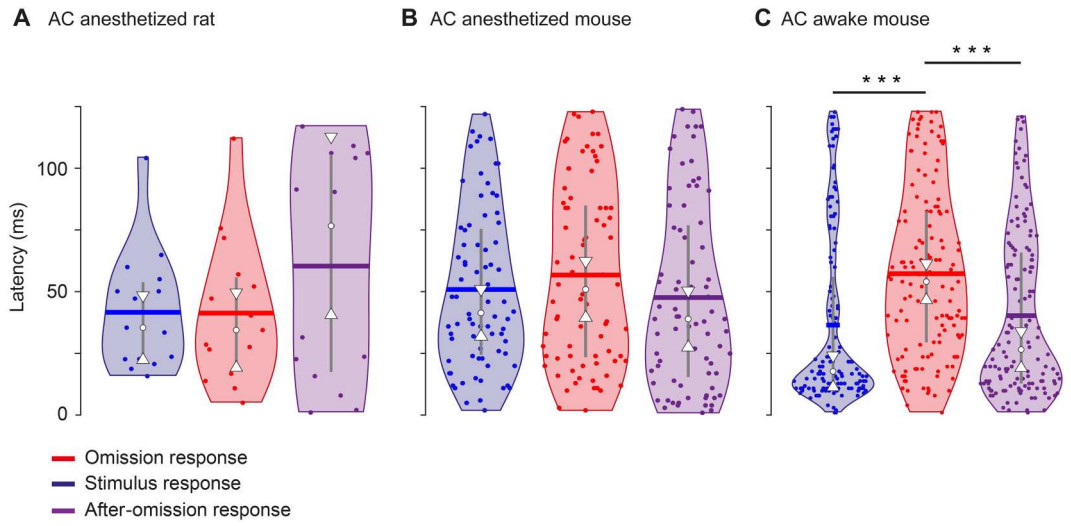

Fig. 5. Comparison of response latencies for omission and stimulus responses. Distribution of response peak latencies (ms) of omission-sensitive neurons in the AC of the anesthetized rat (**A**), anesthetized mouse (**B**), and awake mouse (**C**). The blue, red, and purple violin plots depict the distribution of the sound stimuli, omission, and after-omission latencies (see Fig. 3 for the meaning of the violin plot symbols). Asterisks denote statistical significance between stimuli and omission latencies (***P < 0.001; paired Wilcoxon with Holm-Bonferroni correction; see Table 2).

Table 2. Summary of responses latencies.

Response latency (ms)	AC anesthetized rat	AC anesthetized mouse	AC awake mouse
Mean			
Stimulus	42.8333	50.4474	36.5929
Omission	42.5	56.3289	57.8214
After-omission	61.9	47.1842	40.5
Median			
Stimulus	36.5	41	17.5
Omission	35.5	50.5	54.5
After-omission	78.5	38.5	26.5
***P* values**			
Stimulus/omission	0.8904	0.8904	<0.0001
Stimulus/after-omission	0.5830	0.5830	0.3066
Omission/after-omission	0.4052	0.4052	0.0001

properties in the AC show that omission-sensitive neurons can also have a response to deviant sounds; however, in the awake state, the omission response of the omission-sensitive neurons becomes comparable in size and more specific to omissions (see Discussion for details).

Omission-sensitivity dynamics depend on brain state

Next, we analyzed whether omission-sensitive neurons show a dependence of their response on the history of stimulation, and how this depends on the state of the animal. First, we considered the neural responses as a function of the overall stimulation sequence. As expected, the stimulus response exhibited a fast decay, within just two stimuli under both the anesthetized (Fig. 7A, left, blue) and the awake (Fig. 7A, right, blue) condition. Under the awake condition, a second time scale of adaptation existed with a time constant of ~5 s. The level of the omission responses (red) stayed rather constant over the period of the whole sequence in both states. The iOmi index of omission selectivity (Fig. 7B; see Methods) showed a slow increase, which was more pronounced under the awake case ($r = 0.39$, $P = 1.2 \times 10^{-16}$, Pearson correlation) than under the anesthetized condition ($r = 0.1$, $P = 0.035$). This was probably mostly driven by the adaptation of the standard response, potentially signifying a buildup of predictions (*21*).

Second, we studied the omission-evoked responses in relation to the number of stimuli preceding the stimulus omission. In the anesthetized case, a significant decrease [$P = 0.02$, Kruskal-Wallis analysis of variance (ANOVA)] is observed for the omission response (Fig. 7C, left, red). The response to the first standard after the omission (purple) shows a similar but nonsignificant dependence. Unexpectedly, no dependence with a decrease for shorter sequences of standards is present in the awake case (Fig. 7C, right); conversely, the standard response instead shows a significant decrease ($P = 0.00074$). For the omission response, no dependence is present, although the omission response is on a high level relative to the standards (firing rates are normalized to the average standard response here), which suggests that the omission response might already have reached a plateau level. This possibility is supported by the rapid adaptation of the standard response after the omission (Fig. 7D), which is very salient in the anesthetized case and completes after just two standard stimuli, and even after just one in the awake case. In the latter, this behavior is only apparent if a shorter time window (30 ms) is used for the analysis (Fig. 7D, right, inset), which matches the brief, driven response (see Fig. 2B, right).

In summary, the omission sensitivity shows a significant slow increase over prolonged stimulation, particularly under awake

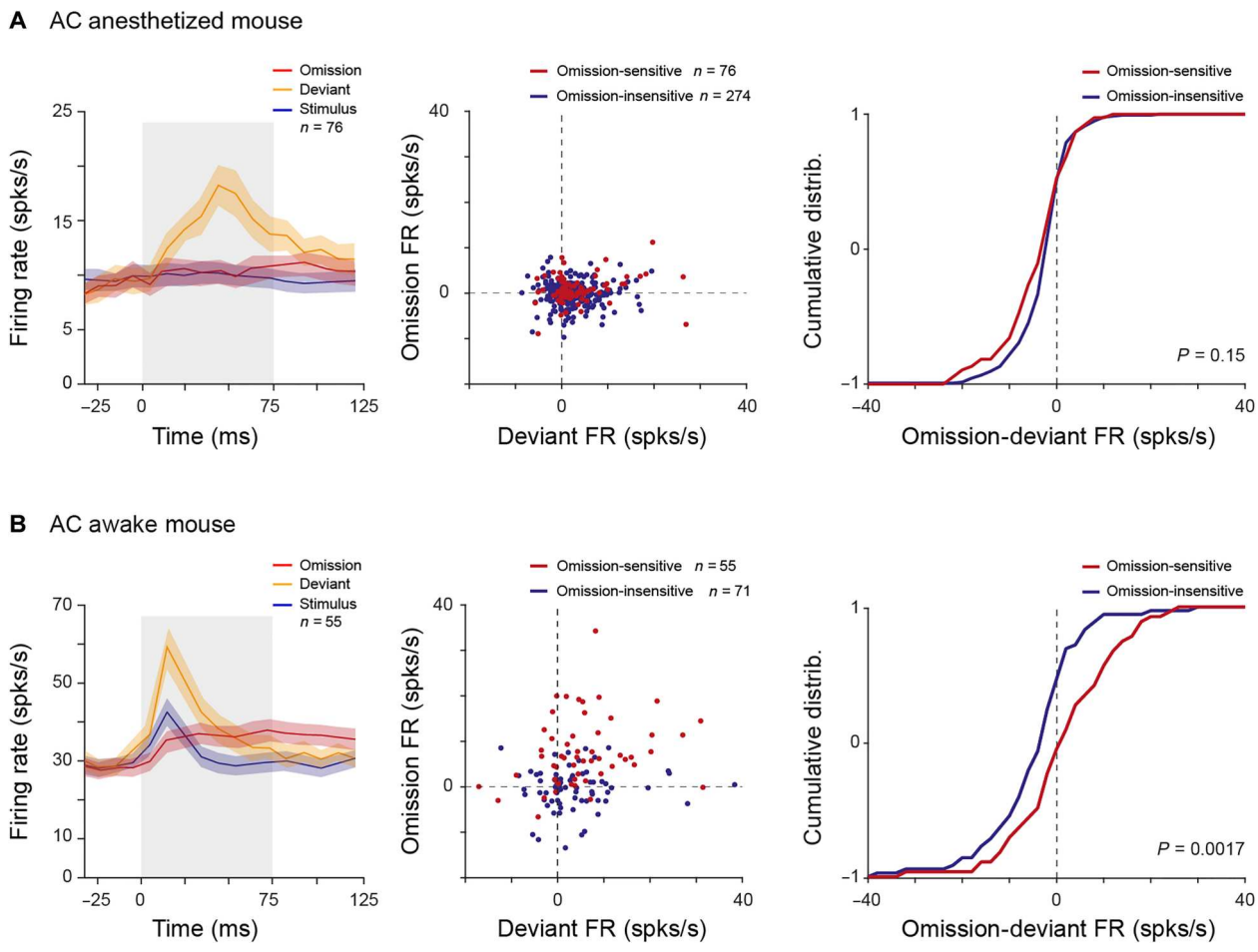

Fig. 6. Omission-sensitive neurons differentiate their response from deviants in the awake state. (**A**) In the AC in the anesthetized mouse, omission-sensitive neurons show a strong response to deviants (orange; left), which substantially exceed the omission (red) and standard stimulus (blue) responses [$P = 0.00018$ and $P = 1.4 \times 10^{-9}$, Wilcoxon signed-rank test (one-sided) between deviant responses relative to omission or standard responses; $n = 76$]. The relative responses of omission-sensitive (red) and omission-insensitive (blue) neurons to omissions and deviant stimuli are statistically indistinguishable (middle), indicated by the overlapping cumulative distributions of difference between omission and deviant responses (right column; $P = 0.15$, Wilcoxon rank sum test between the two populations on omission-deviant responses). Shaded areas in the left column indicate one SEM. All responses are relative to the preomission baseline period. (**B**) In the AC of the awake mouse, the responses are generally larger and the omission response becomes comparable in overall rate to the deviant response ($P = 0.36$), while the deviant response is ~91% larger than the stimulus response ($P = 2.7 \times 10^{-7}$). Many cells, particularly from the omission-sensitive (red) group, show omission responses that are larger than the deviant response (middle; red dots above diagonal). In the awake state, omission-sensitive neurons show a clear and significant separation in the difference between omission and deviant responses ($P = 0.0017$).

conditions. A dependence on the number of preceding standards is found in anesthetized, but not in awake. The latter might indicate that the omission response has already reached a plateau, which we cannot resolve presently, as even shorter sequences of standards (1 to 2) would be required.

Histological distribution of omission responses

The histological analysis of the electrolytic lesions in the IC demonstrates that omission-sensitive neurons are located in the nonlemniscal IC (fig. S3). To test whether omission responses show any specific distribution across the AC fields and/or layers, we analyzed where neurons with omission responses were located in the different AC regions (Fig. 8 and fig. S4).

We analyzed the distribution of omission-sensitive neurons across layers (Fig. 8, A to C). In the AC of anesthetized rats, the proportions of omission-sensitive neurons were 7.1, 35, and 22% for supragranular, granular, and infragranular layers, respectively (Fig. 8A, burgundy bars relative to gray). In the AC of anesthetized mice, these proportions were 26% of the neurons in the supragranular layers that were omission-sensitive, 30% in the granular, and 19% in the infragranular (Fig. 8B, burgundy bars). For awake mice AC neurons, these proportions were 40, 38, and 34% for the supragranular, granular, and infragranular layers, respectively (Fig. 8C, burgundy bars). We performed bootstrapping analysis on all three recording sets, but only found a significant reduction relative to the distribution of expected counts in the supragranular layer ($P = 0.003$, based on 300,000 independent draws, and $P < 0.05$ significance bound), although there appears to be a tendency for a higher fraction of omission-sensitive cells in supragranular layers in the awake compared with the anesthetized mouse. However,

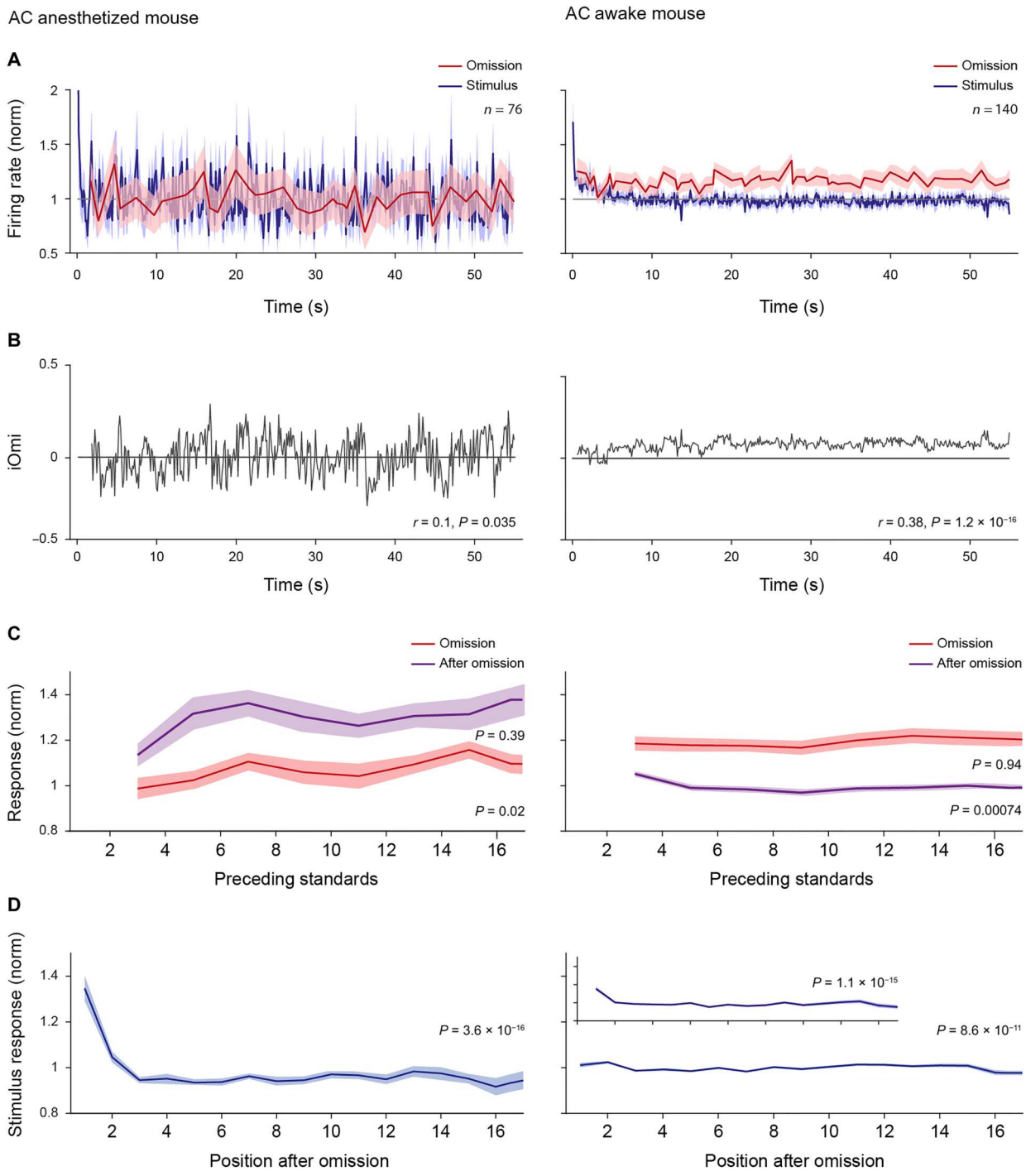

Fig. 7. Omission response progression depends on brain state. (**A**) Responses of the omission-sensitive cells to the standard stimulus (blue) adapt in both the anesthetized (left) and awake (right) state. Adaptation occurs more rapidly in the anesthetized state, reaching baseline already after ~1 s, while in the awake state, two time scales of adaptation are apparent, one very fast (one to two stimuli, i.e., ~125 to 250 ms) and the second with a time constant of ~5 s. The omission response stays rather constant over the entire period under both conditions but is consistently larger in the awake case ($P = 1.2 \times 10^{-22}$, Wilcoxon signed rank test between awake and anesthetized). (**B**) The index of omission sensitivity in relation to the standard responses, iOmi, consequently increases over time in the awake case ($r = 0.38$, $p = 1.2 \times 10^{-16}$, Pearson correlation), while this correlation is weaker and only borderline significant in the anesthetized case ($r = 0.1$, $P = 0.035$). (**C**) In the anesthetized state, the omission response exhibited a significant dependence on the number of standards preceding it [$P = 0.02$, Kruskal-Wallis analysis of variance (ANOVA)]. In the awake state, the omission response already starts at a high level and has no significant dependence on the number of preceding standards, possibly indicating that the dependence has already plateaued. The after-omission response shows a fast and significant decay to a plateau level. (**D**) The response to the standard following an omission decayed quickly, within two stimuli under anesthesia and just one stimulus in the awake (see inset for 20-ms analysis window; *P* values based on Kruskal-Wallis ANOVA). Using our standard analysis window (5 to 120 ms), the effect is also significant, but less pronounced, because of the brevity of the response (see Fig. 2B, right).

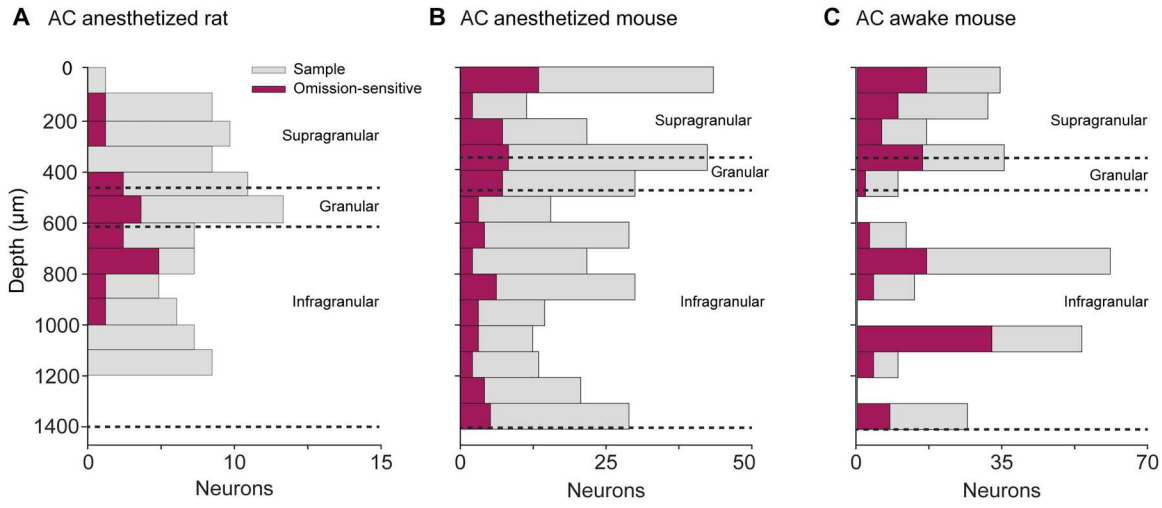

Fig. 8. Distribution of omission-sensitive neurons in the AC layers. (**A**) Anesthetized rat, (**B**) anesthetized mouse, and (**C**) awake mouse. Horizontal dashed lines indicate the boundaries between supragranular, granular, and infragranular layers. While the fraction of omission-sensitive neurons (burgundy bars) relative to the total sample (gray bars) is low in supragranular layers in anesthetized rats, for awake mice, there is a tendency toward a higher proportion of omission-sensitive neurons in the supragranular layers. Note that the depth AC is 1400 μm thick in mice because of the oblique trajectory of the recording electrodes to the pial surface, while in rat, it is 1200 μm thick because of the orthogonal trajectory.

additional research with higher-density probes will be required to fully address this question.

Last, we investigated the location of omission-sensitive neurons in subfields of the AC. Location data were only available in the rat, as the recordings in the mouse were all targeted toward A1 only. As we acknowledge that the number of cells is likely insufficient for a complete map, we provide these data in the supplement as suggestive evidence. To allocate each recorded neuron to a specific field in the rat AC, we recorded the frequency response areas and analyzed the topographical distribution of characteristic frequencies for all units. Each recording was assigned to a dorsoventral and rostrocaudal coordinate relative to bregma as in previous studies (*7*, *8*, *35*, *36*). This analysis allowed us to pool the data from all animals (fig. S4A) and construct a synthetic map of characteristic frequencies across the entire rat AC (*7*, *8*). Similar to these previous works, we found a high-frequency reversal zone between VAF (caudally) and anterior auditory field (AAF; rostrally), a low-frequency reversal zone between A1 and PAF (dorsocaudally), and a high-frequency reversal between VAF and SRAF (ventrally). Thus, we could reliably define the lemniscal (A1, AAF, and VAF) and nonlemniscal (SRAF and PAF) auditory cortical fields as shown in fig. S4A. The omission-sensitive neurons found in this study were located mostly toward the caudal areas of the AC, within the limits of A1, PAF, and SRAF (fig. S4A). When plotting iOmi levels for all significant sequences recorded (in this case, we did not use the average value per unit, because it would not allow to properly map the whole AC), it becomes evident that, although omission responses are distributed in all fields, the highest levels of iOmi were found in SRAF and PAF (fig. S4B).

DISCUSSION

The key finding of the current study is that a subset of neurons in the auditory brain responds to the absence of an expected stimulus, which provides empirical evidence in support of certain elements of predictive coding in a subcortical area and sensory cortex (*1*, *37*–*41*). Specifically, we demonstrate that robust neural activity emerges during the omission of a sound in a regular sequence of repetitive stimuli. These responses are consistent with prediction error signals, as these omissions result in the violation of an expected stimulus when it should occur. We identified several key properties of the omission responses. In particular, our results demonstrate that the omission responses depend on different parameters, including the repetition rate, brain state but are similar across species. According to our findings, omission-sensitive responses are already present under anesthesia and become even more pronounced under the awake condition in both number and strength. The omission responses are likely the earliest neuronal correlate underlying the salient perception of omitted stimuli in humans and can be considered to provide additional support for a hierarchical predictive coding framework (*1*, *37*, *39*, *42*, *43*).

Relation to previous studies

In humans, responses to omissions of tones are primarily observed at rather high presentation rates (*15*, *16*), corresponding to the presently used shortest SOA. To resolve these on the neuronal level, the high temporal resolution available in electrophysiology is highly suited. On the basis of single-unit recordings, our study demonstrates clear omission responses at the spiking level in the auditory system and thus identifies a potential neuronal correlate for those omission responses previously recorded using noninvasive techniques such as EEG/magnetoencephalography in humans (*9*, *16*, *25*, *44*–*49*).

Multiple studies have investigated mismatches between predictions and actual stimuli on the neuronal level using calcium imaging in different sensory cortices. While calcium imaging provides the possibility for highly parallel recordings, its temporal resolution limits the use of comparably fast SOAs in continuous sequences as in the present study. In the visual cortex V1 in the mouse, multiple studies reported responses to sequence violations

[e.g., (*50*–*52*)], as well as in the somatosensory system (*53*). In the auditory system, virtually no, if any, studies have directly looked for omission responses at the cellular level, or have not directly reported them (*7*, *8*, *13*, *34*, *54*, *55*). Two studies have reported potentially related results using calcium imaging: Li and colleagues (*56*) have reported neural responses at the end of a regular, slow train of repetitive stimuli as a persistent evoked response, which they termed echo responses (*56*, *57*). While those echo responses might also signal predictions, the much slower time scales (SOA: 2 to 4 s) suggest different underlying mechanisms. Possibly because of limitations imposed through the calcium dynamics, the studies did not find omission responses at fast rates. Given the shorter SOAs, we observe strong adaptation to the tones, while such adaptation appears to be absent in the longer SOAs for the echo responses, which suggests a difference in the contributing mechanisms. Other differences between omission and echo responses include latency and histological location: The latency of the present omission and stimulus responses was similar, which indicates that the omission responses are time-locked to the expected time of occurrence of the omitted stimuli. In contrast, the latency of the echo responses is significantly longer than that of the stimulus responses (237 versus 83 ms) (*57*). Omission responses are found in subcortical neurons, at the IC level, while the echo responses seem to only emerge at the cortical level (*56*). Moreover, these authors (*56*) also discuss very elegantly how their echo responses differ from the classical omissions recorded under the oddball paradigm as we do here. Li and colleagues (*56*) relate these responses to fit the time scales of motor responses. This is a key aspect of their work as their results strongly support that the neuronal circuits of the AC are critical for coding predictive information and transforming it into anticipatory motor behavior. There is also other work that is also similar in some ways to the echo responses but recorded in the IC, the so-called "long-lasting sound-evoked afterdischarge" responses or LSA neurons (*58*). These authors argue that, because LSA produces long-lasting firing in the absence of sound, it may be relevant to temporary or chronic tinnitus or to some other aftereffect of long-duration sound. While it thus appears that omission, LSA responses, and echo responses rely on different underlying mechanisms, the use of different stimulation paradigms and recording procedures complicates a conclusive comparison.

Earlier theoretical investigations using neural modeling had already suggested the existence of omission responses (*20*, *59*). Omission responses were here created by the difference between the activity of neurons encoding the prediction of the next stimulus and the actual input (see the "Relation to predictive coding theory" section for more details).

Relevance of the current results

We have recorded robust omission responses in the auditory pathway of anesthetized rats and anesthetized and awake mice using single- and multiunit recordings. These statistically significant responses of single neurons evoked by omitted tones had the largest proportion (~36%) observed in the awake AC and the lowest at the urethane-anesthetized AC of rats (~20%) and mice (~22%). The difference in the detected omission responses appears to be determined most strongly by brain state, because we did not find a significant difference between the omission response size in the AC between the anesthetized rat and mouse. The fact that we found omission responses also in anesthetized preparations suggests that omission detection and thus predictive coding are already partially available under the passive condition, without the need for specific attention (*8*, *23*). Furthermore, the proportion of omission responses was only substantially present at the shortest SOA of 125 ms, i.e., at relatively high presentation rates (up to 8 Hz). This time course suggests that if the sounds are close enough in time, then they form a perceptual unit and, hence, compatible with the temporal window of integration (*15*, *16*, *60*, *61*) that integrates neighboring sounds and/or omissions into a single percept.

While we could not find significant differences when the omission responses were preceded by a random number of reference stimuli (random), compared to a fixed number of reference stimuli (periodic), several studies have shown that expected omissions evoke a smaller response than unexpected omissions (*19*, *25*, *45*). It may be that the number of preceding repetitions (nine stimuli) in our periodic sequences is too large for producing an accurate expectation of when it should happen in our rodent models; if the animal loses track of how many repeated stimuli have happened, then these omissions would be perceived as events preceded by a random (albeit large) number of stimuli. This is supported by the rapid dynamics of adaptation or the responses to the standard stimulus following the omission, which return to baseline in just one to two stimuli (Fig. 7). Related to this, we only find a correlation between the number of preceding stimuli and the omission response under the anesthetized condition, while it may have already reached a plateau in the awake case. This finding relates to the previous work by Dürschmid *et al.* (*62*), which demonstrated that transitional probabilities are different in AC and prefrontal cortex by increasing the number of standards before a deviant occurrence. They observed that this increases the expectation of prediction errors in the prefrontal cortex, while this was not the case for the AC (*62*). This is in accordance with our data related to the number of preceding standard responses before an omission that did not show an enhancement but a sustained response. This is important because omission-selective responses have been reported in humans (*19*, *27*, *44*, *63*, *64*), suggesting the preactivation of neural circuits needed to process the actual physical inputs.

Additional related work in humans has shown an interaction between arousal (in the form of attentional set and expectation) and mismatch responses. For example, an elegant study by Auksztulewicz and Friston (*65*) concluded that temporal attention and sensory expectation produced opposing effects on evoked response amplitude, when orthogonally manipulated in an auditory mismatch paradigm. MMN was enhanced by attention, speaking against its supposedly preattentive nature. The distinction between expectation and attention may be useful when interpreting our results in the awake mice. In other words, there is a difference between expecting something and attending to a sensory stream, and these can have opposite effects on the amplitude of mismatch responses (and thus, presumably, omission-related responses).

Methodological considerations

An important strength in our study is that we have used two animal species and two different recording preparations in two different laboratory setups. This approach allowed us to distinguish the effect of species and brain state on the omission responses and demonstrate that the results under anesthesia do not differ significantly between mice and rats, mimicking previous results (*66*–*70*). In contrast, the frequency of omission-sensitive cells and the magnitude of

the omission responses were found to be larger in awake mice than under anesthesia. This would be in line with the differences in the level of response for humans in awake compared to unresponsive wakefulness state [see, e.g., (*67*)]. Furthermore, this is also consistent with our previous work comparing rat, mouse (*8*, *71*, *72*), and others that show a similar structural and functional organization of these rodents' auditory system [e.g., (*73*–*75*)], speaking in favor of the existence of genuine omission responses across species that can be modulated by arousal state.

It is unlikely that the omission responses we observed are not genuine responses or simply the reflection of rebound or entrainment effects as discussed elsewhere in the context of adaptation models (*17*, *76*) and our own control data shown in fig. S5. If these omission responses were just long latency activity evoked by the previous stimulus, then such activity would remain when probing the neurons with longer SOA sequences, but that is not the case in our data (see fig. S5). In addition, such an adaptation model would not account for omissions evoking a larger response than the tone they replaced as occurring in many of our responses; if anything, the effect would be opposite. Moreover, there are also models that support the predictive framework for omission responses. The modeling study by Wacongne *et al.* (*19*, *20*) demonstrated that omission responses were larger than stimulus responses in blocks containing quintuplets of tones where the last one was replaced by an omitted tone, whereas the adaptation model would predict equal omission responses in both instances. Moreover, entrainment should be stronger for periodic sensory stimuli (*77*).

Although there is no question that omission responses occur in AC, a relevant weakness in our study is that AC responses are biased toward A1 (lemniscal field) in the awake mouse and toward the nonlemniscal fields in the anesthetized rat, making it difficult to conclude if the differences in the response magnitude between the two preparations are related to the arousal state or the field location of the recordings. Although the results are in line with the hierarchical organization of prediction error that we have seen in our previous studies (*8*), future studies should clarify this confound.

We found a relatively small percentage (16.7%) of omission neurons in the IC of the anesthetized rat, at least compared to the amount of omission neurons in the anesthetized rats (19.5%) and mice (21.7%), as well as awake mice AC (35.6%). In the split data analysis, the IC responses are revealed to be less robust or statistical deviations. While the omission responses in the IC are thus not as robust as in the AC, the fact that the IC recordings were underpowered and were only conducted in the anesthetized state preclude a conclusion on the existence of omission-sensitive responses in the IC. For example, a recent study showed that a small proportion of IC neurons were pattern sensitive (*78*) and that a sparse set (~5%) of neurons in AC showed a high-rate prolonged burst firing responses to trained sounds (*79*). Further studies in the IC under the awake state with greater neuron numbers are required to resolve this question.

Relation to predictive coding theory

As in other sensory systems, where omission responses have been best explained by a deviation between expected and actual visual stimulus (*50*), our results are consistent with a predictive coding framework, in which sensory input is compared to an internal model of the environment to detect deviations from expectations. Because bottom-up inputs cannot account for omission responses, our results are consistent with the hypothesis that prediction is a hierarchical process encompassing subcortical and cortical neuronal circuitries and can be observed in two species and two brain states. Together, these findings are in agreement with two recent studies that have combined 9.4-T functional magnetic resonance imaging and high-density electrocorticographic recordings with a local-global auditory sequence paradigm to assess the hierarchical depth of auditory sequence processing in the marmoset brain (*80*, *81*). These authors demonstrate that the neural responses to omissions cannot be explained by any modulation of feedforward propagation and should contain specific information of upcoming predictive information (*80*, *82*). Hence, omission responses thus allow the study of top-down prediction signals decoupled from bottom-up input signals, i.e., without sensory input. Such a perspective supports the notion of an endogenous neural activity that could reflect the generation of predictions (*83*, *84*).

An important issue to be considered is whether responses encoding predictions can be disentangled from responses encoding prediction errors. According to predictive coding, omission responses can provide rather clear access to the representation of the prediction; as in this case, the prediction error is a, in the forward path inverted, copy of the prediction (*26*, *85*). Because the omission responses that we detected are elevations in firing rate, they likely provide access to the neural representation of prediction in the AC (*64*, *81*, *86*). Another distinction between prediction error and prediction responses may be feasible in time-frequency measures (*87*, *88*). Thus, positive omission responses are likely related to predictions (*10*, *21*) and within predictive coding theory represented by interneuron-mediated modulation of pyramidal output. Hence, they may share the neuronal and local circuitry of stimulus-specific adaptation that involves multiple neuron types (*35*, *89*, *90*), supporting feedforward and feedback inhibition and excitation of pyramidal output, which can detect deviations from regularity (*35*, *59*). Our data do not allow us to definitely distinguish whether we recorded from excitatory or inhibitory interneurons; we have observed omission responses in multiple AC layers that encompass different neuron types, suggesting that omission responses are generated and enhanced at the network level through a hierarchical process consistent with the predictive coding perspective (*1*, *37*–*39*, *43*, *84*, *91*). Canonical microcircuit formulations of predictive coding are quite consistent: They suggest that excitatory pyramidal cells encode prediction errors (*92*, *93*). Their activity is the difference between ascending stimulus information and the activity of interneurons. In this formulation, the interneurons represent the predictions, e.g., derived from regularities in the environment. The pyramidal cells are hypothesized to be located in superficial and granular layers, while the prediction carrying inhibitory neurons are hypothesized to be located in supragranular layers. However, the latter activity is also thought to be passed to infragranular pyramidal cells (*92*). This architecture makes it difficult to have a simple hypothesis of where omission-related responses should be found. This follows because they could be associated with predictions in deep pyramidal cells or the inhibitory interneurons in superficial layers. However, a more definitive interpretation would probably rest upon tracing studies or optogenetic characterization of the cells recorded. Thus, future studies are needed to separate pyramidal neurons from inhibitory interneurons to get a clearer picture of predictive coding in canonical microcircuits.

Another interesting, yet difficult, issue to resolve is how the different components described in the classical adaptation studies, i.e., prediction error and repetition suppression (*8*), relate to the deviant and omission responses. To address this issue, it would have been necessary to carry out additional control recordings using the cascade or many-standard sequence as in, e.g., (*8*, *23*, *35*, *94*). Unfortunately, these sequences are very time consuming and the current inclusion of other conditions (multiple SOAs, deviant) precluded the recording of these additional controls. This is definitely an interesting and open question but a limitation of the current study that should be explored in the future. In summary, the demonstration of omission responses in IC and AC, particularly in awake but also in anesthetized preparations, confirms that the auditory system does not require an external stimulus trigger to detect a deviation from expectations (*95*) and indicates that the auditory brain internally generates a prediction of future sensory input.

MATERIALS AND METHODS

Experimental procedures

Experiments were performed on 22 anesthetized adult female Long-Evans rats (9 rats were used for IC recordings and 13 rats for AC recordings) and 6 C57/B6 mice (3 awake and 3 under urethane anesthesia). The body weight ranged from 200 to 300 g in rats (9 to 17 weeks of age) and 25 to 35 g in mice (14 to 18 weeks of age). Each individual animal was used to record from a single auditory station, either IC or AC. Experimental procedures in anesthetized rats were carried out at the University of Salamanca, and all the experimental procedures and protocols were adjusted to the directives of the Directive of the European Communities (86/609/CEE, 2003/65/CE, and 2010/63/UE) and RD53/2013 Spanish Legislation for the use and care of animals. All the details of the study were approved by the Bioethics Committee of the University of Salamanca (USAL-ID-195 and USAL-ID-574). Experiments in awake mice were performed at the Central Dierenlaboratorium at the Radboud University Medical Center. The experimental procedures and protocols were approved by the Dutch central commission for animal research (Centrale Commissie Dierproeven) and implemented according to approved work protocols from the local animal welfare body (project number 2017-0041).

Experimental procedures in anesthetized rats

The experiments were carried out inside a chamber with acoustic insulation and electrical protection. Sound stimuli were generated using the RZ6 Multi I/O processor [Tucker-Davis Technologies (TDT)]. Sounds were presented monaurally (right ear) through a closed system using a custom-made earphone (1 to 45 kHz) coupled to a custom-made cone, as a substitute for traditional ear bars. Thus, sounds were presented through the speaker under a closed-field condition to the ear contralateral to the left IC or AC.

The software was programmed with OpenEx Suite (TDT) and MATLAB. The sound system response was flattened with an on-site calibrated finite impulse response system using a one-fourth-inch condenser microphone (model 4136, Brüel & Kjaer), a conditioning amplifier (Nexus, Brüel & Kjaer), and a dynamic signal analyzer (Photon+, Brüel & Kjaer). The speaker output was adjusted to ensure a flat spectrum (±2 dB) between 0.5 and 44 kHz, and the second and third harmonic components in the signal were >40 dB below the level of the fundamental at the highest output level [~76 dB of sound pressure level (SPL)]. A single neuron was recorded at a time, using a self-made glass-coated tungsten electrode whose impedance ranged from 1.5 to 3 megohm at 1 kHz.

Analog signals were digitized with an RZ6 multi-I/O processor, Medusa RA16PA preamp, and ZC16 main stage (TDT) at 25 kHz of sample rate and amplified 251×. The neurophysiological signals for multi- or single-unit activity were band-pass filtered between 0.5 and 4.5 kHz.

Experimental procedures in anesthetized and awake mice

The experiments were carried out inside an acoustically insulated and electromagnetically shielded and grounded booth. Sound stimuli were generated and recorded using a multichannel data acquisition device (USB-6351, National Instruments) through a custom-written MATLAB GUI (Controller). Sounds were presented to both ears using a speaker (T250D, Fostex) placed in front and above the animal. The output of the speaker was calibrated to have a flat spectral profile over the range of 2 to 80 kHz within 5 dB using an inverse linear filter, estimated before the experiment using an ultrasonic microphone (CM16/CMPA, Avisoft Bioacoustics) corrected for its own frequency-dependent sensitivity curve.

Surgical procedures in anesthetized rats

The initial surgical procedures were the same for the two auditory areas to be recorded (IC and AC). Electrophysiological procedures differed only in craniotomy location and recording electrode placement for each station.

Anesthesia was induced and maintained with urethane [1.9 g/kg, intraperitoneally (ip)] with supplementary doses (~0.5 g/kg, ip) administered as necessary. These replenishments were given to ensure a deep and stable anesthetic level whenever corneal or pedal retraction reflexes appeared. Urethane maintains a balanced neuronal activity better than other anesthetic agents that have a slight effect on inhibitory and excitatory synapses and that is why it was the selected anesthesia method (*96*).

At the beginning of surgery, both dexamethasone (0.25 mg/kg) and atropine (0.1 mg/kg) were administered to reduce cerebral edema and bronchial secretions, respectively. Lidocaine was also injected around the pinna tissue to achieve a higher anesthetic level in these areas (*8*). In addition, an isotonic glucosaline solution [5 to 10 ml every 6 to 8 hours, subcutaneously (sc)] was periodically administered to avoid dehydration. During all the experimental procedures, the animals were artificially ventilated, controlling the CO_2 levels, and the temperature was monitored with a rectal probe (36° to 38°C) and maintained with a heating blanket (Cibertec) placed under the animal.

Once the animal reached a surgical state of anesthesia, the ears were prepared by removing the cartilage to obtain a greater exposure of the ear canal. The trachea was cannulated to maintain ventilation artificially, and corneal and pedal withdrawal reflexes were constantly monitored to ensure that we maintained a deep anesthetic level during surgery and as uniform as possible throughout the recording procedure.

Once the animal was prepared, it was placed on the stereotactic frame; the upper jaw was attached to a bite bar and the restraint was carried out using ear bars. At this time, the speaker was also placed on the right ear of the animal, while the left ear canal was covered with plasticine.

Surgical procedures for IC (anesthetized rats)

For IC recordings, a craniotomy was performed on the left parietal bone to expose the cerebral cortex overlying the left IC. The dura was removed and the surrounding tissue was covered with cotton balls soaked in 0.9% saline solution to maintain hydration of the area.

Surgical procedures for AC (anesthetized rats)

For AC recordings, the skin and temporal muscles were removed from the left side of the skull and a 6-mm by 5-mm craniotomy was performed on the left temporal bone to expose the entire AC. The dura was removed and the cisterna magna was drained to prevent brain herniation. The exposed cortex area and surrounding tissue were covered with a transparent layer of agar to prevent desiccation and, thus, stabilize the recordings.

Surgical procedures for AC (awake and anesthetized mice)

Mice were implanted with a headpost for head fixation at the ages of 8 to 12 weeks. In the second surgery, performed when animals were 12 to 16 weeks old, mice were implanted with a silicon NeuroNexus neural probe aiming at the left primary AC, field A1, based on stereotaxic coordinates (3.2 mm post-bregma, 5.9 mm lateral from the midline) measured on the skull, estimated from (*97*), and confirmed preimplantation via intrinsic optical imaging of noise burst sequences (0.2-s long, 0.1 s interstimulus interval, 70 dB of SPL, 10 sounds per trial, 30 trials). A craniotomy (~1 mm by 2 mm) was opened using a microdrill centered on the part of AC that showed the strongest response in the intrinsic imaging. In the awake mice, the implant was chronic, mounted on a custom-designed drive (variant of the EDDS drive, Microprobes for Life Science), allowing the electrode array to be repositioned. The surgery was performed under general isoflurane anesthesia (1.5 to 2% dosage; E-Z Anesthesia, E-Z Systems Corporation). From 24 hours before to 48 hours after the surgery, the animal received an analgesic dissolved in water (1 ml/liter; carprofen (Rimadyl cattle), Zoetis], supplemented by another dose of carprofen at the start of the surgery (5 mg/kg, sc). In the anesthetized mice, the electrode array was inserted acutely for the period of the recordings under urethane anesthesia using one initial dose (1.7 g/kg, ip) and one to two supplementary doses (0.2 g/kg, ip). In addition, dexamethasone (0.2 mg/kg, sc) was given under both conditions after induction of anesthesia to reduce local bulging of the brain, and a ground screw was implanted over the right frontal cortex.

Electrophysiological recording procedures

Auditory brainstem response recording in anesthetized rats

Once the animal was under anesthesia, before starting the surgery and therefore the recording sessions, the auditory brainstem responses were recorded using subcutaneous electrodes to ensure that the animal had normal hearing, using the RZ6 Multi I/O processor (TDT) as hardware and BioSig software (TDT). The auditory brainstem response stimuli were generated following standard procedures (0.1ms clicks presented at a rate of 21 Hz, applied monaurally to the right ear in 10 dB of upward steps between 10 and 90 dB of SPL using a closed-field speaker).

Procedures for electrophysiological recording in IC (anesthetized rats)

For measurements in the IC, an electrode was placed orthogonal to the surface of the brain (forming an angle of 20° with the horizontal plane, oriented caudally), advanced between 7500 and 10,000 μm from lambda to bregma and 500 and 3000 μm to the left ear, and then lowered into the brain between 4400 and 5600 μm using a piezoelectric micromanipulator (Sensapex) until we observed a strong spike activity synchronized with the search stimulus train.

Procedures for electrophysiological recording in AC (anesthetized rats)

Once the AC was exposed and the tissue was stabilized, an enlarged image of the exposed surface was taken (×25). The image included a pair of landmarks previously marked before the craniotomy, on the dorsal border of the temporal bone, indicating the absolute scale and position of the image relative to bregma. This image was displayed on a computer screen, and a grid was overlaid on it that would serve as a guide so we would be able to mark the recording electrode placement for each recording. The snapshot was taken with a single lens digital reflex camera (D5100, Nikon) coupled to the surgical microscope (Zeiss) through a lens adapter (TTI Medical) (*7*).

For AC measurements, we placed the electrode in contact with the AC and as perpendicular as possible to its surface. After this, we advanced it between 0 and 2000 μm in depth. The recording tracks were spaced 250 to 500 μm and placed through the cortical regions of interest, while blood vessels were avoided. The vascular pattern was used as a local reference to mark the position on the image where the tract was made, considering that this map varies between animals. At the end of the experiment, the limits and the relative position of the auditory fields were identified according to the pure-tone frequency response topographies in rats (*7*). We estimated the depth of each neuron from the reading of the micromanipulator relative to the brain surface (Fig. 8A). We used the depths of the layers in the rat AC as stated by Pérez-González *et al.* (*35*) (i.e., the granular layer would extend between 457 and 614 μm).

The characteristic frequency of each recording track was calculated as the average characteristic frequency of all neurons recorded on that track, including a rapid multiunit activity frequency response area recording performed between 400 and 550 μm in depth, corresponding to layers IIIb to IV. The reversals of the characteristic frequency progression defined the boundaries between the cortical fields (*98*), so that most recordings could be assigned to one specific field: primary or secondary and their corresponding subdivisions: AAF, VAF, A1, PAF, and SRAF.

Procedures for electrophysiological recording in AC (awake mice)

For the time of the recording, the animal was placed on a platform located in the middle of a booth and head-fixated using an implanted headpost. All recordings were performed using NeuroNexus silicon probes with 64 channels. The recording sites were distributed differently per probe; in particular, we used two 4x16 (A4x16-Poly2-5mm-23s-200-177 and A4x16-2.5mm-tet/lin-300/125-333-121/177-PC) configurations. Data were digitized using a combination of a 64-channel (Intan Technologies) headstage connected to an Open Ephys recording system (Open Ephys, Cambridge, USA). Data were collected at a sampling rate of 30 kS/s, band-pass filtered between 0.3 and 6 kHz, and spike-sorted to get multi- and single-unit responses using the openly available function autoSortC from the Controller package. The sorting used automatic criteria for cluster-cutting rather than human decisions, which are prone to be variable from day to day. Sorting was performed separately for each prong. The average number of cells/electrode in a single

session was 0.71 after spike-sorting, which is a typical yield, e.g., in comparison to other recording techniques (0.625 cells per electrode) (*99*). We estimated the depth of each cell from the depth of the array relative to the brain surface and the position of the recording sites in each array configuration (Fig. 8). The depths of the layers were estimated from a coronal section of the mouse AC in the Allen Brain Atlas (*100*) (i.e., the granular layer would extend between 355 and 477 μm).

Location of cells and recording of the frequency response area (anesthetized rat)

The sounds used to search for neuronal activity were trains of noise or pure tones (1 to 4 stimuli/s). These stimuli had a short duration (30 ms) to avoid a strong adaptation. Sound parameters such as frequency, intensity, presentation rate, or type of sound such as white noise, narrow band noise, or pure tones were manually varied as necessary to facilitate mismatch.

For each neuron recorded, the frequency response area was calculated, which is the response magnitude map for each pair of frequency/intensity data. This was calculated in the first place to ensure that the frequencies and intensities used were contained in the response range. To obtain this frequency response area, a sequence of tones was presented at a rate of 4 Hz, randomly varying the frequency and intensity of the tones presented (three to five repetitions of each tone).

For the AC recordings, the coordinates of the neurons over the AC extension were measured from the micromanipulator as the position of the recording electrode in reference to bregma. For the IC recordings, at the end of the recording session, a 5-μA current was driven for 5 s through the recording electrode to produce an electrolytic lesion. Animals were euthanized with a lethal dose of pentobarbital, and the head was removed and immersed in a mixture of 1% paraformaldehyde and 1% glutaraldehyde in 1 M phosphate-buffered saline. After fixation, tissue was cryoprotected in 30% sucrose and sectioned in a freezing microtome to obtain 40-μm-thick coronal sections. The sections were stained using 0.1% cresyl violet to facilitate identification of cytoarchitectural boundaries.

Online viewing

For the anesthetized experiments, we visualized the electrophysiological recordings online using custom-written software with MATLAB (MathWorks) and OpenEx Suite (TDT). Multiple-unit activity was automatically extracted by manually setting a unilateral action potential threshold above the background noise as an accurate estimate of neuronal population dynamics (*101*). Once a neuron was isolated and confirmed to be stable, the stimulation protocol described in the next section was applied. For the awake experiments, the activity was monitored online using the Open Ephys GUI, and stimuli were presented if single-unit neural activity could be visually detected.

Stimulation parameters

The sounds used for stimulation were sinusoidal tones of 75-ms duration, including up and down ramps of 5 ms, at a frequency and intensity within the response area of the neuron. In the single-electrode recordings in the rat, the frequency-intensity combination could be chosen specifically for the single neuron recorded at a time. In the many-electrode recordings in the mouse, we chose a set of frequencies that made a good match with the frequency response areas of the currently recorded cells. We used a fixed set of three intensities in the mouse ([50,60,70] dB of SPL) that were intense enough to activate all recorded neurons. These sounds were presented in an oddball sequence of 400 tones long. The oddball sequence consisted of a repeating tone (90% standard probability) that was occasionally omitted (10% deviant probability).

The omission of the tone was presented in two different ways within the oddball sequence: periodically or randomly, always with the same probability of appearance. A minimum of three standard tones were presented before each deviant. These sequences were presented with different SOAs (125, 250, and 500 ms) to control for confusion between actual responses to omissions and responses to previous standard stimuli. To double-check that no sound was played during omissions, we recorded the output of the speaker while playing the stimulation sequence to check that there was no acoustic signal during the omissions (fig. S1).

In a second set of recordings, we compared deviant tones with omission responses in the AC of anesthetized rats and awake mice (Fig. 6). For this purpose, identical sequences were used with either deviant tones or omissions occurring at the same positions in the sequence. In the single-electrode recordings in the rat, the standard and deviant frequencies were chosen to lie symmetrically around the characteristic frequency at the same intensity to elicit similar response rates (Fig. 6A). The paradigm was run with either of the two stimuli as standard and deviant. In the multielectrode recordings in the mouse, we chose a pair of frequencies that provided the best match to the currently recorded cells and also ran the paradigm with both frequencies for standard and deviant. All subsequent analyses for omissions and deviants were identical. Comparisons were then performed on the set of omission-sensitive neurons.

The output of the system was also recorded using a one-fourth-inch condenser microphone (model 4136, Brüel & Kjaer) to ensure the absence of any sound or noise during omissions (fig. S1). The spectrogram in fig. S1A shows a portion of the presented periodic omission sequence, reflecting the intensity of the sounds that the system reproduces. The power spectrum shown in fig. S1B allows comparison between the signal produced during a real stimulus (blue) and the omitted signal (red) and confirms that no sound was reproduced during the omission.

Data and statistical analysis

After the single- and multiunit response times were established, we selected the cells that elicited responses for omissions. We did that by comparing firing rates during omitted tones to the pre-stimulus firing rates. For this purpose, comparison windows had to be defined. The pre-stimulus/stimulus windows were defined individually for each SOA. These windows were chosen after visual inspection of the responses, aiming to include the bulk of the evoked responses while leaving enough time to calculate the pre-stimulus activity for the next trial. Because of the long AC responses, for the 125 SOA recordings, there is some overlap between the pre-stimulus and stimulus windows. The pre-stimulus window start was defined as 25, 75, and 195 ms before the stimulus onset for 125, 250, and 500 ms of SOA, respectively. All pre-stimulus windows ended 5 ms after the start of the stimulus, because the evoked response latency was always longer great than 5 ms. This time also marks the start of the "stimulus window." Stimulus windows ended at 120, 150, and 225 ms for 125, 250, and 500 ms

of SOA, respectively. Note that stimulus here refers to both tone and omission. These values are summarized in Table 3.

Firing rates were computed in all of the predefined windows and used in subsequent analyses to compare the responses under the tested conditions. PSTHs (10-ms bins; Fig. 2 and fig. S5) were aligned to show the average response around the omission. Peak latencies were calculated for each tone or omission as the time (relative to stimulus onset) of the maximum value in the stimulus PSTH (1-ms bins).

Omission responses were identified as an elevated firing rate during the omitted tones. Specifically, responses during the omission window were considered significant if their mean firing rate was significantly larger than the mean firing rate of the cell's activity, immediately preceding the omission window.

Using these time windows, we collected for each omission the firing rates of preomission activity and the firing rates of omission activity. To avoid a positive bias due to double dipping, we used split data analysis (*32*), i.e., only every other omission was used for statistical testing, while the complementary set was used for all subsequent analyses. These sets are referred to as "statistics set" and "analysis set." The starting point, the first or second omission, for the division into the two sets was randomized independently between cells, i.e., either using the omissions at positions [1, 3, 5, ...] or [2, 4, 6,...] for the statistics set and, correspondingly, the complement for the analysis set. In the statistics set, the preomission activity was compared against the periomission activity over the length of the stimulus window (see above) using a single-sided paired Wilcoxon signed-rank test. A neuron was termed an "omission-sensitive neuron" if the P value was <0.05. False positives in this classification will not translate to elevated omission responses, based on the split data analysis, where only systematic differences, present in both splits of the data, are retained in the plotting. The significance on the population level is then subsequently tested on the part of the data not used for statistical testing (see Fig. 3).

The iOmi used to quantify the comparison between sound- and omission-evoked firing rate (Fig. 4A) was defined as: iOmi = (Omi FR − Stim FR)/(Omi FR + Stim FR). The firing rate for stimuli was averaged from all stimulus presentations.

The statistical analysis on the population level was performed using ANOVA (Kruskal-Wallis analysis for one-way comparisons) followed by pairwise comparisons between individual conditions using Wilcoxon signed-rank test with Bonferroni correction for the number of tests performed. Rates were transformed to approximately normal distributions by taking their logarithm, given that neural responses are distributed exponentially particularly at low rates. For differences between firing rates, e.g., stimulus versus omissions, we computed the logarithm of the difference in rates, before applying ANOVA.

For testing whether the percentage of omission-sensitive neurons in each layer was as expected if these neurons were randomly distributed across layers, we sampled the same number of omission-sensitive neurons according to the empirical distributions across layer groups (i.e. granular, infragranular, and supragranular) using bootstrapping (300,000 samples) and then compared the actual distribution of omission-sensitive cells to the bootstrapped densities. The P values represent their location in the distribution at the closest end of the density.

Table 3. Times of the analysis windows, relative to stimulus/omission onset.

SOA	Pre-stimulus window start	Pre-stimulus window stop/stimulus window start	Stimulus window stop
125	−25 ms	5 ms	120 ms
250	−75 ms	5 ms	150 ms
500	−195 ms	5 ms	225 ms

Supplementary Materials

This PDF file includes:
Figs. S1 to S5
Legend for data S1

Other Supplementary Material for this manuscript includes the following:
Data S1

View/request a protocol for this paper from *Bio-protocol*.

REFERENCES AND NOTES

1. K. Friston, A theory of cortical responses. *Phil. Trans. R. Soc. B* **360**, 815–836 (2005).
2. I. Winkler, Interpreting the mismatch negativity. *J. Psychophysiol.* **21**, 147–163 (2007).
3. M. I. Garrido, K. J. Friston, S. J. Kiebel, K. E. Stephan, T. Baldeweg, J. M. Kilner, The functional anatomy of the MMN: A DCM study of the roving paradigm. *Neuroimage* **42**, 936–944 (2008).
4. H. E. M. Den Ouden, K. J. Friston, N. D. Daw, A. R. McIntosh, K. E. Stephan, A dual role for prediction error in associative learning. *Cereb. Cortex* **19**, 1175–1185 (2009).
5. H. E. M. Den Ouden, P. Kok, F. P. de Lange, How prediction errors shape perception, attention, and motivation. *Front. Psychol.* **3**, 548 (2012).
6. G. Stefanics, P. Astikainen, I. Czigler, Visual mismatch negativity (vMMN): A prediction error signal in the visual modality. *Front. Hum. Neurosci.* **8**, 1074 (2015).
7. J. Nieto-Diego, M. S. Malmierca, Topographic distribution of stimulus-specific adaptation across auditory cortical fields in the anesthetized rat. *PLOS Biol.* **14**, e1002397 (2016).
8. G. G. Parras, J. Nieto-Diego, G. V. Carbajal, C. Valdés-Baizabal, C. Escera, M. S. Malmierca, Neurons along the auditory pathway exhibit a hierarchical organization of prediction error. *Nat. Commun.* **8**, 2148 (2017).
9. A. Bendixen, I. SanMiguel, E. Schröger, Early electrophysiological indicators for predictive processing in audition: A review. *Int. J. Psychophysiol.* **83**, 120–131 (2012).
10. G. V. Carbajal, M. S. Malmierca, The neuronal basis of predictive coding along the auditory pathway: From the subcortical roots to cortical deviance detection. *Trends Hear.* **22**, 233121651878482 (2018).
11. G. V Carbajal, M. S. Malmierca, Novelty processing in the auditory system: Detection, adaptation or expectation?, in *The Senses: A Comprehensive Reference*, B. Fritzsch, B. Gothe, Eds. (Elsevier, ed. 2, 2020), pp. 749–776.
12. A. Yuille, D. Kersten, Vision as Bayesian inference: Analysis by synthesis? *Trends Cogn. Sci.* **10**, 301–308 (2006).
13. F. M. Antunes, I. Nelken, E. Covey, M. S. Malmierca, Stimulus-specific adaptation in the auditory thalamus of the anesthetized rat. *PLOS ONE* **5**, e14071 (2010).
14. R. P. N. Rao, D. H. Ballard, Predictive coding in the visual cortex: A functional interpretation of some extra-classical receptive-field effects. *Nat. Neurosci.* **2**, 79–87 (1999).
15. M. Tervaniemi, J. Saarinen, P. Paavilainen, N. Danilova, R. Näätänen, Temporal integration of auditory information in sensory memory as reflected by the mismatch negativity. *Biol. Psychol.* **38**, 157–167 (1994).
16. H. Yabe, M. Tervaniemi, K. Reinikainen, R. Näätänen, Temporal window of integration revealed by MMN to sound omission. *Neuroreport* **8**, 1971–1974 (1997).
17. P. J. C. May, H. Tiitinen, Mismatch negativity (MMN), the deviance-elicited auditory deflection, explained. *Psychophysiology* **47**, 66–122 (2010).
18. J. Horváth, D. Müller, A. Weise, E. Schröger, Omission mismatch negativity builds up late. *Neuroreport* **21**, 537–541 (2010).

19. C. Wacongne, E. Labyt, V. Van Wassenhove, T. Bekinschtein, L. Naccache, S. Dehaene, Evidence for a hierarchy of predictions and prediction errors in human cortex. *Proc. Natl. Acad. Sci. U.S.A.* **108**, 20754–20759 (2011).
20. C. Wacongne, J. P. Changeux, S. Dehaene, A neuronal model of predictive coding accounting for the mismatch negativity. *J. Neurosci.* **32**, 3665–3678 (2012).
21. M. Heilbron, M. Chait, Great expectations: Is there evidence for predictive coding in auditory cortex? *Neuroscience* **389**, 54–73 (2018).
22. Y. M. Fonken, A. Mukerji, R. Jimenez, J. Lin, P. Brunner, G. Schalk, R. T. Knight, Unexpected sound omissions are signaled in human posterior superior temporal gyrus: An intracranial study. bioRxiv 733212 [Preprint]. 14 August 2019. https://doi.org/10.1101/733212.
23. L. Casado-Román, G. V. Carbajal, D. Pérez-González, M. S. Malmierca, Prediction error signaling explains neuronal mismatch responses in the medial prefrontal cortex. *PLOS Biol.* **18**, e3001019 (2020).
24. A. Bendixen, E. Schröger, I. Winkler, I heard that coming: Event-related potential evidence for stimulus-driven prediction in the auditory system. *J. Neurosci.* **29**, 8447–8451 (2009).
25. A. Todorovic, F. van Ede, E. Maris, F. P. de Lange, Prior expectation mediates neural adaptation to repeated sounds in the auditory cortex: An MEG study. *J. Neurosci.* **31**, 9118–9123 (2011).
26. E. Schröger, S. A. Kotz, I. SanMiguel, Bridging prediction and attention in current research on perception and action. *Brain Res.* **1626**, 1–13 (2015).
27. M. Cornella, A. Bendixen, S. Grimm, S. Leung, E. Schröger, C. Escera, Spatial auditory regularity encoding and prediction: Human middle-latency and long-latency auditory evoked potentials. *Brain Res.* **1626**, 21–30 (2015).
28. D. J. M. Kraemer, C. N. Macrae, A. E. Green, W. M. Kelley, Sound of silence activates auditory cortex. *Nature* **434**, 158 (2005).
29. M. S. Malmierca, Auditory system, in *The Rat Nervous System*, G. Paxinos, Ed. (Elsevier–Academic Press, ed. 4, 2015), pp. 865–946.
30. M. S. Malmierca, D. K. Ryugo, Descending connections of auditory cortex to the midbrain and brain stem. *Audit. Cortex*, 189–208 (2011).
31. R. Näätänen, A. W. K. Gaillard, S. Mäntysalo, Early selective-attention effect on evoked potential reinterpreted. *Acta Psychol. (Amst)* **42**, 313–329 (1978).
32. N. Kriegeskorte, W. K. Simmons, P. S. Bellgowan, C. I. Baker, Circular analysis in systems neuroscience: The dangers of double dipping. *Nat. Neurosci.* **12**, 535–540 (2009).
33. K. S. Button, Double-dipping revisited. *Nat. Neurosci.* **22**, 688–690 (2019).
34. M. S. Malmierca, S. Cristaudo, D. Pérez-González, E. Covey, Stimulus-specific adaptation in the inferior colliculus of the anesthetized rat. *J. Neurosci.* **29**, 5483–5493 (2009).
35. D. Pérez-González, G. G. Parras, C. J. Morado-Díaz, C. Aedo-Sánchez, G. V. Carbajal, M. S. Malmierca, Deviance detection in physiologically identified cell types in the rat auditory cortex. *Hear. Res.* **399**, 107997 (2021).
36. D. B. Polley, H. L. Read, D. A. Storace, M. M. Merzenich, Multiparametric auditory receptive field organization across five cortical fields in the albino rat. *J. Neurophysiol.* **97**, 3621–3638 (2007).
37. M. I. Garrido, J. M. Kilner, K. E. Stephan, K. J. Friston, The mismatch negativity: A review of underlying mechanisms. *Clin. Neurophysiol.* **120**, 453–463 (2009).
38. Z. C. Chao, K. Takaura, L. Wang, N. Fujii, S. Dehaene, Large-scale cortical networks for hierarchical prediction and prediction error in the primate brain. *Neuron* **100**, 1252–1266.e3 (2018).
39. K. Friston, S. Kiebel, Cortical circuits for perceptual inference. *Neural Netw.* **22**, 1093–1104 (2009).
40. F. P. de Lange, M. Heilbron, P. Kok, How do expectations shape perception? *Trends Cogn. Sci.* **22**, 764–779 (2018).
41. H. C. Barron, R. Auksztulewicz, K. Friston, Prediction and memory: A predictive coding account. *Prog. Neurobiol.* **192**, 101821 (2020).
42. K. Friston, Hierarchical models in the brain. *PLOS Comput. Biol.* **4**, e1000211 (2008).
43. F. Lieder, J. Daunizeau, M. I. Garrido, K. J. Friston, K. E. Stephan, Modelling trial-by-trial changes in the mismatch negativity. *PLOS Comput. Biol.* **9**, e1002911 (2013).
44. T. Raij, L. McEvoy, J. P. Mäkelä, R. Hari, Human auditory cortex is activated by omissions of auditory stimuli. *Brain Res.* **745**, 134–143 (1997).
45. S. Chennu, V. Noreika, D. Gueorguiev, Y. Shtyrov, T. A. Bekinschtein, R. Henson, Silent expectations: Dynamic causal modeling of cortical prediction and attention to sounds that weren't. *J. Neurosci.* **36**, 8305–8316 (2016).
46. T. T. Dercksen, A. Widmann, E. Schröger, N. Wetzel, Omission related brain responses reflect specific and unspecific action-effect couplings. *Neuroimage* **215**, 116840 (2020).
47. T. T. Dercksen, A. Widmann, F. Scharf, N. Wetzel, Sound omission related brain responses in children. *Dev. Cogn. Neurosci.* **53**, 101045 (2022).
48. D. A. Prete, D. Heikoop, J. E. McGillivray, J. P. Reilly, L. J. Trainor, The sound of silence: Predictive error responses to unexpected sound omission in adults. *Eur. J. Neurosci.* **55**, 1972–1985 (2022).
49. S.-L. Joutsiniemi, R. Hari, Omissions of auditory stimuli may activate frontal cortex. *Eur. J. Neurosci.* **1**, 524–528 (1989).
50. A. Fiser, D. Mahringer, H. K. Oyibo, A. V. Petersen, M. Leinweber, G. B. Keller, Experience-dependent spatial expectations in mouse visual cortex. *Nat. Neurosci.* **19**, 1658–1664 (2016).
51. G. B. Keller, T. Bonhoeffer, M. Hübener, Sensorimotor mismatch signals in primary visual cortex of the behaving mouse. *Neuron* **74**, 809–815 (2012).
52. A. Pak, S. T. Kissinger, A. A. Chubykin, Impaired adaptation and laminar processing of the oddball paradigm in the primary visual cortex of Fmr1 KO mouse. *Front. Cell. Neurosci.* **15**, 668230 (2021).
53. H. Mohan, Y. Gallero-Salas, S. Carta, J. Sacramento, B. Laurenczy, L. T. Sumanovski, C. P. J. De Kock, F. Helmchen, S. Sachidhanandam, Sensory representation of an auditory cued tactile stimulus in the posterior parietal cortex of the mouse. *Sci. Rep.* **8**, 7739 (2018).
54. N. Ulanovsky, L. Las, I. Nelken, Processing of low-probability sounds by cortical neurons. *Nat. Neurosci.* **6**, 391–398 (2003).
55. B. J. Farley, M. C. Quirk, J. J. Doherty, E. P. Christian, Stimulus-specific adaptation in auditory cortex is an NMDA-independent process distinct from the sensory novelty encoded by the mismatch negativity. *J. Neurosci.* **30**, 16475–16484 (2010).
56. J. Li, X. Liao, J. Zhang, M. Wang, N. Yang, J. Zhang, G. Lv, H. Li, J. Lu, R. Ding, X. Li, Y. Guang, Z. Yang, H. Qin, W. Jin, K. Zhang, C. He, H. Jia, S. Zeng, Z. Hu, I. Nelken, X. Chen, Primary auditory cortex is required for anticipatory motor response. *Cereb. Cortex* **27**, 3254–3271 (2017).
57. M. Wang, R. Li, J. Li, J. Zhang, X. Chen, S. Zeng, X. Liao, Frequency selectivity of echo responses in the mouse primary auditory cortex. *Sci. Rep.* **8**, 49 (2018).
58. M. Ono, D. C. Bishop, D. L. Oliver, Long-lasting sound-evoked afterdischarge in the auditory midbrain. *Sci. Rep.* **6**, 20757 (2016).
59. V. S. C. Chien, B. Maess, T. R. Knösche, A generic deviance detection principle for cortical On/Off responses, omission response, and mismatch negativity. *Biol. Cybern.* **113**, 475–494 (2019).
60. H. Yabe, M. Tervaniemi, J. Sinkkonen, M. Huotilainen, R. J. Ilmoniemi, R. Näätänen, Temporal window of integration of auditory information in the human brain. *Psychophysiology* **35**, 615–619 (1998).
61. Y. Mori, H. Hoshino, Y. Osakabe, T. Wada, K. Kanno, T. Shiga, S. Itagaki, I. Miura, H. Yabe, Omission mismatch negativity of speech sounds reveals a functionally impaired temporal window of integration in schizophrenia. *Clin. Neurophysiol.* **132**, 1144–1150 (2021).
62. S. Dürschmid, E. Edwards, C. Reichert, C. Dewar, H. Hinrichs, H. J. Heinze, H. E. Kirsch, S. S. Dalal, L. Y. Deouell, R. T. Knight, Hierarchy of prediction errors for auditory events in human temporal and frontal cortex. *Proc. Natl. Acad. Sci. U.S.A.* **113**, 6755–6760 (2016).
63. H. C. Hughes, T. M. Darcey, H. I. Barkan, P. D. Williamson, D. W. Roberts, C. H. Aslin, Responses of human auditory association cortex to the omission of an expected acoustic event. *Neuroimage* **13**, 1073–1089 (2001).
64. I. SanMiguel, A. Widmann, A. Bendixen, N. Trujillo-Barreto, E. Schröger, Hearing silences: Human auditory processing relies on preactivation of sound-specific brain activity patterns. *J. Neurosci.* **33**, 8633–8639 (2013).
65. R. Auksztulewicz, K. Friston, Attentional enhancement of auditory mismatch responses: A DCM/MEG study. *Cereb. Cortex* **25**, 4273–4283 (2015).
66. T. A. Bekinschtein, S. Dehaene, B. Rohaut, F. Tadel, L. Cohen, L. Naccache, Neural signature of the conscious processing of auditory regularities. *Proc. Natl. Acad. Sci. U.S.A.* **106**, 1672–1677 (2009).
67. U. Górska, A. Rupp, T. Celikel, B. Englitz, Assessing the state of consciousness for individual patients using complex, statistical stimuli. *NeuroImage. Clin.* **29**, 102471 (2021).
68. K. V. Nourski, M. Steinschneider, A. E. Rhone, H. Kawasaki, M. A. Howard, M. I. Banks, Auditory predictive coding across awareness states under anesthesia: An intracranial electrophysiology study. *J. Neurosci.* **38**, 8441–8452 (2018).
69. K. V. Nourski, M. Steinschneider, A. E. Rhone, B. M. Krause, H. Kawasaki, M. I. Banks, Cortical responses to auditory novelty across task conditions: An intracranial electrophysiology study. *Hear. Res.* **399**, 107911 (2021).
70. C. A. Smout, M. F. Tang, M. I. Garrido, J. B. Mattingley, Attention promotes the neural encoding of prediction errors. *PLOS Biol.* **17**, e2006812 (2019).
71. D. Duque, M. S. Malmierca, Stimulus-specific adaptation in the inferior colliculus of the mouse: Anesthesia and spontaneous activity effects. *Brain Struct. Funct.* **220**, 3385–3398 (2015).
72. Y. A. Ayala, D. Pérez-González, M. S. Malmierca, Stimulus-specific adaptation in the inferior colliculus: The role of excitatory, inhibitory and modulatory inputs. *Biol. Psychol.* **116**, 10–22 (2016).
73. M. S. Malmierca, D. K. Ryugo, Auditory system, in *The Mouse Nervous System* (Elsevier, 2012), pp. 607–645.

74. D. Choy Buentello, D. C. Bishop, D. L. Oliver, Differential distribution of GABA and glycine terminals in the inferior colliculus of rat and mouse. *J. Comp. Neurol.* **523**, 2683–2697 (2015).
75. H. Foley, M. Matlin, The auditory system, in *Sensation and Perception* (Psychology Press, 2015), pp. 258–284.
76. P. J. C. May, H. Tiitinen, Auditory scene analysis and sensory memory: The role of the auditory N100m. *Neurol. Clin. Neurophysiol.* **2004**, 19 (2004).
77. L. Gao, X. Meng, C. Ye, H. Zhang, C. Liu, Y. Dan, M. M. Poo, J. He, X. Zhang, Entrainment of slow oscillations of auditory thalamic neurons by repetitive sound stimuli. *J. Neurosci.* **29**, 6013–6021 (2009).
78. M. S. Malmierca, G. V Carbajal, C. Escera, Deviance detection and encoding acoustic regularity in the auditory midbrain, in *The Oxford Handbook of the Auditory Brainstem*, K. Kandler, Ed. (Oxford Univ. Press, 2019), pp. 706–740.
79. M. Wang, X. Liao, R. Li, S. Liang, R. Ding, J. Li, J. Zhang, W. He, K. Liu, J. Pan, Z. Zhao, T. Li, K. Zhang, X. Li, J. Lyu, Z. Zhou, Z. Varga, Y. Mi, Y. Zhou, J. Yan, S. Zeng, J. K. Liu, A. Konnerth, I. Nelken, H. Jia, X. Chen, Single-neuron representation of learned complex sounds in the auditory cortex. *Nat. Commun.* **11**, 4361 (2020).
80. Y. Jiang, M. Komatsu, Y. Chen, R. Xie, K. Zhang, Y. Xia, P. Gui, Z. Liang, L. Wang, Constructing the hierarchy of predictive auditory sequences in the marmoset brain. *eLife* **11**, e74653 (2022).
81. Y. Suda, M. Tada, T. Matsuo, K. Kawasaki, T. Saigusa, M. Ishida, T. Mitsui, H. Kumano, K. Kirihara, T. Suzuki, K. Matsumoto, I. Hasegawa, K. Kasai, T. Uka, Prediction-related frontal-temporal network for omission mismatch activity in the macaque monkey. *Front. Psych.* **13**, 557954 (2022).
82. G. Demarchi, G. Sanchez, N. Weisz, Automatic and feature-specific prediction-related neural activity in the human auditory system. *Nat. Commun.* **10**, 3440 (2019).
83. E. Schröger, A. Marzecová, I. Sanmiguel, Attention and prediction in human audition: A lesson from cognitive psychophysiology. *Eur. J. Neurosci.* **41**, 641–664 (2015).
84. A. Braga, M. Schönwiesner, Neural substrates and models of omission responses and predictive processes. *Front. Neural Circuits.* **16**, 799581 (2022).
85. B. Korka, A. Widmann, F. Waszak, Á. Darriba, E. Schröger, The auditory brain in action: Intention determines predictive processing in the auditory system—A review of current paradigms and findings. *Psychon. Bull. Rev.* **29**, 321–342 (2022).
86. I. SanMiguel, K. Saupe, E. Schröger, I know what is missing here: Electrophysiological prediction error signals elicited by omissions of predicted "what" but not "when". *Front. Hum. Neurosci.* **7**, 407 (2013).
87. L. H. Arnal, V. Wyart, A. L. Giraud, Transitions in neural oscillations reflect prediction errors generated in audiovisual speech. *Nat. Neurosci.* **14**, 797–801 (2011).
88. L. H. Arnal, A. L. Giraud, Cortical oscillations and sensory predictions. *Trends Cogn. Sci.* **16**, 390–398 (2012).
89. R. G. Natan, W. Rao, M. N. Geffen, Cortical interneurons differentially shape frequency tuning following adaptation. *Cell Rep.* **21**, 878–890 (2017).
90. J. M. Ross, J. P. Hamm, Cortical microcircuit mechanisms of mismatch negativity and its underlying subcomponents. *Front. Neural Circuits* **14**, 13 (2020).
91. H. E. M. Den Ouden, J. Daunizeau, J. Roiser, K. J. Friston, K. E. Stephan, Striatal prediction error modulates cortical coupling. *J. Neurosci.* **30**, 3210–3219 (2010).
92. A. M. Bastos, W. M. Usrey, R. A. Adams, G. R. Mangun, P. Fries, K. J. Friston, Canonical microcircuits for predictive coding. *Neuron* **76**, 695–711 (2012).
93. S. Shipp, Neural elements for predictive coding. *Front. Psychol.* **7**, (2016).
94. A. M. H. Lesicko, C. F. Angeloni, J. M. Blackwell, M. De Biasi, M. N. Geffen, Corticofugal regulation of predictive coding. *eLife* **11**, e73289 (2022).
95. A. Bendixen, E. Schröger, W. Ritter, I. Winkler, Regularity extraction from non-adjacent sounds. *Front. Psychol.* **3**, 143 (2012).
96. K. Hara, R. A. Harris, The anesthetic mechanism of urethane: The effects on neurotransmitter-gated ion channels. *Anesth. Analg.* **94**, 313–318 (2002).
97. H. Tsukano, M. Horie, R. Hishida, K. Takahashi, H. Takebayashi, K. Shibuki, Quantitative map of multiple auditory cortical regions with a stereotaxic fine-scale atlas of the mouse brain. *Sci. Rep.* **6**, 22315 (2016).
98. W. Guo, A. R. Chambers, K. N. Darrow, K. E. Hancock, B. G. Shinn-Cunningham, D. B. Polley, Robustness of cortical topography across fields, laminae, anesthetic states, and neurophysiological signal types. *J. Neurosci.* **32**, 9159–9172 (2012).
99. J. Voigts, J. Siegle, D. L. Pritchett, C. I. Moore, The flexDrive: An ultra-light implant for optical control and highly parallel chronic recording of neuronal ensembles in freely moving mice. *Front. Syst. Neurosci.* **7**, 8 (2013).
100. Allen Institute for Brain Science, Allen Reference Atlas. Mouse Brain [brain atlas] (2011); http://atlas.brain-map.org/atlas?atlas=1&plate=100960228#atlas=1&plate=100960069&resolution=8.38&x=6782&y=4142&zoom=-3&z=6.
101. E. M. Trautmann, S. D. Stavisky, S. Lahiri, K. C. Ames, M. T. Kaufman, D. J. O'Shea, S. Vyas, X. Sun, S. I. Ryu, S. Ganguli, K. V. Shenoy, Accurate estimation of neural population dynamics without spike sorting. *Neuron* **103**, 292–308.e4 (2019).

Acknowledgments: We thank Y. Boubenec, F. de Lange, J. L. Peña, B. Shinn-Cunningham, and E. Schröger for comments on a previous version of the manuscript. **Funding:** This work was supported by project PID2019-104570RB-I00 funded by MCIN/AEI/10.13039/501100011033 (to M.S.M.) and Foundation Ramón Areces grant CIVP20A6616 (to M.S.M. and D.P.-G.), European Union's Horizon 2020 grant agreement no. 952378—BrainTwin (to M.S.M., D.P.-G., and A.B.L.-R.), Foundation Ramón Areces grant CIVP20A6616 (to M.S.M. and D.P.-G.), NWO-VIDI grant 016.VIDI.189.052 (to B.E., K.P., and A.A.), NWO-ALW-Open grant (ALWOP-346) (to K.P.), iNavigate grant H2020-MS-CA-RISE-2019-873178 (to E.Y.), and NeurotechEU grant EPP-EUR-UNIV-2020-101004080 (to E.Y.). **Author contributions:** A.B.L.-R. performed experiments in anesthetized rats, data curation and analysis under the guidance of D.P.-G. and M.S.M., and writing—original draft. K.P. performed experiments in the awake mouse and analyzed the data under the guidance of B.E., as well as writing—review and editing. A.A. performed experiments in the awake and anesthetized mouse and contributed to data analysis. E.Y. performed experiments in the anesthetized mouse. D.P.-G. performed conceptualization, software, data curation, formal analysis, and writing—review and editing. B.E. performed conceptualization, supervision, project administration, funding acquisition, contributed to data analysis and writing—review and editing. M.S.M. performed conceptualization, methodology, supervision, project administration, funding acquisition, and writing—original draft, review, and editing. **Competing interests:** The authors declare that they have no competing interests. **Data and materials availability:** All data needed to evaluate the conclusions in the paper are present in the paper and/or the Supplementary Materials.

Submitted 25 June 2022
Accepted 9 May 2023
Published 14 June 2023
10.1126/sciadv.abq8657